Vertical Motions in the Mesosphere.

by

Damian John Murphy B.Sc. (Hons)

A thesis presented for the degree of

Master of Science

at the University of Adelaide

(Department of Physics)

December 1984

For my parents, who taught me that the more string you let out, the tighter it gets.

Dedicated to...

The Collingwood Football Club.

STATEMENT:

I declare that this thesis contains no material which has been accepted for the award of any other degree or diploma in any university and that, to the best of my knowledge, the thesis contains no material previously published or written by another person, except where due reference is made in the text. I consent to the thesis being made available for photocopying and loan if applicable, if accepted for the award of the degree of Master of Science.

Damian Murphy

TABLE OF CONTENTS

TABLE OF CONTENTS (continued)

Acknowledgements:

As small repayment of a great debt I would like to extend my sincere thanks to.....

- Dr Bob Vincent for his well directed supervision and for generally making it all possible.
- Dr Basil Briggs for numerous crystallising discussions.
- Dr Dave Fritts for his assistance in Chapter one and for our many helpful and interesting discussions.
- Dr Wayne Hocking for his help in Chapter three and for the occasional push along.
- Dr Graham Elford for his ubiquitous support.
- Mr Ron Craig and Mr George Joss for there unlimited computer knowledge.
- Mr Alex Didenko for his technical and giraffe handling skills.
- Mrs Mercia Fuss for her time and wealth of experience in typing everything.
- Mr Jack Szeszycki for all the diagrams/creations.
- Mr Brian Fuller for all sorts of things including continually beating me at squash.
- My colleagues in the Atmospheric Physics group and maybe even the Cosmic Ray group.
- Last but not least, the girls, Linda and Janet, for putting up with me for the duration.

Thanks.

Summary

Vertical motions are difficult to measure in the mesosphere and the measurements that have been made have been found to contradict the theoretically predicted results. It is this contradiction that this thesis seeks to address.

The principles responsible for the theoretical predictions are presented in Chapter one in the form of a review of the relevant literature. There is also some suggestion of misinterpretation of the theory.

Experimental causes of error are addressed in the second chapter, with particular emphasis on the possibility of the radar receiving beam not being truly vertical. Some evidence was found for an effective beam tilt but this was considered to be largely due to the scatterers themselves.

Chapter three describes an experiment that compares the vertical velocities obtained through radar beams of differing characteristics. It is concluded, on the basis of the results of chapters two and three that the current method of analysis is susceptible to contamination from the horizontal wind. A possible alternative is suggested.

The fourth and final chapter reviews the work of the thesis and makes proposals for future work.

Preface:

The experiments described in chapters two and three and to a small extent, chapter four of this thesis, were carried out at the University of Adelaide's Buckland Park Field Station. Although information of particular importance is presented as part of the discussions of the experiments being described, it may be in the interest of the reader to become familiar with Appendix 1, which describes the experimental facility in general terms.

The operational height range of the radar stretches from 60 to 98 km. This encompasses the mesosphere and lower thermosphere, and results are generally presented over the entire available height range. It is noted that, when discussing experiments and in the title, the word "mesosphere" is used to describe the 60 to 98 km height range, for convenience.

D.J.M.

CHAPTER 1 : INTRODUCTION AND BACKGROUND

1.1 The Mean Circulation

1.2 Atmospheric Momentum Transport

1.3 Interpretation Considerations

Summary

1. INTRODUCTION AND BACKGROUND

The work presented in this thesis concerns the measurement of vertical velocities in the altitude range 60-100km, which encompasses the mesosphere and lower thermosphere. Before any results can be considered, however, the mechanisms thought to be responsible for these vertical motions should be addressed.

The following section reviews the observations, problems, and resulting theories that lead us to believe vertical motions exist in the mesosphere.

1.1 The Mean Circulation

The understanding of any physical system requires familiarisation via both theory and observations. In this case, it was observations that raised doubts about theories of the mean atmospheric circulation, so it is with observations that this investigation will start.

Rocket-grenade measurements of temperature and wind in the mesosphere were made at Fort Churchill, Canada (55° N, 94° W) by Stroud, Nordberg, Bandeen, Bartman and Titus (1960) using methods described by Ference, Stroud, Walsh and Weisner (1956) and Weisner (1956). In this experiment, Stroud et al. (1960) found the winter mesosphere to be approximately 40K warmer than the mesosphere in summer at the same height. This was consistent with the findings of Kellogg and Schilling (1951), and in part with the work of Murgatroyd and Goody (1958). In the latter paper, the authors calculated the temperature changes, both positive and negative, in the atmosphere due to absorption of solar radiation and reradiation, by ozone, molecular oxygen and carbon dioxide. They found that only from 30° latitude in the winter hemisphere to 60° latitude in the summer hemisphere is the atmosphere very close to being in radiative equilibrium. Outside this region, they suggest that non-radiative effects would need to be invoked to account for the disagreement.

A similar study was made of the stratosphere by Ohring (1958). The result was a radiative source and sink distribution like that of Murgatroyd and Goody even though it was based on different assumptions, adding support to the latter authors' findings.

The suggestion that the non-radiative processes required are dynamical was made by Haurwitz (1961) who argued that, because the mesosphere was warmer at high winter latitudes than elsewhere, horizontal advection alone could not explain the observations. This would be in violation of the Second Law of Thermodynamics. On these grounds Haurwitz proposed vertical motions over the poles due to a meridional circulation. The way in which a poleward flow requires vertical motion due to convergence and the requirements of continuity is illustrated in Fig. (1-1). The proposal was also made that the high ozone content of the polar atmosphere at the end of winter, which cannot be attributed to photochemical production, could be explained by the vertical transport mechanism described above.

Further evidence for the existence of vertical motions near the poles comes from attempts to explain the presence of noctilucent clouds which are observed during local summer. In a recent paper, Reid (1975) makes the popular suggestion that these are ice clouds and proposes a model for their formation. However, to obtain the conditions required, a persistent upward motion must exist.

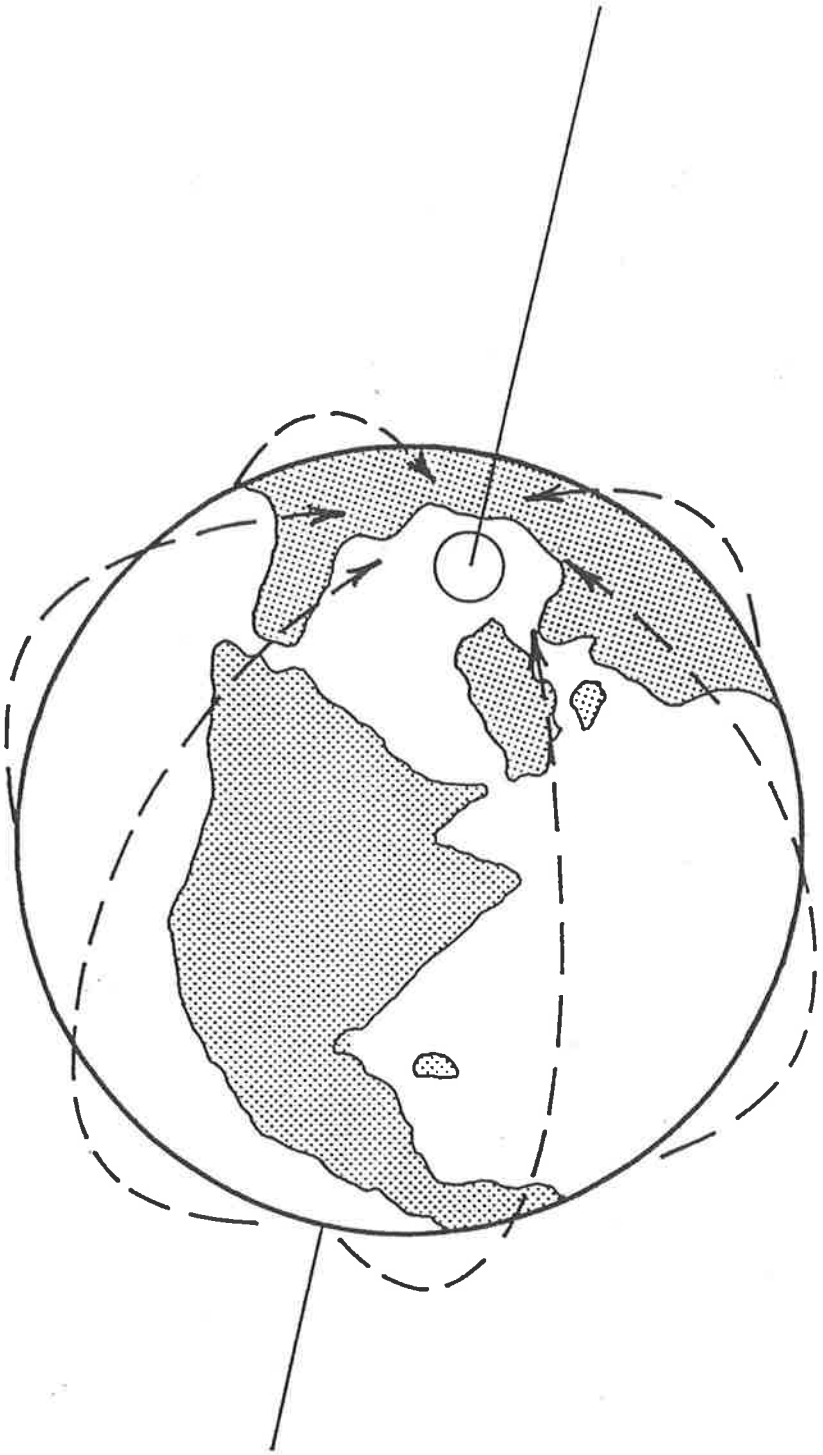

Figure 1-1. " A meridional flow requires vertical motion over the poles to satisfy continuity "

These observations and discussions imply that the presence of a meridional circulation would explain several atmospheric phenomena if it could be justified. This justification, however, does not come easily at all and will be the subject of much of this discussion from here on. Before this, however, it will be advantageous to expand our observational data set to a full meridional cross-section so that comparisons between theory and observations can be made at all latitudes.

To do this, we refer to the oft-quoted work of Murgatroyd (1969) and in particular the temperature and zonal wind profiles reproduced in Fig. (1-2). The cross-sections shown are for the solstices and are obtained by averaging zonally the data from radiosonde, rocketsondes, and rocket-grenade experiments over a number of years, principally in the Northern Hemisphere.

With this observational base we can now look at attempts to recreate features consistent with Fig (1-2) using theoretical models. One of the first groups of workers to do this was Murgatroyd and Singleton (1961) who calculated the vertical and meridional motions required to transport heat between the radiative sources and sinks suggested by Ohring (1958) and Murgatroyd and Goody (1958). The resulting circulations are consistent with observations of the paths of radioactive debris, as well as being qualitatively what was required to explain the vertical motions over the polar mesosphere. As is stated by the authors, however, there is one thing missing in

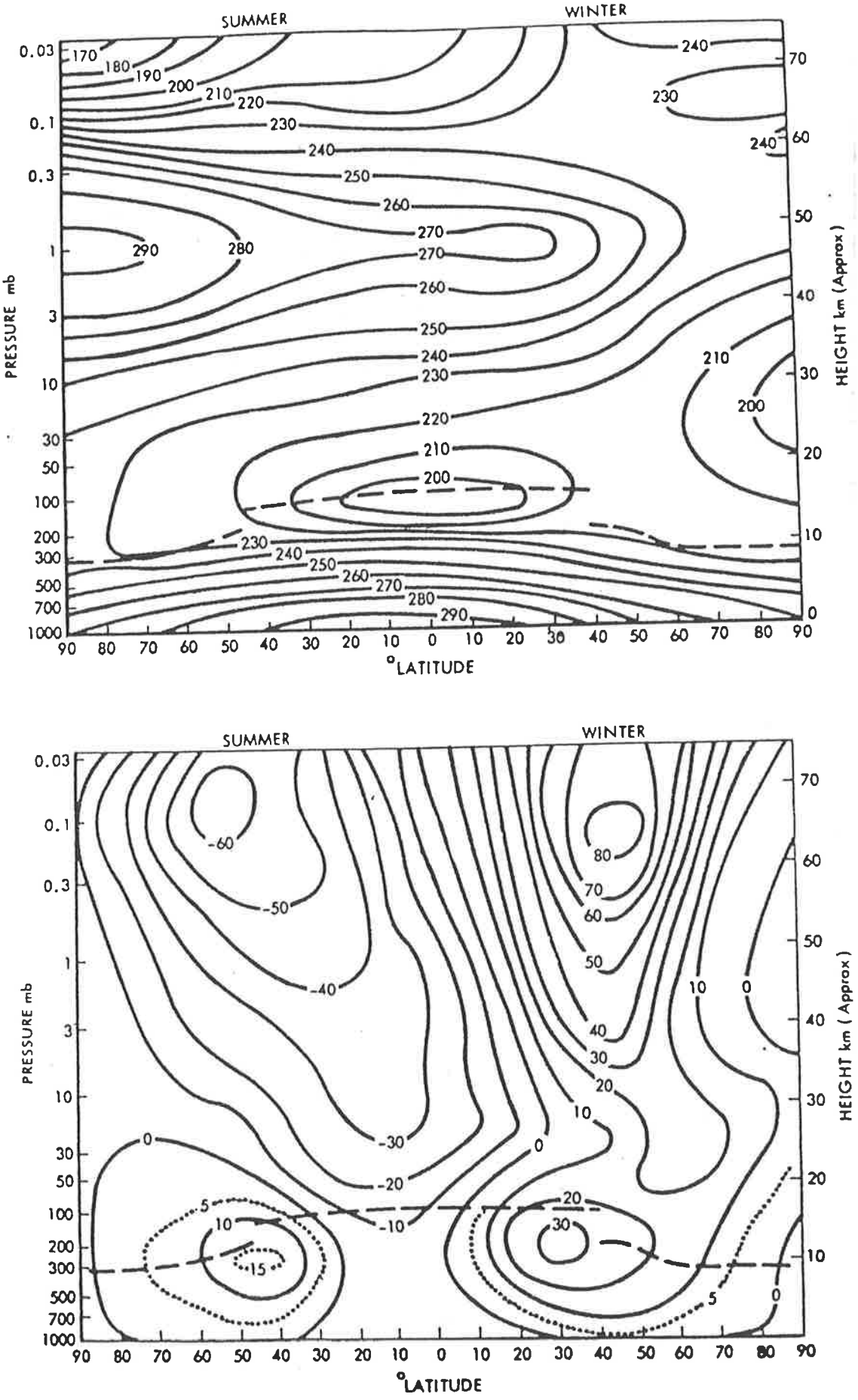

Figure 1-2. Observed meridional cross-sections of temperature (upper, °K) and zonal wind (lower, ms^{-1}) for solstice, after Murgatroyd (1969).

their model. This is that it does not attempt to balance the angular momentum budget of the atmosphere.

The seriousness of this omission is illustrated by the profiles from Geller (1983) shown in Fig (1-3). The first of these shows the atmospheric temperature as a function of height and latitude due to radiative effects only. This "Radiative Equilibrium" or Local Thermodynamic Equilibrium (LTE) cross-section is that obtained when local solar heating and infrared cooling are in balance. This representation does not allow for transport of heat from outside the local environment by advection, so Fig (1-3a) does not include heating or cooling due to horizontal or vertical motions. The wind field that will result from this temperature distribution can be found via the geostrophic wind equation which balances the pressure gradient force due to the thermal structure, with the force experienced by a parcel of air which tries to move in a way that would change the total angular momentum of the atmosphere. The latter is known as the Coriolis force. As the earth's atmosphere is isolated in space, the total angular momentum must be constant so it is appropriate to use the geostrophic wind equation and utilise its inherent angular momentum conservation. The results are presented in Fig (1-3b). The gap over the equatorial regions is due to the inapplicability of the geostrophic equation in this region, but is of little consequence to the arguments used here. Comparison of Fig (1-3) with the observations in Fig (1-2) show summer and winter mesopheric winds of the correct sign but of extremely large magnitude and the wind

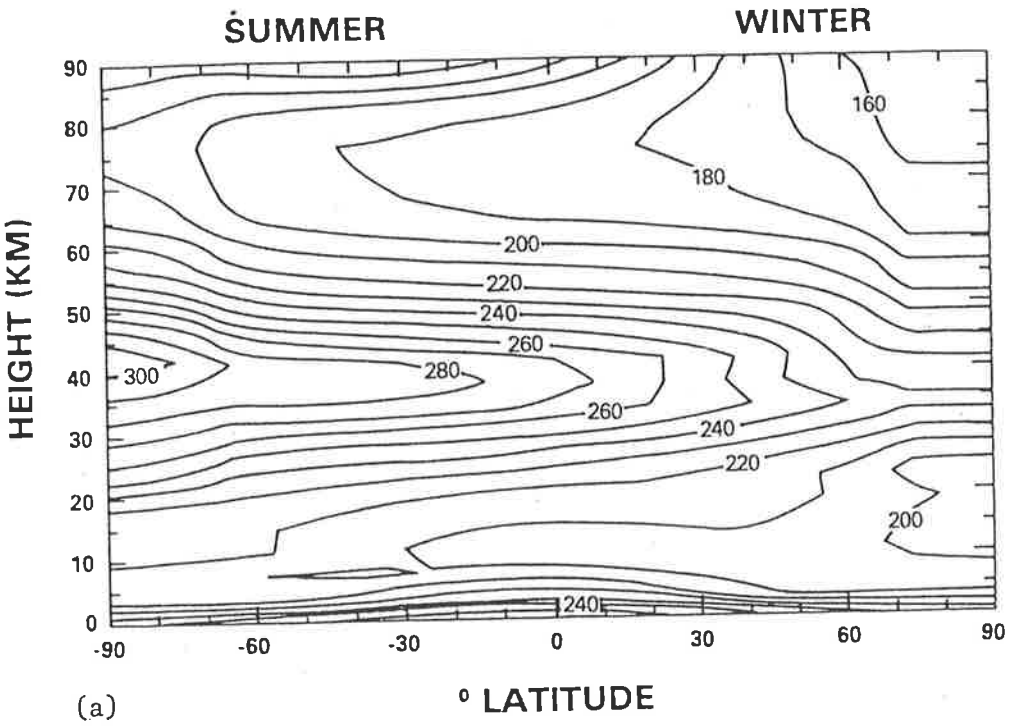

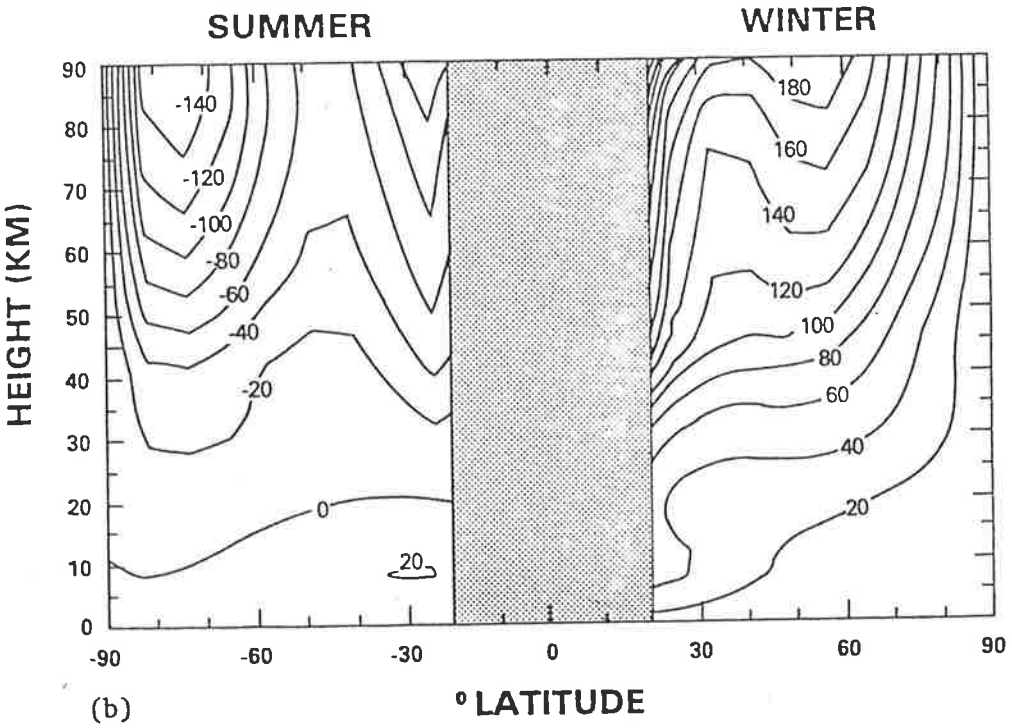

Figure 1-3. Meridional cross-sections of
a) Local Thermodynamic Equilibrium temperature distribution, and b) Zonal geostrophic wind resulting from the above temperature distribution.

profiles in Fig (1-3b) do not close over at the top, but continue to increase upward out of the model domain. Finally, this wind field is an equilibrium state so that the flow shown is a steady state for this radiation forcing configuration. Thus we have settled into a momentum "niche" and any flows that affect this balance cannot be allowed. Unfortunately, vertical and meridional flows fall into this category so that this model does not allow for their existence.

This suggests that the model is incomplete. To have meridional and vertical flow, another source of momentum must be introduced to keep the mesospheric momentum budget in balance. A landmark in attempts to do this came in the work of Haurwitz (1961). In this paper two possible mechanisms were proposed to allow meridional flow. The first was a zonal pressure gradient. This would cause a meridional flow but only an oscillating one that would not give rise to a mean mass transport along latitude lines. The second suggestion was that friction due to eddy viscosity decelerated the mean zonal flow. This would obviously result in a momentum change and in turn a meridional flow to maintain the momentum balance. Calculations based on this principle showed qualitative agreement with observations in a broad sense. It seemed that the right ideas were now there to be built on.

Another important work appeared a few years later and was due to Leovy (1964). In this, a set of linearised equations requiring momentum and energy conservation were

used to model the atmosphere; however, these equations contained some significant refinements. In his treatment of heating Leovy included terms due to radiation, which were a function of season and temperature, as well as terms which accounted for differences due to transport, from the zonal mean temperature. He also assumed that there was no exchange of radiation with adjacent layers, just to and from space. This was later termed the "Cooling to Space Approximation". Leovy also recognised that mechanical dissipation of the zonal flow, (which would drive the meridional circulation) would cause heat transport making this effect extremely difficult to parameterise with the data available. This was simplified by gathering these effects into a Rayleigh friction term which acted to decelerate the mean flow. For all the cases treated the Rayleigh friction coefficient was held constant with height although some different values were used. The results were once again in fair qualitative agreement with observations.

Leovy's use of a constant Rayleigh friction coefficient was in the interest of simplicity and it would not be expected to be so in actuality. However, the extent and nature of variation with height is not in the least obvious and the bulk features of the Rayleigh friction profile required to balance both the energy and momentum budgets were found with no knowledge of the effects responsible. This may in part explain the long period of time that elapsed before the next major work in this field appeared. However, much important work was done in improv-

ing the understanding and parameterisation of atmospheric heating and cooling during this time (e.g., Dickinson 1973 and references found in the following papers). In particular, ozone concentrations were investigated and it was this work that produced the next attempt at atmospheric modelling.

We have not so far been explicitly interested in the transport of atmospheric constituents. The model by Cunnold, Alyea, Phillips and Prinn (1975) was produced for just this purpose. Based on the balance equations and greatly improved heating formulations the model produced results showing improved agreement with observations. The results, however, were discussed mainly in terms of ozone transport. The friction term used was derived from eddy flux arguments with a coefficient that was not constant but increased with height above 25km.

Because of its emphasis, the previous paper is often not referenced and it is the work of Schoeberl and Strobel (1978) that is discussed. In this important paper, the basic model of Leovy (1964) was upgraded with improved heating parameterisations (e.g., Strobel 1978) and allowance was made for contributions to the heat and momentum budgets of planetary waves with zonal wavenumbers 1 and 2. The lack of knowledge of the required Rayleigh friction was allowed for by making this an adjustable parameter.

Improved agreement with observations resulted when a Rayleigh friction profile of the form

$$k_r = k_o \exp(z/c)$$

(where z is height) with c=4.1km, k_o=30 days was used. This expression resulted from the need to drive the meridional circulation at greater heights but not damp the quasi biennial oscillation further down. Thus the main features of the momentum input required were now known.

Further improvements to the models by Holton and Wehrbein (1980), Wehrbein and Leovy (1982) and Apruzese, Schoeberl and Strobel (1982) involved changes to the treatment of heating and the drag profiles required to maintain agreement with observations. However, it is stated in Holton and Wehrbein (1980) that the mechanical dissipation (represented by Rayleigh friction) is supposedly due to turbulence associated with gravity waves and tides. Therefore it is important to remember that the Rayleigh drag idea was a simplification and misleading when considering the true nature of the processes involved. The nature of this process is also not immediately obvious, thus we will turn our attention to the mechanisms responsible for the "drag".

1.2 Atmospheric Momentum Transport

In the previous section, it was described how attempts to provide mechanical dissipation via local effects such as eddy viscosity, and to balance the mesospheric momentum budget, did not give quantitative agreement with observations (Haurwitz, 1961). This suggests that the required momentum is being transported into the mesosphere from sources at other levels. To understand how this occurs, it is necessary to know the nature of the momentum sources, and the properties of the transport mechanism which enables momentum to be conveyed straight through some levels and deposited into others. Experience in other fields of physics would suggest that the process was probably wave-like, but the question is: of what kind?

A theory to explain wave-like features of upper atmosphere wind profiles was proposed by Hines (1960) and internal atmospheric gravity waves (or buoyancy waves) came to the fore. Hines suggested that these waves could be responsible for energy transport, and mechanical dissipation due to the generation of turbulence. Recently, these proposals have been shown to be correct but before they can be discussed, an understanding of these waves is required. Therefore, the theory, assumptions and characteristics of internal atmospheric gravity waves will be reviewed briefly. For further information on the subject the reader is referred to Hines (1960), Hines (1974) and Gossard and Hooke (1975).

The frequency with which a parcel of air in an horizontally stratified fluid will oscillate if displaced vertically from its mean position is known as the Brunt-Vaisala frequency, N defined as

$$N^2(z) = \frac{g}{\bar{T}} \left[\frac{\partial \bar{T}}{\partial z} + \Gamma_d \right]$$

In terms of potential temperature θ,

$$N^2(z) = \frac{g}{\bar{\theta}} \frac{\partial \bar{\theta}}{\partial z}$$

where z is the height co-ordinate, T temperature, Γ_d the dry adiabatic lapse rate and g the acceleration due to gravity. Overbars denote mean values.

The Brunt-Vaisala frequency can be regarded as the resonant frequency of oscillation for fluid parcels under the influence of gravity and thus will represent a frequency limit of some kind. It is in fact the high frequency limit for gravity wave oscillations. The low frequency limit is known as the inertial frequency and is defined as

$$f = 2 \Omega \sin \phi$$

where Ω is the angular velocity of the earth and ϕ the latitude.

These limitations make it possible to disregard some of the terms in the continuity, force (momentum) and conservation of energy equations, which are only of interest when studying oscillations of a longer or shorter time scale. These equations may be further simplified by assuming the fluid is incompressible and in hydrostatic balance and that the co-ordinate axes can be aligned,

without loss of generality, such that the oscillations occur in the x-z plane. If the field variables such as pressure, density etc. are then represented by a mean, and a perturbation about that mean

$$\psi(x,z,t) = \bar{\psi}(z) + \psi'(x,z,t)$$

(the overbar denoting a mean as before and the primed variable a perturbation), and terms involving products of primed quantities are ignored, the solutions, of the form

$$\psi'(x,z,t) \sim e^{z/2H} \; e^{i(kx + mz - kct)}$$

(with m and $\bar{u}$ slowly varying) can be found. Here k and m are the horizontal and vertical wavenumbers, $\bar{u}$ the mean horizontal wind and c the horizontal phase velocity of the wave. These then yield the dispersion relation

$$m^2 = \frac{k^2(N^2 - \omega^2)}{(\omega^2 - f^2)}$$

or

$$\omega^2 = \frac{k^2N^2 + m^2f^2}{(k^2 + m^2)}$$

where $\omega = k(\bar{u}-c)$ is the intrinsic frequency of the wave motion, i.e., the frequency seen by an observer moving with the mean wind. Similar manipulation of the equations give relations between the field variables - the so-called "polarisation relations" (see appendix 2 for details).

Further study of the dispersion relations shows that high intrinsic frequency oscillations involve small horizontal displacements and large vertical displacements whereas the inverse is true for low frequency oscillations. Thus the phase fronts for low frequency waves are aligned

more nearly horizontally than those of high frequency waves. It can also be shown (Hines, 1960) that for $\omega << N$, the phase and group velocities of a gravity wave are perpendicular to each other with downward propagating phase implying upward going energy.

While propagating through an environment where $\bar{u}$ varies, it is possible that a gravity wave will encounter a region where its horizontal phase speed equals the background wind velocity and the quantity $(\bar{u}-c)$ becomes zero. This represents a singularity in the linear, inviscid, steady state mathematical treatment of gravity waves and such layers are called critical levels. It has been shown (Bretherton, 1966; Booker and Bretherton, 1967) that gravity waves are strongly attenuated by critical layers so that they act as a gravity wave screen to higher levels.

Finally, to conserve wave energy as a gravity wave propagates upward through the decreasing density of the atmosphere, the wave amplitude must increase. This wave growth goes as $e^{z/2H}$.

Although the above outline relies on many assumptions, the relations given can be applied successfully throughout the atmosphere to explain many atmospheric phenomena, and are thus of considerable significance.

It is considered likely that these gravity waves propagate upward from the troposphere, as this region of the atmosphere has the greatest energy density. This would suggest that mesospheric gravity waves should be mainly

upgoing but it is difficult to test this hypothesis. This problem was addressed by Vincent (1984) who considered the properties of low frequency gravity waves observed above Adelaide (35° S, 138° E). These motions are affected by Coriolis forces making the velocity vector of the wave rotate in a known fashion. The sense of rotation is different for upgoing and downgoing waves and can be found using the vector spectral decomposition technique. Vincent, using the method outlined by Leaman and Sanford (1975) for the oceans, estimated that about 70% of the long period wave energy over Adelaide is upgoing.

Similar conclusions were reached by Balsley, Ecklund and Fritts (1983) for the Arctic mesosphere. In this work, the MST echoes seen at Poker Flat, Alaska, were attributed to the breakdown of upgoing gravity waves.

Therefore, it seems likely that sources of gravity waves lie in the troposphere. But what mechanism or mechanisms are responsible for their excitation? The first and probably most well-known involves prevailing wind flow over large scale topography such as mountain ranges. The resulting downwind oscillations are known as lee-waves. Convection above "heat islands" is also thought to perturb the atmosphere in such a way as to produce gravity wave oscillations. Instabilities arising from wind shears are also considered. Gravity waves will be produced and will propagate away from the shear level in both directions (upward and downward).

With these momentum sources and the momentum transport properties of gravity waves in mind, we must now consider how momentum might be deposited in the mesosphere. The key work in this field was due to Lindzen, (1981) and it is largely this work that will be discussed. It is by no means complete but illustrates some important points. The author was also aided by the exhaustive review due to Fritts (1984) which contributes to much of this discussion. This review is recommended as a source of further information on the subject.

Most treatments of this topic begin with the Taylor-Goldstein equation, which describes the vertical perturbation velocity of a gravity wave under the assumptions used in our previous theoretical development. It is stated here for the case of gravity wave propagation parallel to the x-axis with $\bar{u}_{zz}$, k^2 and $\frac{1}{4H^2}$ all considered small, H being the scale height. Under these assumptions this equation becomes

$$w'_{zz} + m^2 w' = 0$$

where the subscript denotes differentiation. Here $m = \frac{N}{(\bar{u}-c)}$ is the vertical wavenumber as before. This equation has the approximate WKB solution (Bender and Orszag, 1978) for m slowly varying:

$$w'(z) = A\, m^{-\frac{1}{2}}\, e^{-i\int m\, dz'}$$

or more simply

$$w'(x,z,t) = A\, m^{-\frac{1}{2}}\, e^{i(kx + mz - kct)}$$

This can be used to find other perturbation quantities in terms of w' , importantly

$$u' = \frac{-mw'}{k}$$

from continuity and from the adiabatic energy equation ...

$$\theta' = \frac{-\bar{\theta}_z}{ik(\bar{u}-c)}$$

Wave breaking requires the presence of some form of instability, in this case it is thought to be a static instability. This occurs when the total temperature (mean plus perturbation) lapse rate exceeds the adiabatic lapse rate. Expressed in terms of the potential temperature we have the condition

$$(\bar{\theta} + \theta')_z < 0$$

By assuming the $e^{z/2H}$ and $\bar{\theta}_z$ terms do not vary rapidly with height, the above expressions for w' and θ' can be combined and differentiated to yield the conditions for instability in terms of u', $\bar{u}$ and c viz:

$$u' > c - \bar{u}$$

That is, the atmosphere is statically unstable when the total (Eulerian) parcel velocity exceeds the intrinsic phase speed of the wave.

These results must now be considered in relation to the exponential growth of gravity waves with height. Through much of the atmosphere, gravity waves will perturb the mean flow but will not make it unstable. The process could be considered reversible with all the momentum being

retrieved as the wave packet leaves the level being considered.

Eventually, however, perturbation amplitudes grow to the point such that the presence of the gravity wave makes regions of the atmosphere unstable. The resulting stabilising processes rob the total flow (background plus perturbation) of momentum and the wave, which cannot retrieve this momentum, dissipates.

To parameterise these effects, Lindzen (1981) made the assumption of earlier workers (Hodges, 1967, 1969 and Lindzen, 1967) that convective instabilities in the wave field produce only that level of turbulence necessary to maintain near neutral static stability. This means that momentum will be deposited into the flow above the level of onset of breaking and that apart from generating enough turbulence to keep perturbation amplitudes constant (for $\bar{u}(z)$ constant), the wave is unaffected. If we define the level at which saturation occurs as z_s , then we know that the mean flow acceleration is

$$\bar{u}_t = \frac{-1}{\rho_o} \left(\rho_o \overline{u'w'}\right)_z \begin{cases} = 0 & z < z_s \\ \neq 0 & z \geq z_s . \end{cases}$$

(Eliassen and Palm, 1960).

Given that $(c-\bar{u})$ does not increase faster than $e^{z/2H}$ we know that the horizontal perturbation velocity above z_s will be

$$|u'_s| = |c - \bar{u}|$$

which combined with our previous expression for u', gives

$$w_s' = -\frac{k}{m} u_s' = \frac{k}{N} (\bar{u} - c)^2$$

From this we get

$$\overline{u_s' w_s'} = -\frac{\rho_o}{2} \frac{k}{N} (\bar{u}-c)^3$$

In differentiating, both the density ρ_o and $(\bar{u}-c)$ must be considered, yielding an expression in two terms:

$$\bar{u}_t = \frac{-k (\bar{u}-c)^2}{2N} \left[\frac{(\bar{u}-c)}{H} - 3 \bar{u}_z \right]$$

which simplifies, for little variation in $\bar{u}$ to

$$\bar{u}_t = \frac{-k(\bar{u}-c)^3}{2NH}$$

Inspection of this shows that when $\bar{u}>c$, the mean flow is decelerated, and for $\bar{u}<c$ the flow is accelerated. The mean flow tends to be driven toward the horizontal phase velocity of the wave, which need not be in the zonal direction.

We can now see that Rayleigh friction does not suitably describe the processes responsible for decelerating the mean flow. Previously, large drag was only possible for large $\bar{u}$. A linear term was being used where a $\bar{u}^3$ dependence was required and Rayleigh drag was forcing the flow to zero while this new process forces it towards the wave phase speed. However, the modelling results of the previous section showed that on average the mean flow must be decelerated (not accelerated) therefore, there must be some limitations on c in the mesosphere to ensure that this process normally results in deceleration. This will be discussed shortly.

Turbulence also results from gravity wave breaking and Lindzen (1981) shows that the eddy diffusion coefficient D_{eddy} (with the y-direction wave number $\ell=0$ as in the above formulation) is

$$D_{eddy} = \frac{k\,(\bar{u} - c)^4}{N^3} \left[\frac{1}{2H} - \frac{3}{2} \frac{\bar{u}_z}{(\bar{u} - c)} \right]$$

Lindzen also states that, because mean flow acceleration cannot be produced by turbulence, both these effects must be related but separate manifestations of wave breaking.

The work of Lindzen, although an important advance, does have its shortfalls. These include the neglect of wave superposition, wave-wave interaction, wave packet localisation and wave and mean flow transience (Fritts, 1984). It was, however, a good base on which to build.

The question of wave-wave interaction was approached by Lindzen and Forbes (1983), who included the possibility of breakdown of stable waves via the parametric subharmonic instability of McComas and Bretherton (1977) to produce turbulence, into Lindzen's (1981) work. It was found that the results were not greatly affected.

Dunkerton (1982) included the effects of Lindzen (1981) in his earlier studies of wave transience (Dunkerton, 1981) to yield a quasi-linear treatment of the topic and a non-linear theory was developed by Weinstock (1982) completing a spectrum of approaches to the problem of gravity wave saturation.

It is now possible to construct an overall picture of the mechanisms that balance the atmospheric momentum budget while allowing meridional and vertical flows. As gravity waves propagate upward through the atmosphere and their perturbation amplitudes increase, they may be affected in a variety of ways. Of principal interest here is the possibility of the gravity wave (a) saturating (i.e., u' becomes equal to $c-\bar{u}$) or (b) encountering a critical level $(c-\bar{u})=0$ before saturation occurs. These gravity waves blocked by critical levels below the mesosphere will not contribute to the mesopheric momentum budget. Inspection of Fig 1-2 shows that, in both hemispheres for the solstices, the flow in the stratosphere is in the opposite direction to that in the mesosphere. If we consider a spectrum of gravity waves propagating up from the troposphere with phase speeds symmetric about zero, part of this distribution will be filtered out in the stratosphere by critical level encounters. This is illustrated in Fig 1-4 a,b (adapted from Lindzen, 1981). Upon reaching the mesosphere, only the phase speeds of opposite sense to the flow at or above the breaking level remain, so the effect of bringing the mean flow speed to the wave phase speed is equivalent to a deceleration. Once again this is an illustrative simplification of the real case, as only zonal phase speeds are considered. The more correct approach of using an isotropic gravity wave spectrum was taken by Matsuno (1982) to examine the above stratospheric filtering effects.

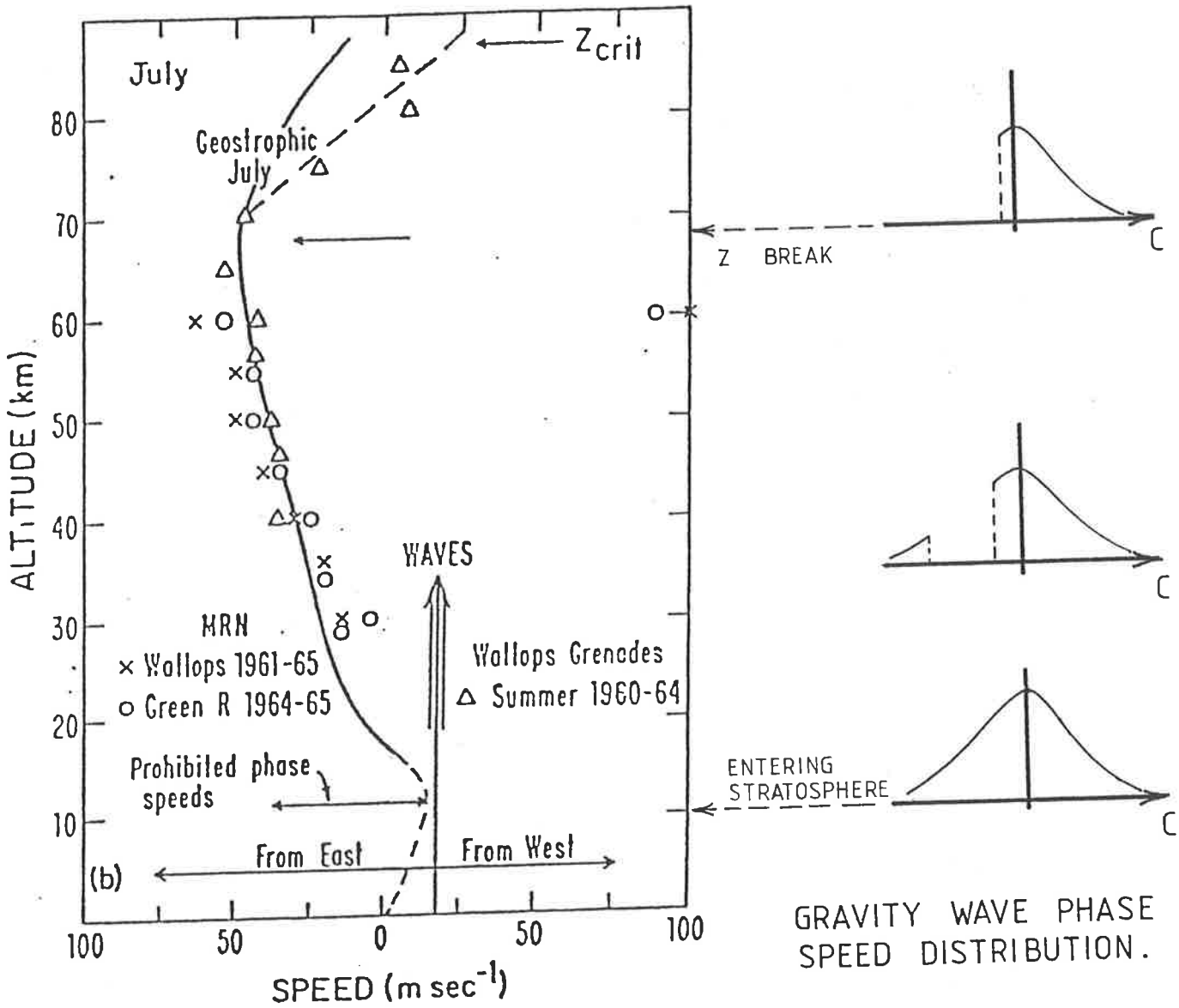

Figure 1-4. a) Gravity wave filtering in the Northern Hemisphere local summer (after Lindzen 1981).

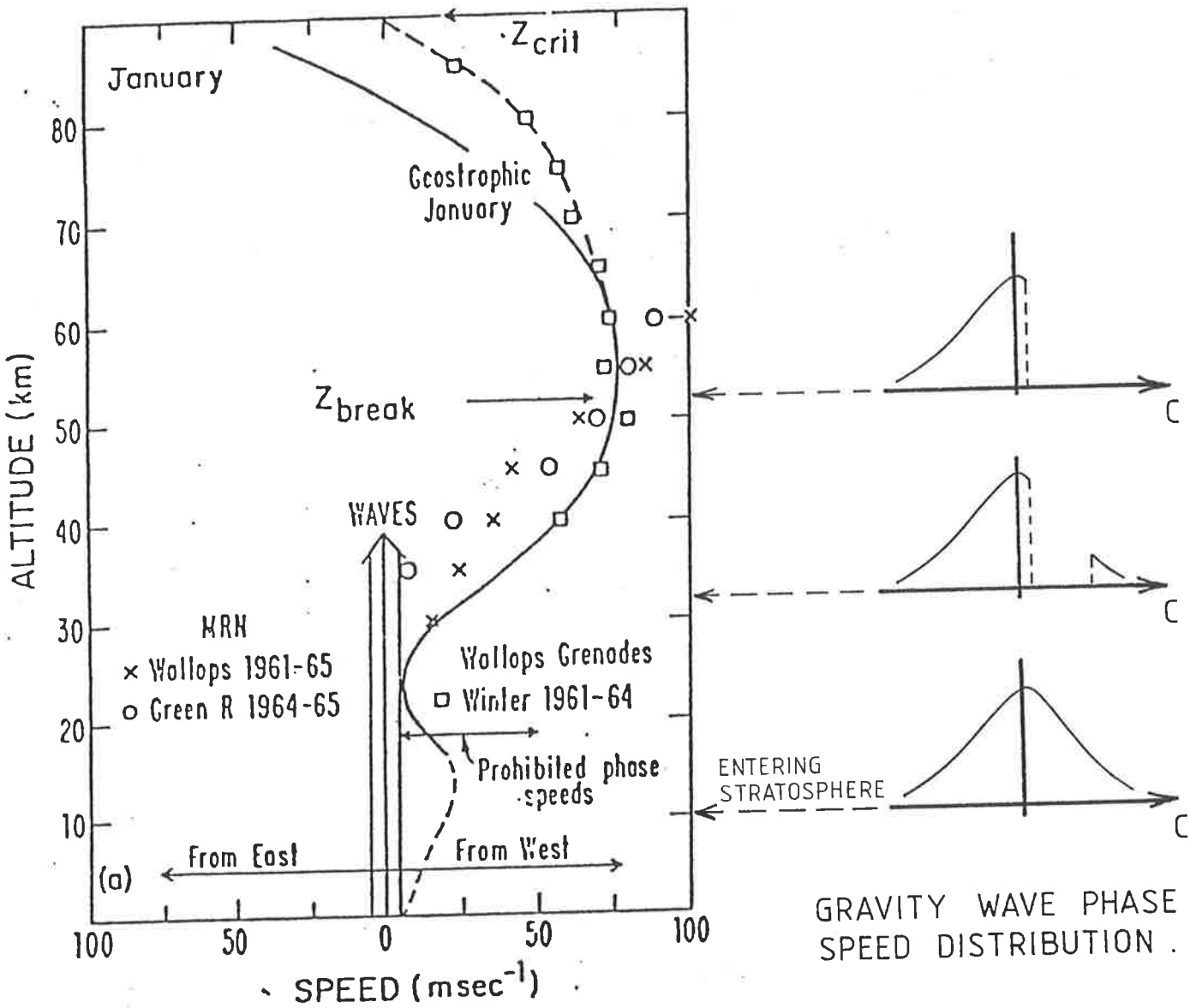

Figure 1-4. b) Gravity wave filtering in the Northern Hemisphere local winter (after Lindzen 1981).

It is possible that tides (see e.g., Lindzen, 1967; Forbes, 1982) also make some contribution to the momentum budget of the atmosphere. Lindzen (1981) concluded that the propagating diurnal mode was a primary contributor to this but only at tropical latitudes. However, it was noted by Schoeberl, Strobel and Apruzese (1983) that, because of the qualitative success of Rayleigh friction, the true momentum deposition process must depend upon the zonal wind velocity relative to the earth's surface velocity. Because tides have phase velocities that are large relative to the earth, the arguments proposed for gravity waves would not result in a deceleration. Thus tides are not thought to contribute greatly to the mesospheric momentum budget outside the tropics.

Planetary waves have also been considered as a momentum source, however, momentum transport is required into both the summer and winter mesospheres. As planetary waves only occur in winter, they are not thought to be of key importance (Houghton, 1978).

The gravity wave saturation results of Lindzen (1981) were used to replace Rayleigh friction in the model of Holton (1983) with good results. Thus it may be accepted that the breaking of upward propagating gravity waves provides the mesospheric momentum required to balance the angular momentum budget of the atmosphere.

1.3 Interpretation Considerations

The principal aim of this thesis is to consider the possible causes of error in vertical velocity measurements. In most regards this is an experimental problem but recently there have been some suggestions that the theoretical interpretation of results so far obtained has been lacking. These suggestions will now be briefly discussed.

In contrast to theoretical expectations, Balsley and Riddle (1984) measure downward velocities in the summer mesosphere. A discussion of possible sources of error concludes that this effect cannot be explained away experimentally so a polar circulation cell is proposed.

More recently, however, it has been suggested (Fritts, private communication) that it is the interpretation that is at fault. Fluid dynamics offers two representations of velocity for fluid flow. The Lagrangian velocity is the velocity of a particular parcel of air and it is this velocity that arises from large scale model studies. The Eulerian velocity which is thought to be the main contributor to ground based radar studies, is the velocity of air parcels moving through a fixed point. It is possible that these quantities differ and that difference is known as the Stokes drift defined (for vertical components) as

$$w^S = w^L - w^E$$

The mesospheric temperature structure outlined earlier and the adiabatic heating and cooling associated with vertical motion suggest that the Lagrangian component

is small (a few cm s^{-1}), however, it can be shown using mass transport arguments that the Eulerian component for gravity waves may be large in comparison (10-20 cm s^{-1}). This means that there is an associated Stokes drift and care must be taken in interpreting the measured velocities.

It is unlikely, however, that observations made so far are devoid of the experimental problems discussed later in this thesis. The above arguments will account for some but not all of the difference between theory and observation.

Summary

The mean atmospheric circulation in the mesosphere has been investigated theoretically using global scale models. The more useful of these models were found to be those that attempted to satisfy the energy (heat) and momentum equations simultaneously. It was found however, that the features predicted by the models with no momentum sources included were vastly different from observations. Zonal flows were predicted but meridional and vertical flows were not. This was in contrast with observations which suggested there were vertical motions over the poles and a related meridional flow.

It was later found that a secondary source of momentum was required to reproduce the features observed in the mesosphere. This source was parameterised using Rayleigh drag to decelerate the mean flow, with considerable success. The true momentum source was found to be non-local: gravity waves transporting momentum from the energy dense troposphere and depositing it via wave breaking in the mesosphere. In transit, parts of the gravity wave phase speed spectrum are filtered out by prevailing winds making the wave breaking process drag-like.

The inclusion of this secondary source of momentum in theoretical models results in zonal and meridional flows similar to those observed. This is not so for the vertical velocities, which are found to be significantly different from those predicted by theory. The possibility that this may be due to errors of measurement is dealt with later in

this thesis; however, there has been some suggestion that a Stokes drift associated with gravity wave activity could be causing a misinterpretation of the vertical velocities being measured.

CHAPTER 2 : AN INVESTIGATION OF SYSTEMATIC ERRORS IN VERTICAL VELOCITY DETERMINATION

2.1 The Effects of an Off-Vertical Beam

2.1.1 Statistical analysis of the Buckland Park Data

2.1.2 Results

2.1.3 Discussion

2.2 Other Effects Causing Apparent Vertical Velocities

Summary

2. AN INVESTIGATION OF SYSTEMATIC ERRORS IN VERTICAL VELOCITY DETERMINATION

> But not being at that time in a disposition to philosophize upon this phenomenon, I rather chose to observe ...
>
> Jonathan Swift, Gulliver's Travels

Some possible experimental causes of the disagreement between theoretical and measured vertical velocities are discussed in this and the following chapter of this thesis.

The most likely cause of experimental error is considered to be a "vertical" beam that does not point exactly vertically. An attempt to find the off-vertical angle and direction (if any) of the BP array is now presented. A discussion of other possible causes of experimental error in vertical velocity determination then follows.

The vertical velocities used in this chapter were obtained using the phase of the autocorrelation function (see Rastogi and Woodman, 1974). Possible alternative methods to this are discussed in chapter 3.

2.1 The Effects of an Off-Vertical Beam

Introduction

Scatterers moving horizontally across a monostatic radar beam which is pointing truly vertically will produce no Doppler shift in the returned signal and a zero radial velocity will result when a suitable Doppler analysis is used. However, attaining a truly vertical beam is difficult, particularly at HF where large arrays (e.g., 1km in diameter at Buckland Park, Briggs *et al.*, 1969) are required to produce the narrow beams considered desirable. The pointing accuracy required for measurements of the vertical velocity is illustrated when we consider the effect of a horizontal velocity of, say, $50ms^{-1}$, which is typical of the mesosphere. If the beam is off-vertical at an angle θ, then the radial velocity is $v_r = 50 \sin\theta \simeq 50\,\theta$, for θ small. The tilt in a nominally vertical beam required to produce an apparent $0.5ms^{-1}$ (typically measured in the mesosphere) "vertical velocity" by leakage into the beam of horizontal motions is given by $\sin^{-1}(0.5/50) = 0.57°$. Even off-vertical tilts of the order of 0.1° will make considerable contributions to the inferred vertical velocities and are thus undesirable. These tilts are determined by the characteristics of the array ground plane. This, however, is difficult to measure directly. Thus statistical attempts were made to find the beam pointing angle of the Buckland Park (BP) array.

2.1.1 Statistical analysis of Buckland Park data

If the measured vertical velocities are in fact due to the folding or leakage into the beam of horizontal motions, then a comparison of the "vertical" and horizontal velocities should show a correlation. This section describes a statistical method used in an attempt to find a correlation of this kind for the BP array. The ultimate aim was to find the effective pointing angle so that the inferred vertical velocities can be corrected by removing the effects of horizontal motions.

The routine operation of the BP 2MHz radar currently provides horizontal winds in real time, using the spaced antenna method (Briggs, 1977) and Doppler inferred "vertical" winds using the whole array with all elements connected in phase to produce a narrow "vertical" beam. (Details of these methods of analysis are given in chapter 3.) The half power half width of this beam is 4.5° (Hocking, 1981) and samples are taken every 2km in height from 60 to 100km. These vertical and horizontal winds suitably averaged form the data base for this analysis.

If we use the Cartesian components

$\bar{u}$ = zonal (E-W) component

$\bar{v}$ = meridional (N-S) component

$\bar{w}$ = vertical component

(with an overbar denoting a long-term average) to represent a three-dimensional wind velocity vector $\underline{v}(\bar{u},\bar{v},\bar{w})$ passing through the sampling volume of a radar beam, and

denote the direction in which the beam is pointing by the unit vector $\underline{b}$ then the Doppler shift detected by the beam will be proportional to the scalar product $\underline{V}.\underline{b}$. It is convenient at this stage to introduce spherical polar co-ordinates to represent the beam vector $\underline{b}(b_1, b_2, b_3)$ where

$$\begin{aligned} b_1 &= \sin\theta \sin\phi \\ b_2 &= \sin\theta \cos\phi \\ b_3 &= \cos\theta \end{aligned} \qquad (2\text{-}1)$$

where θ is the zenith angle and ϕ the angle measured clockwise from north to the projection of $\underline{b}$ on to the horizontal plane (see Fig 2-1). Thus

$$\bar{w}_m = \underline{V}.\underline{b} = \bar{u} \sin\theta \sin\phi + \bar{v} \sin\theta \cos\phi + \bar{w} \cos\theta \qquad (2\text{-}2)$$

will be the mean measured Doppler velocity observed with the beam in the direction $\underline{b}$.

If we assume at this stage that the values of $\bar{u}$ and $\bar{v}$ contained within our database are true velocities, then we can infer θ and ϕ without any knowledge of what the true vertical velocity is. All that is required of $\bar{w}$ is that its seasonal variations make only a small contribution to variations in $\bar{w}_m$.

If we let the terms in Eq (2.2) involving the horizontal velocities by X i.e.

$$X = \bar{u} \sin\theta \sin\phi + \bar{v} \sin\theta \cos\phi \qquad (2\text{-}3)$$

and compare X with the measured "vertical" velocity $\bar{w}_m$ using the BP narrow beam, then for the correct combination of (θ, ϕ), we should find a correlation. This comparison

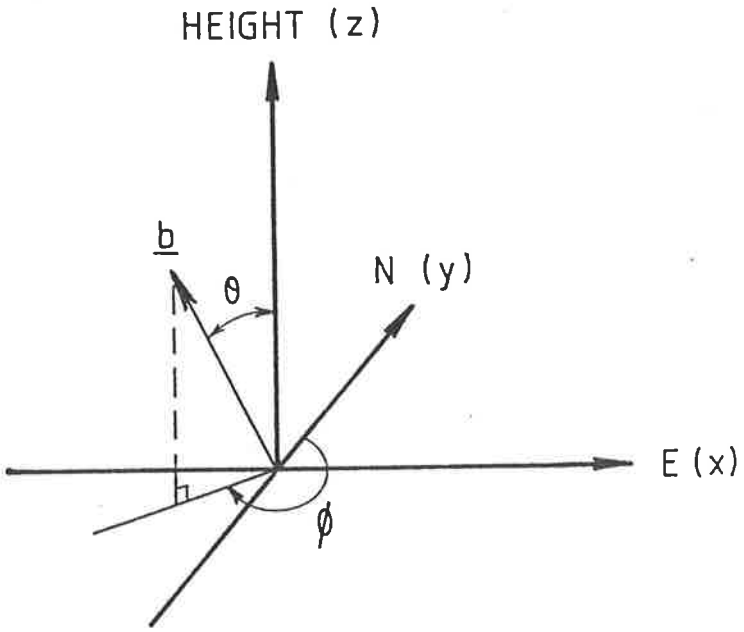

Figure 2-1. Coordinate system used in Chapter 2

was made graphically using sets of $(X,\bar{w}_m)$ values and linear regression techniques were used.

When the correct values of (θ,ϕ) are chosen, $(\bar{w}_m,X)$ values would appear as in Fig (2-2). Therefore, to obtain an estimate of the true (θ,ϕ) values, we need to find those values which give closest correspondence to Fig (2-2).

Results of the least square analysis (as outlined in appendix 3) are in the form of the following parameters:

a	$\bar{w}_m$ axis intercept
σ_a	error in a
c	slope of line
σ_c	error in slope
d^2	residual sum of squares

(i.e., square of the vertical distances from points to the fitted line)

where

$$\bar{w}_m = a + c\,X$$

An estimate of the correlation coefficient (ρ) is also derivable from d^2 (see appendix 3).

Inspection of Eq (2-3) shows that for constant ϕ, $\bar{u}$ and $\bar{v}$, the value X is a function of θ. This means that a variation in θ corresponds to a stretch in the X-direction, which will not affect the distance between the individual data points and the fitted line. This in turn means that ρ, a and d^2 will not vary with θ making the method of finding the correct θ and ϕ simple. Firstly, ϕ is chosen to give the highest correlation coefficient ρ. Then the value of θ (for

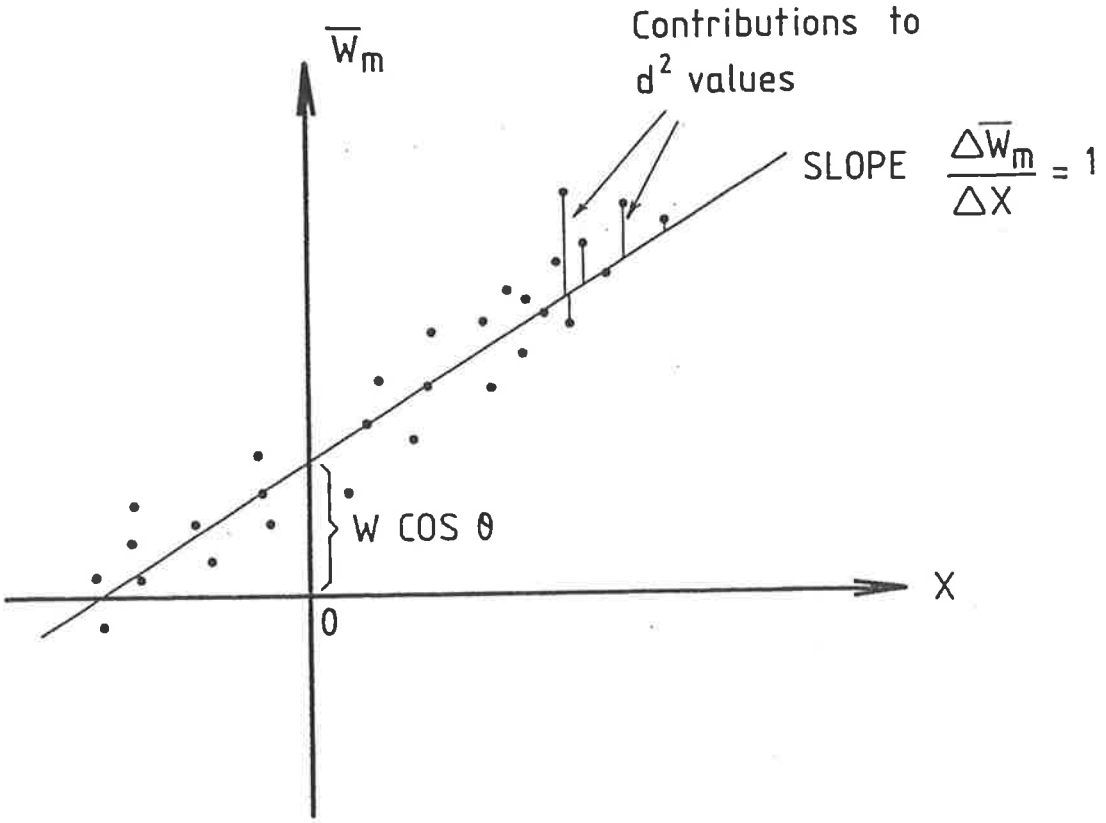

Figure 2-2. Characteristics of required correlation for true θ and ϕ .

this computed ϕ) is varied until the value is found that gives the line of best fit a slope of 1.0. This fully determines the pointing angle (see Fig 2-3).

An advantage of this method, and the reason we had to assume that $\bar{w}$, the true vertical velocity does not show much variation over the data base when compared with $\bar{w}_m$, is that the true $\bar{w}$ will not affect the slope, only the intercept. Thus pointing angles can be inferred without any knowledge of the true average vertical velocity. It may even be possible to find the long-term average of $\bar{w}$ using the intercept and the value of θ.

2.1.2 Results

Data sets made up of weekly averaged horizontal and apparent vertical velocities were analysed using the method outlined in the previous section. The long-time averages were used to remove any correlations due to real physical effects. Gravity wave and tidal theories predict a relationship between the horizontal and vertical velocities which would appear as a correlation if data of a short-time scale were used. By averaging over 7 days, effects of this kind should be removed.

Real time analysis of Buckland Park data provides wind velocities at 2km height intervals. (Successive heights, however, do not give independent results because of the transmitter pulse width that is used, see appendix 1.) The results presented here are obtained using data from three successive height gates. This means that more

Figure 2-3. (Facing Page)

The optimal values of θ and ϕ are obtained from the computer output by finding the maximum ρ value in the upper table. The corresponding ϕ value can be noted and used to find θ. This must be done in the lower table as the upper table values are invariant in θ. By noting where the slope is closest to 1.0 for the previously determined ϕ, the appropriate θ value can be read off.

SLOPE AND UNCERTAINTY FOR HEIGHTS (KMS) 68 70 72

THESE PARAMETERS DO NOT VARY WITH THETA

PHI	RHO	DSQUARED	INTERCEPT	ERROR
0.0	-.33477900	1.305491	-.115620	.001091
15.0	-.61321641	.917401	-.061904	.000949
30.0	-.61491981	.914325	-.056639	.000979
45.0	-.60493391	.932235	-.056712	.001005
60.0	-.59552331	.948845	-.057514	.001025
75.0	-.58675975	.964078	-.058498	.001042
90.0	-.57783306	.979363	-.059634	.001057
105.0	-.56764265	.996526	-.061037	.001074
120.0	-.55430507	1.018527	-.062984	.001094
135.0	-.53343988	1.051896	-.066178	.001123
150.0	-.49076767	1.116155	-.072935	.001171
165.0	-.34938893	1.290795	-.094330	.001264
180.0	.33477914	1.305491	-.115620	.001091
195.0	.61321642	.917401	-.061904	.000949
210.0	.61491981	.914325	-.056639	.000979
225.0	.60493391	.932235	-.056712	.001005
240.0	.59552331	.948845	-.057514	.001025
255.0	.58675975	.964078	-.058498	.001042
270.0	.57783305	.979363	-.059634	.001057
285.0	.56764265	.996526	-.061037	.001074
300.0	.55430506	1.018527	-.062984	.001094
315.0	.53343988	1.051896	-.066178	.001123
330.0	.49076766	1.116155	-.072935	.001171
345.0	.34938888	1.290795	-.094330	.001264

MAX ρ * *

⇒ $\phi \approx 210.0°$

TABLE OF SLOPES

THETA----------> THETA ⟶

PHI ⟶

PHI	.100	.200	.300	.400	.500	.600	.700	.800
0.00	-7.022	-3.511	-2.341	-1.756	-1.404	-1.170	-1.003	-.878 ← SLOPE
	(*****	(*****	(*****	(.7182	(.4596	(.3192	(.2345	(.1795 ← ERROR IN SLOPE
15.00	-6.433	-3.217	-2.144	-1.608	-1.287	-1.072	-.919	-.804
	(*****	(.5049	(.2244	(.1262	(.0808	(.0561	(.0412	(.0316
30.00	-3.900	-1.950	-1.300	-.975	-.780	-.650	-.557	-.487
	(.7356	(.1839	(.0817	(.0460	(.0294	(.0204	(.0150	(.0115
45.00	-2.840	-1.420	-.947	-.710	-.568	-.473	-.406	-.355
	(.4110	(.1027	(.0457	(.0257	(.0164	(.0114	(.0084	(.0064
60.00	-2.334	-1.167	-.778	-.583	-.467	-.389	-.333	-.292
	(.2914	(.0729	(.0324	(.0182	(.0117	(.0081	(.0059	(.0046
75.00	-2.090	-1.045	-.697	-.522	-.418	-.348	-.299	-.261
	(.2446	(.0612	(.0272	(.0153	(.0098	(.0068	(.0050	(.0038
90.00	-2.008	-1.004	-.669	-.502	-.402	-.335	-.287	-.251
	(.2366	(.0591	(.0263	(.0148	(.0095	(.0066	(.0048	(.0037
105.00	-2.059	-1.030	-.686	-.515	-.412	-.343	-.294	-.257
	(.2623	(.0656	(.0291	(.0164	(.0105	(.0073	(.0054	(.0041
120.00	-2.259	-1.129	-.753	-.565	-.452	-.376	-.323	-.282
	(.3384	(.0846	(.0376	(.0211	(.0135	(.0094	(.0069	(.0053
135.00	-2.677	-1.339	-.892	-.669	-.535	-.446	-.382	-.335
	(.5300	(.1325	(.0589	(.0331	(.0212	(.0147	(.0108	(.0083
150.00	-3.475	-1.737	-1.158	-.869	-.695	-.579	-.496	-.434
	(*****	(.2798	(.1244	(.0700	(.0448	(.0311	(.0228	(.0175
165.00	-4.420	-2.210	-1.473	-1.105	-.884	-.737	-.631	-.552
	(*****	(*****	(.4591	(.2583	(.1653	(.1148	(.0843	(.0646
180.00	7.022	3.511	2.341	1.756	1.404	1.170	1.003	.878
	(*****	(*****	(*****	(.7182	(.4596	(.3192	(.2345	(.1795
195.00	6.433	3.217	2.144	1.608	1.287	1.072	.919	.804
	(*****	(.5049	(.2244	(.1262	(.0808	(.0561	(.0412	(.0316
210.00	3.900	1.950	1.300	.975	.780	.650	.557	.487 ⟶ $\theta \approx 0.4°$
	(.7356	(.1839	(.0817	(.0460	(.0294	(.0204	(.0150	(.0115
225.00	2.840	1.420	.947	.710	.568	.473	.406	.355
	(.4110	(.1027	(.0457	(.0257	(.0164	(.0114	(.0084	(.0064
240.00	2.334	1.167	.778	.583	.467	.389	.333	.292
	(.2914	(.0729	(.0324	(.0182	(.0117	(.0081	(.0059	(.0046
255.00	2.090	1.045	.697	.522	.418	.348	.299	.261
	(.2446	(.0612	(.0272	(.0153	(.0098	(.0068	(.0050	(.0038
270.00	2.008	1.004	.669	.502	.402	.335	.287	.251
	(.2366	(.0591	(.0263	(.0148	(.0095	(.0066	(.0048	(.0037
285.00	2.059	1.030	.686	.515	.412	.343	.294	.257
	(.2623	(.0656	(.0291	(.0164	(.0105	(.0073	(.0054	(.0041
300.00	2.259	1.129	.753	.565	.452	.376	.323	.282
	(.3384	(.0846	(.0376	(.0211	(.0135	(.0094	(.0069	(.0053
315.00	2.677	1.339	.892	.669	.535	.446	.382	.335
	(.5300	(.1325	(.0589	(.0331	(.0212	(.0147	(.0108	(.0083
330.00	3.475	1.737	1.158	.869	.695	.579	.496	.434
	(*****	(.2798	(.1244	(.0700	(.0448	(.0311	(.0228	(.0175
345.00	4.420	2.210	1.473	1.105	.884	.737	.631	.552
	(*****	(*****	(.4591	(.2583	(.1653	(.1148	(.0843	(.0646

data points contribute to each correlation calculation for the same time span giving greater significance to the results.

The results of the analysis for three time spans are presented in Figs 2-4a), b) and c). These represent the summer solstice (SS, 6/11/83 to 30/1/84), autumn equinox (AE, 7/2/84 to 30/4/84) and winter solstice (WS, 8/5/84 to 20/8/84), respectively, each containing 12 weeks of data. With the exception of WS which was interrupted by another experiment, the data blocks cover the six weeks before and after the representative date (solstice or equinox). Each figure displays the value of ϕ (direction in degrees clockwise from north) and zenith angle θ . The values of residual sum of squares, d^2 are displayed in Fig 2-5. In all cases the vertical axis represents height with results being plotted next to the mid-range value of the three contributing heights.

The error values listed in the upper part of Fig 2-3 are the uncertainties of the given intercept values. Similarly, the bracketed quantities in the lower section of Fig 2-3 are the errors in the slope. These are not included in the presentation of the results as each error cannot be considered in isolation. An error in ϕ will cause an error in the slope and thus θ . For this reason, simulation studies are used to find uncertainties. A beam pointing direction is assumed and real horizontal wind values are projected on to it to obtain a simulated vertical wind. Random fluctuations are added at various

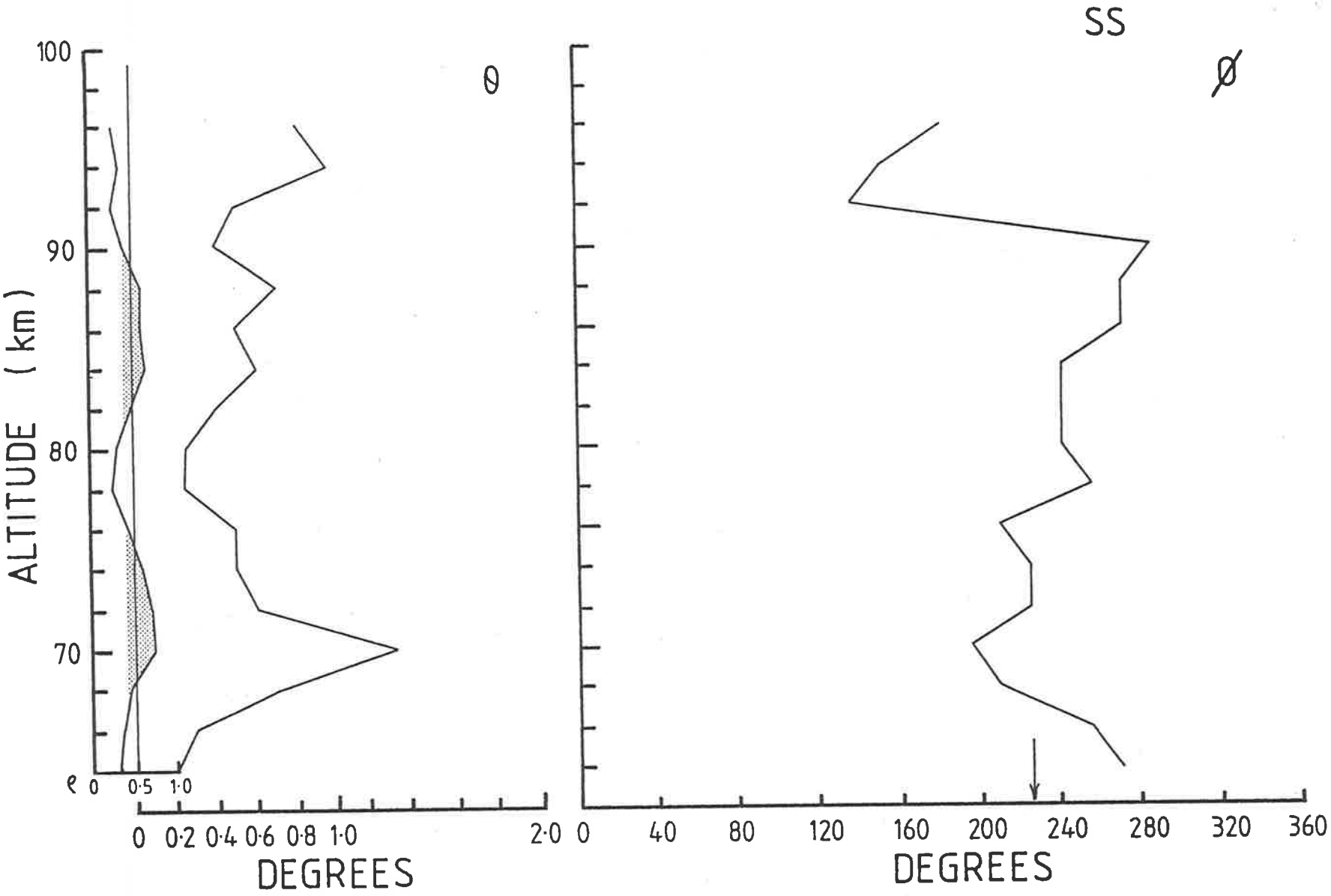

Figure 2-4. a) θ and ϕ values, and their correlation levels for the SS data set.

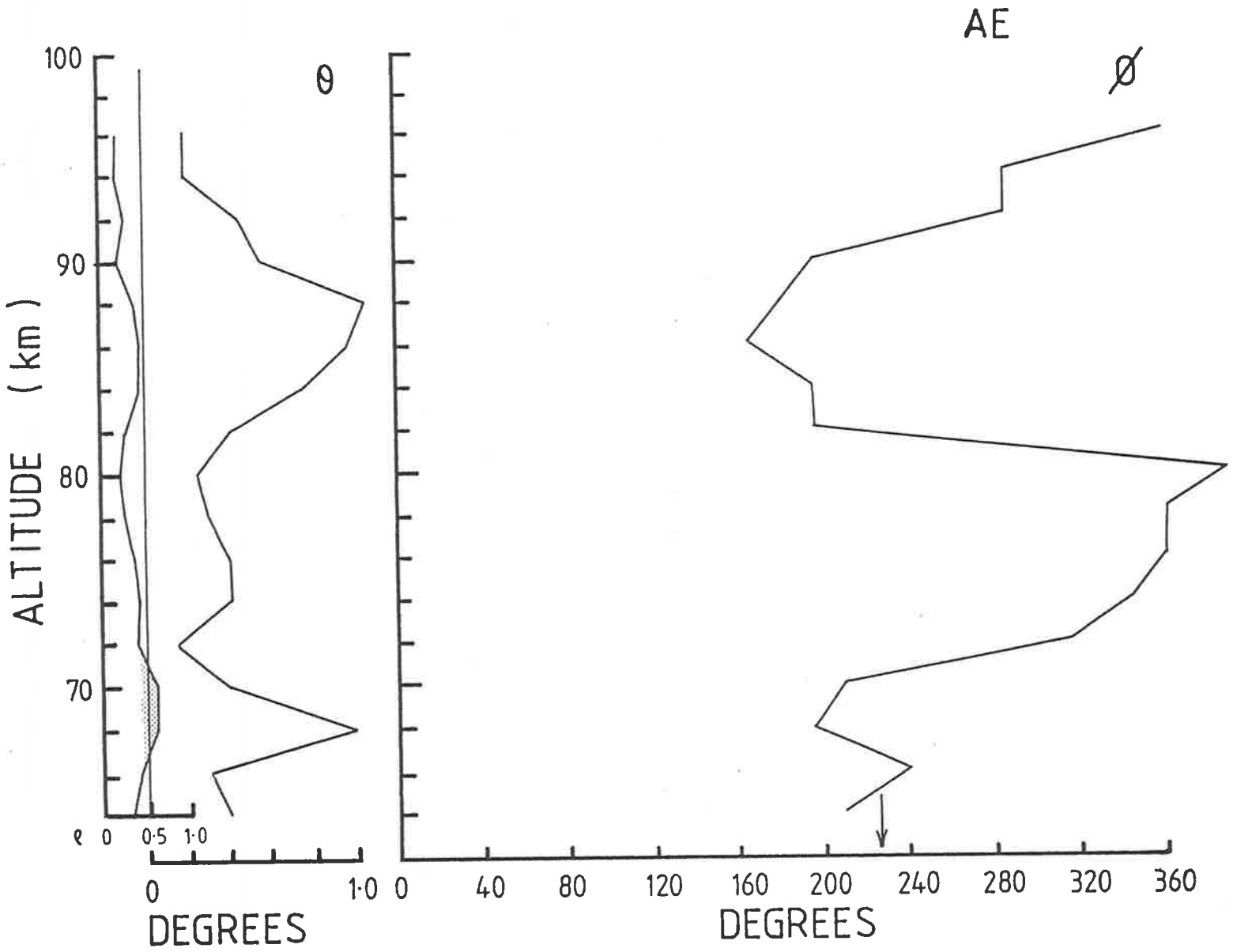

Figure 2-4. b) θ and ϕ values, and their correlation levels for the AE data set.

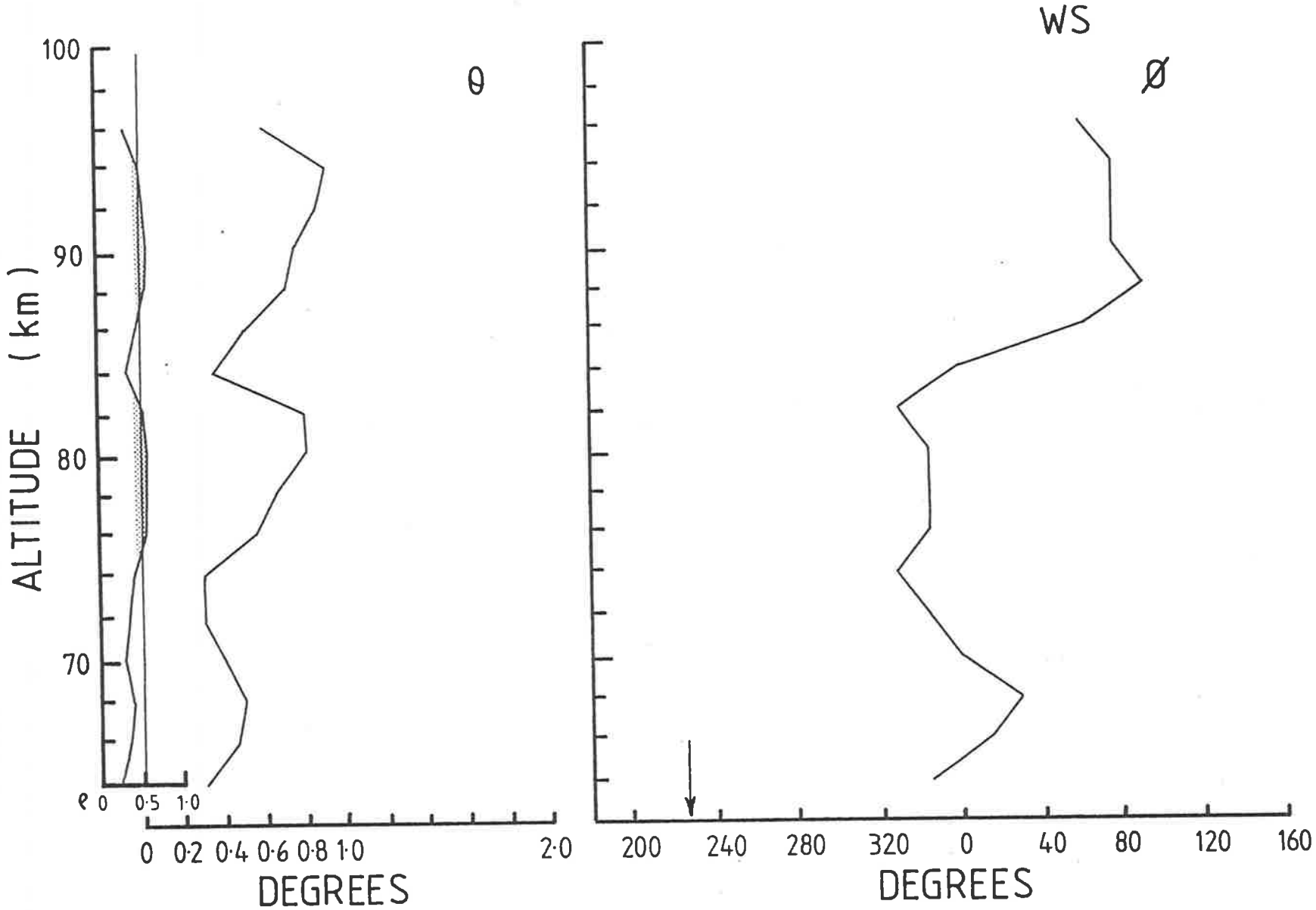

Figure 2-4. c) θ and ϕ values, and their correlation levels for the WS data set.

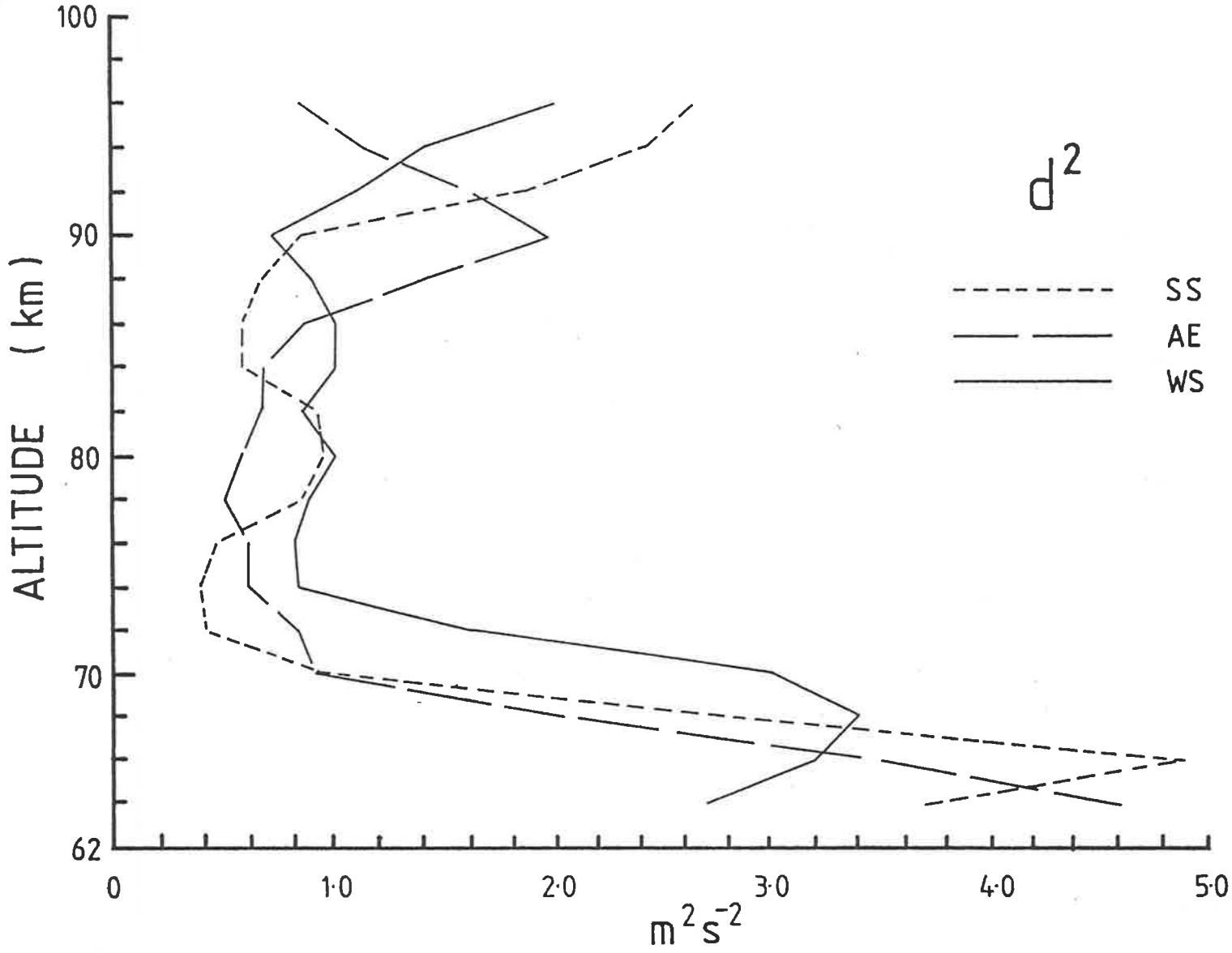

Figure 2-5. d^2 values for the SS, AE and WS data sets.

amplitudes to reproduce the scatter apparent in the real vertical wind data. The amplitude of fluctuation can be varied making it possible to recreate approximate values of d^2, the residual sum of squares.

Repeated use of this kind of simulation makes it possible to build up a scatter distribution of θ and ϕ about known input values, for various values of d^2. The range and standard deviation of these scatter distributions can then be used as a direct measure of the errors.

This technique has the advantage that it uses the same method of finding θ and ϕ as does the actual regression analysis and is thus susceptible to the same error sources.

Using this analysis, approximate errors in θ and ϕ were found for three values of d^2. Because of the random fluctuations used it was impractical to attempt to recreate d^2 exactly. It was not difficult, however, to "tune" the simulation parameters to give results close to the required value of d. These results are presented in table 2-1.

Table 2-1

approx d^2	0.5	1.0	2.0
$\Delta\phi$ (°)	30	30	60
σ_θ (°)	0.2	0.2	0.5

The magnitude of the errors in θ and ϕ show that rounding to the nearest 0.05° in θ and 15° in ϕ when reading off the computer tables (see Fig 2-3) was justified and interpolation was not necessary.

Finally, we must consider the correlation coefficient ρ. The maximum value of this quantity was used to obtain the value presented but it was possible that even this value did not represent a meaningful result. Elementary statistical arguments can be used to obtain a value of the correlation coefficient ρ_{95} such that if $\rho > \rho_{95}$, it can be accepted that there is a positive correlation at a 95% significance level (see e.g., Spiegel, 1972). For the data obtained over a 12-week period and for 3 height blocks as presented here, $\rho_{95} = 0.44$. (This assumes 22 degrees of freedom as the data is not entirely independent.)

The results of Fig 2-4 are redrawn, without those points with correlation levels less than 0.44, in Fig 2-6. In rejecting the low correlation points, the high d^2 points were removed thus all the error bars drawn in Fig 2-6 correspond to the $d^2 = 0.5$ or 1.0 cases. The autumn equinox case is not included in Fig 2-6 because only two points satisfy the significance criteria and the lower of these (midrange 68km) is probably affected by data gaps at 66km.

Many checks were performed on the results presented above. In the most convincing of these, the raw velocity data was plotted in $\bar{u}$ vs $\bar{w}_m$ and $\bar{v}$ vs $\bar{w}_m$ form for each height range. Visual inspection of these diagrams in many cases yielded obvious correlations which could be used to infer the quadrant in which the beam was pointing. These were found to agree with the linear regression analysis results presented here.

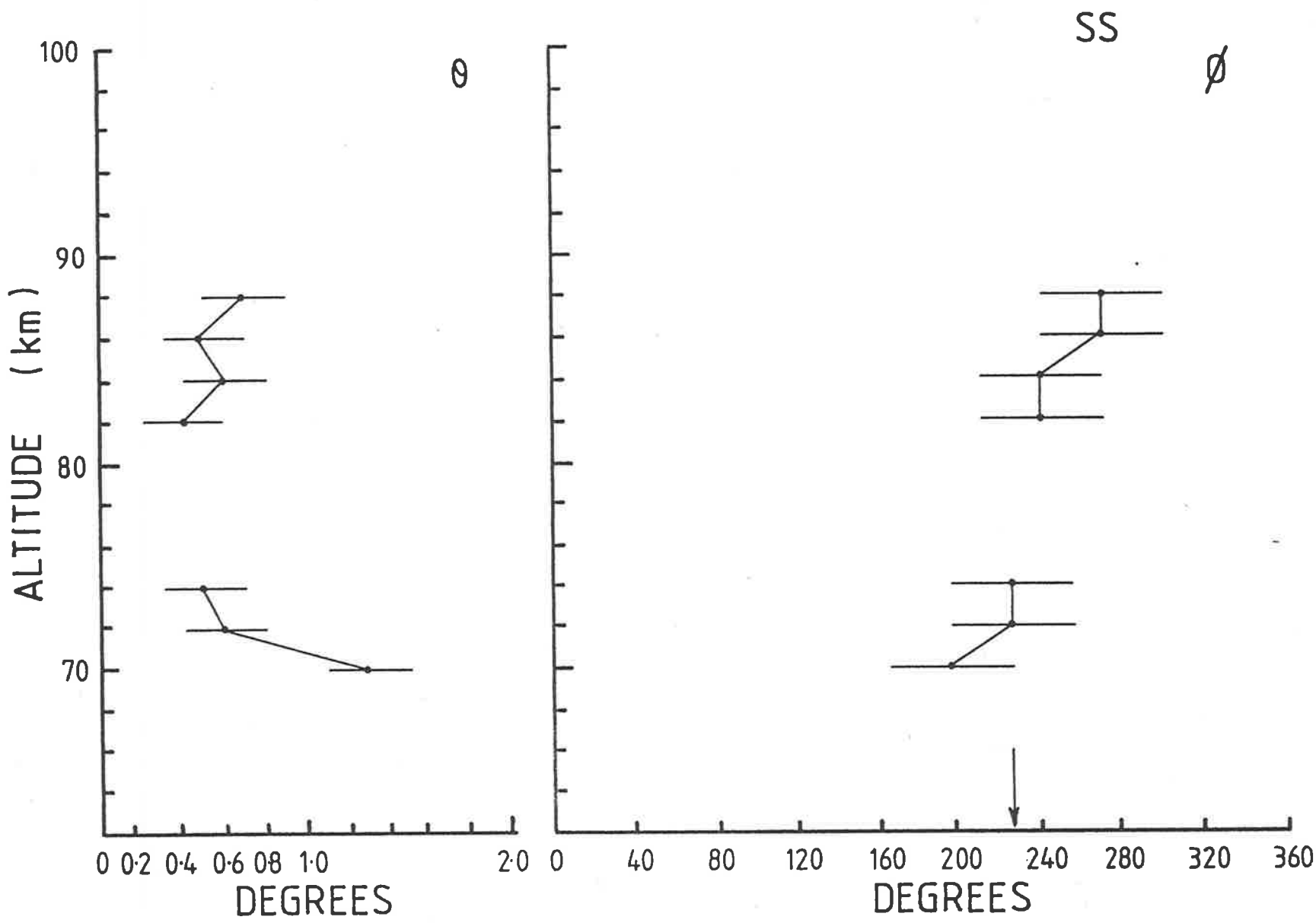

Figure 2-6. a) θ and ϕ values with correlation levels greater than ρ_{95} for SS.

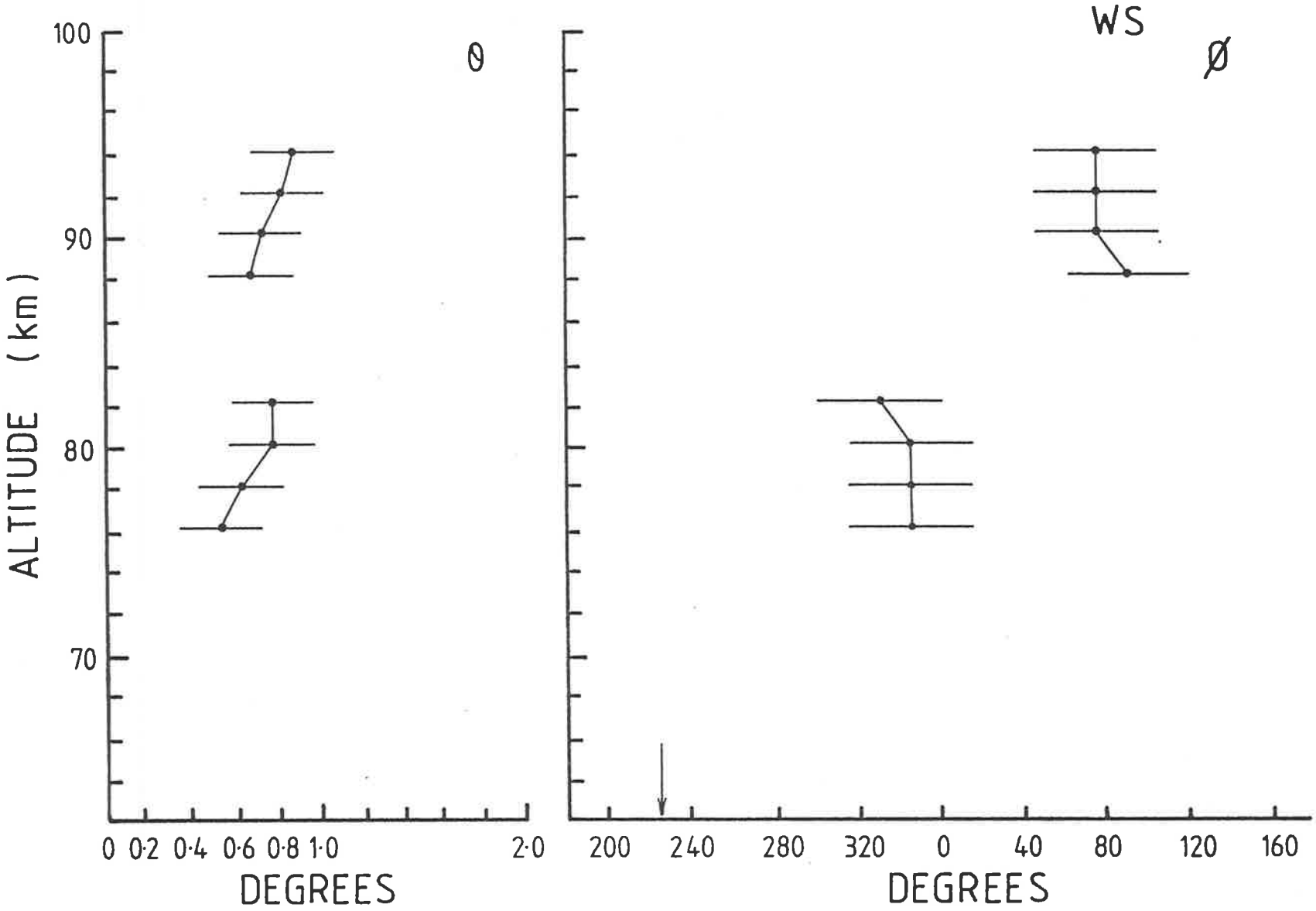

Figure 2-6. b) θ and ϕ values with correlation levels greater than ρ_{95} for WS.

The $\bar{w}_m$ -axis intercept values for the accepted data are presented in Fig 2-7. These values can be used to infer the average vertical velocity over the data period (see Fig 2-2, $\cos\theta \simeq 1$), with the effects of beam tilts removed.

2.1.3 Discussion

Some idea of the beam pointing angle and direction can be obtained by considering the make-up of the BP array itself. A general description of the array is given in appendix 1 so that it is the aspects of the array directly relevant to the pointing angle problem that are presented here.

During construction of the array, it was decided that the dipoles would be suspended at a constant height from the base of the pole. This means that the array level will follow the lie of the land. The array is situated on coastal plane which is flat except for small horizontal and vertical scale undulations. These undulations are not thought to have a systematic effect on the array level. They are considered to cause random fluctuations about the mean level not affecting the pointing direction of the whole array. However, the pointing direction also depends on the images of the dipoles in the array ground plane therefore, this structure must also be considered.

The BP site was surveyed by Reid (1984) and his results are presented in Fig 2-8. (A creek bed passes through the centre top of this diagram affecting the

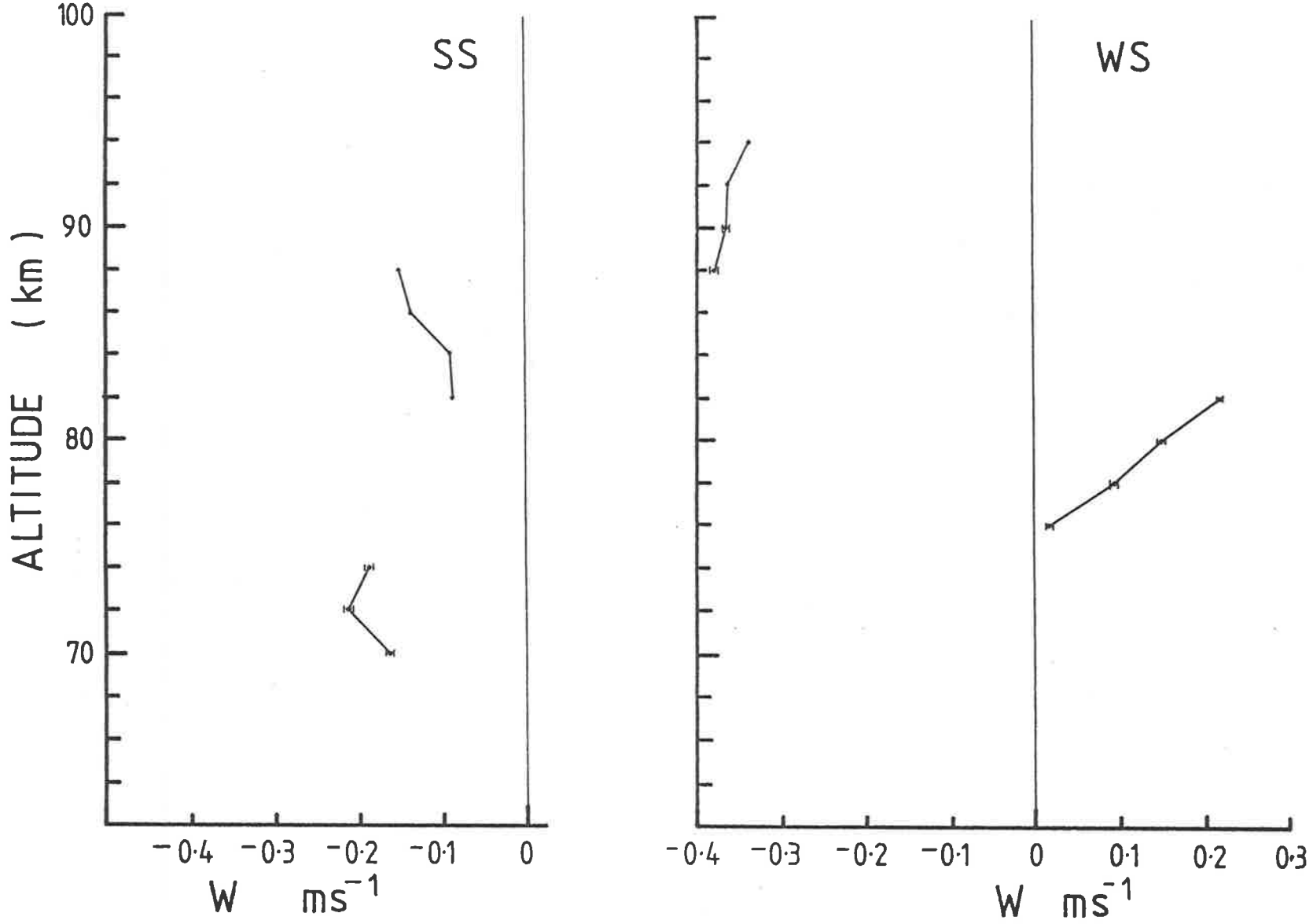

Figure 2-7. Vertical velocities for the SS and WS data from the $\bar{W}_m$ intercept values.

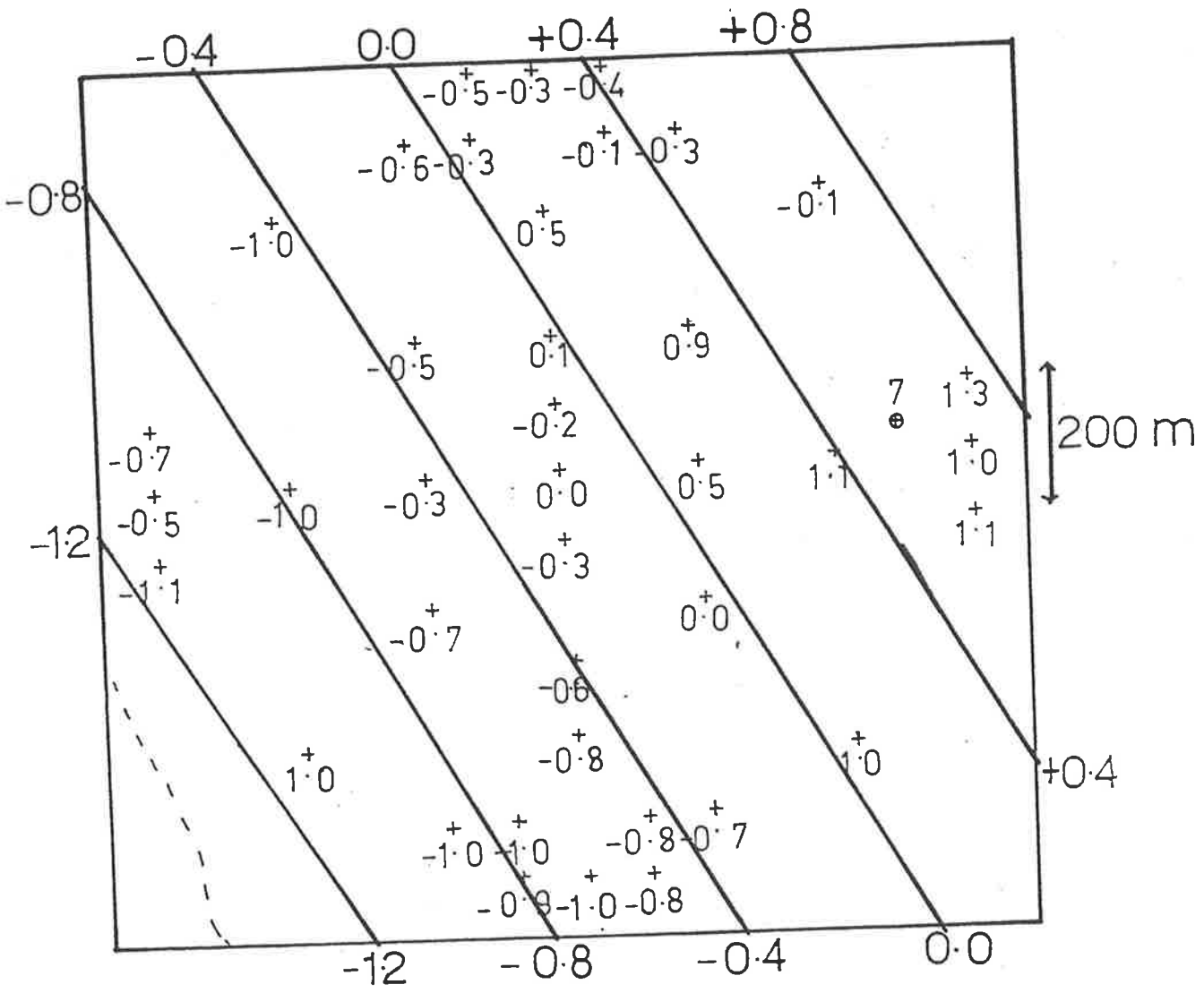

Figure 2-8. Contour plot of the Buckland Park site. Spot heights obtained using a level and staff are represented by a cross. The corresponding height relative to the centre of the array is written next to each. The crossed circle indicates a spot height relative to sea level. The contours represent a plane fitted to all of the spot heights using a multiple regression analysis.
From Reid (1984).

quality of the fit in that region.) Inspection of this diagram suggests that, assuming that the ground plane follows the slope of the ground, the beam will point roughly toward the south-west.

Studies of ground plane characteristics have been carried out by Hocking (1981) and Groves (1983). Hocking used the soil type to calculate a range of reflection coefficients R for the surface of the ground at BP. He suggested that Re(R) was somewhere between -0.6 and -0.9 with Im(R) less than about 0.15. From these it can be seen that $0.62<|R|<0.9$. Hocking also calculated a skin depth of the soil at BP of $\delta \simeq 9$ metres.

The Buckland Park site lies adjacent to salt pans and the sea, and the underground water table is quite salty and thus a good reflector. Groves (1983) found, from reports on two bores on the site, that the water-table never falls below 5-6 metres from the surface as there is a layer of sand and water beginning at this level. However, at times of high rainfall, the site can become quite boggy (Ball, 1981) and the water-table lies at the surface. Inspection of a summer aerial photograph of the area can give a fair indication of the surface geology as there is less vegetation than at other times of the year. The shallow creeks on the site can be seen but no geological formations large enough to appreciably affect the array ground plane are visible. Therefore, we can assume that the water-table is planar.

The orientation of the water-table is less simple to treat. If there is a flow, a pressure head must exist which will slope the water-table's upper surface. It is likely that any flow will be toward the sea so that the upper surface normal will point toward the west. In the case of no flow, the water table will probably follow the lie of the land.

Because the ground conditions will vary with season it is likely the ground plane characteristics will vary between the following two cases:

Dry conditions - A partial reflection occurs at the ground surface ($0.62 < |R| < 0.9$) giving the beam a component toward the south-west (225° clockwise from the north, 0.1° from zenith). However, around 30% of the radiation not reflected at this surface is reflected from the water-table and radiates out again (Hocking, 1981) making a slight westward component (270° clockwise from north) possible.

Wet conditions - The water-table resides at the surface so that the beam points in accordance with the slope of the land (i.e., 225° clockwise from north, 0.1° from zenith).

Because it is expected that the beam will point somewhere around 225° clockwise from north, this direction has been marked by an arrow in Figs 2-4a), b) and c) and Figs 2-6a) and b).

The SS results of Fig 2-6a) show good agreement between the ϕ value predicted and that inferred using this analysis. The θ values, however, do not include (errors withstanding) the predicted value of 0.1°. The WS results (Fig 2-6b)), not only fail to agree with the expected θ, but also fail in ϕ, with a beam pointing direction steady at approximate north for 76-82km and east for 88-94km. The AE period displayed in Fig 2-4b) seems to be "bound" to each of the SS and WS states for part of the height range. In an attempt to ascertain when the transition from SS to WS state occurred, the AE data set was split into pre-AE and post-AE blocks each of six weeks duration. The result was good correlation over most of the lower heights and a pointing direction steady around 225° for the pre-AE data block. The post-AE block, however, was similar to Fig 2-4b) in that the correlation was poor and the pointing direction was swinging from 225° (SW) through 0° (N) to 90° (E).

The six-week block analyses should be treated with care because they contain fewer points and are thus more likely to produce spurious results. However, the high correlation observed in the pre-AE data and the smooth way in which those values vary with height around 225° strongly suggests that it is not until after the autumnal equinox that the beam pointing direction moves from its SS state, viz. south-west - consistent with ground plane considerations, to it's WS state, viz. between north and east.

How, then, can the beam of a fixed broadside array appear to move around the sky? The effects of the water-table previously discussed could move the beam around within the SW quadrant but certainly not to the extent exhibited here.

A clue to what is happening may lie in Fig 2-6b). The inferred ϕ value is significantly different for the two different height ranges. The data producing these results, however, was obtained simultaneously from the same beam. This suggests that the scatterers are changing the effective beam pointing angle. This possibility is now considered.

The effective array polar diagram, and the resulting pointing angle, is determined by the polar diagrams of the transmitter, scatterers and receiving array combined. In this case the transmitter polar diagram is broad (see appendix 1) so that it is the latter two polar diagrams that need to be considered. This is done with the aid of Fig 2-9. The case of isotropic scatter is represented (for two dimensions) in Fig 2-9a). The product of the receiving and scatter polar diagrams gives a result that is largely the same as the original receiving polar diagram. For a more specular reflector at an angle to the horizontal θ_s, the polar diagram is greatly affected (Fig 2-9b)). The effective beam pointing angle in this case is almost wholly determined by the scatterer. Thus if the nature of the scatterers varies with height between these two cases, the effective beam pointing angle will also vary.

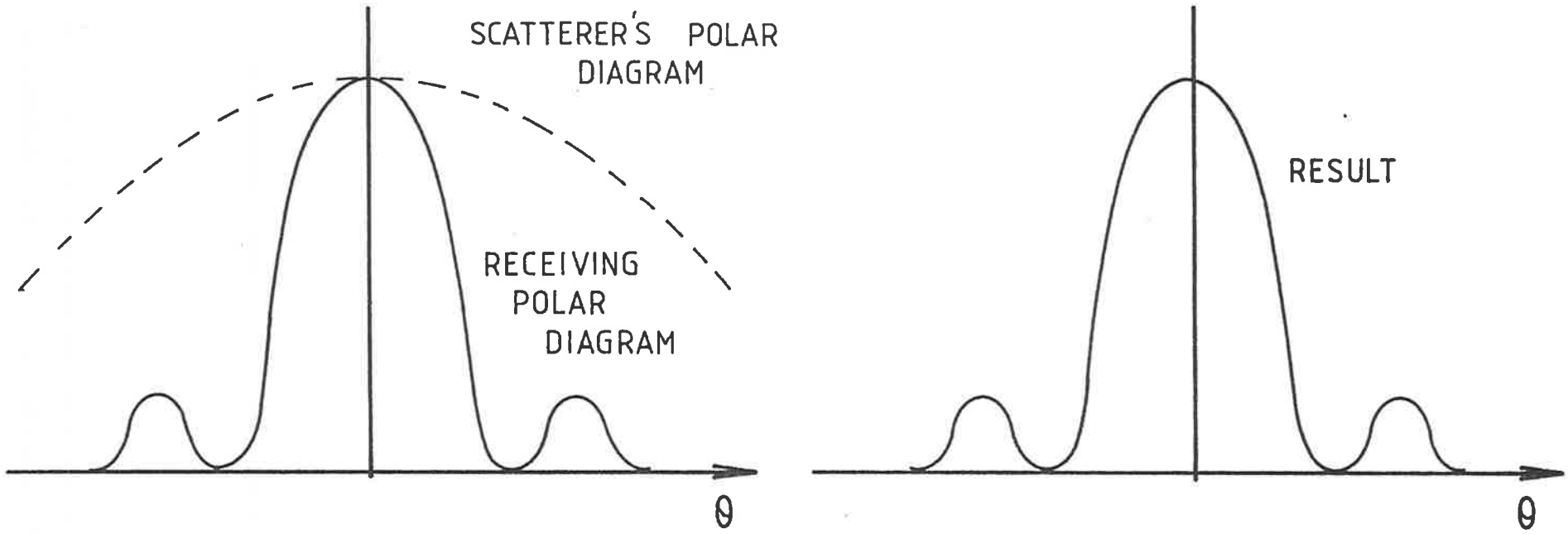

Figure 2-9. a) Resulting effective polar diagram for isotropic scatter.

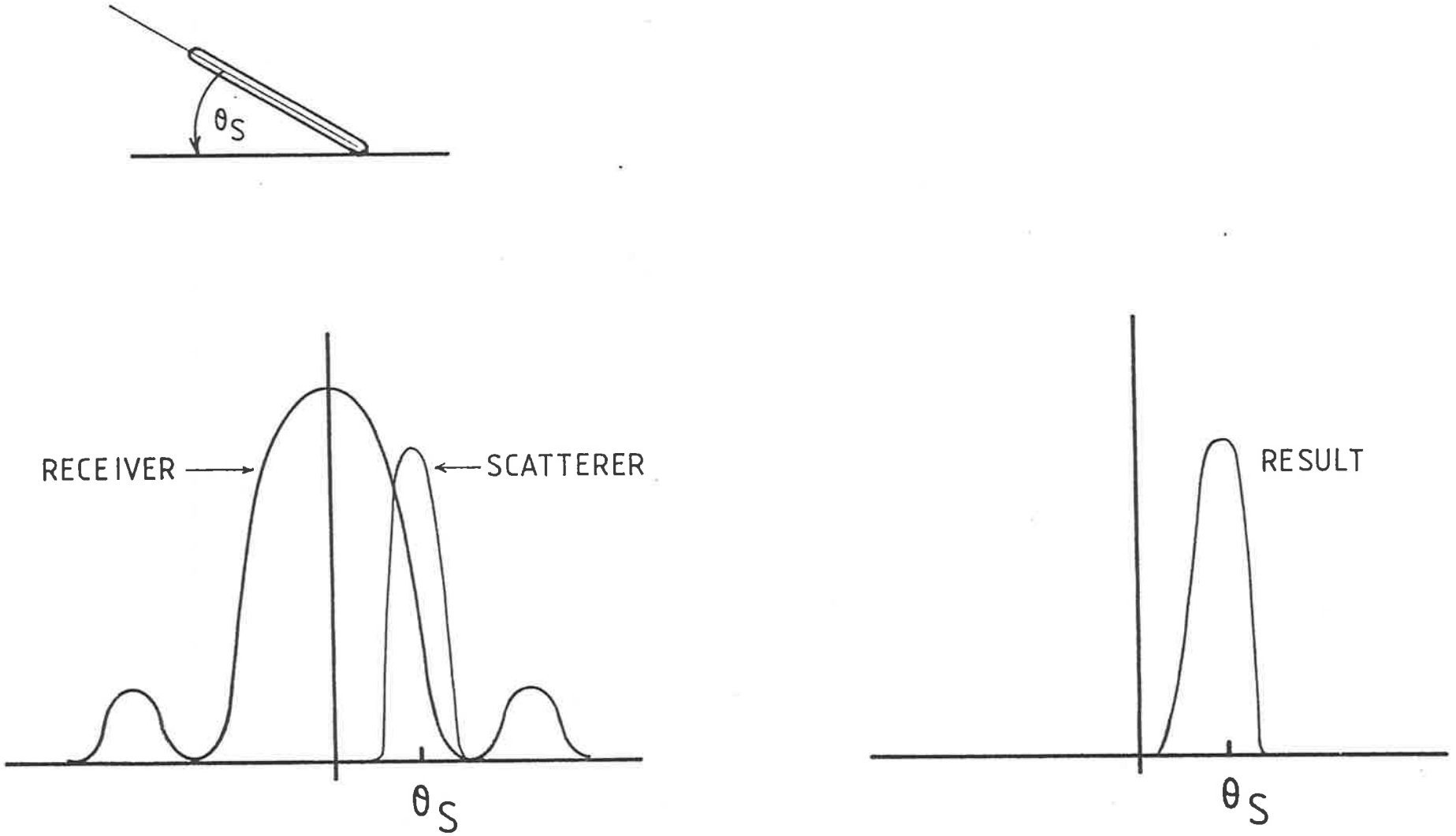

Figure 2-9. b) Resulting effective polar diagram for a specular scatterer.

Unfortunately, neither purely specular nor isotropic scatterers are observed in the real atmosphere. Some atmospheric irregularities scatter over a broad range of angles and are thus termed isotropic. Others scatter over narrow ranges of angles and are called specular but each have some of the characteristics of the other. The mechanisms responsible for these types of irregularities are beyond the scope of this thesis and are not discussed here. It is simply noted that they have been observed in the mesosphere (Hocking and Vincent, 1982; Hocking, 1983). It is important to note, however, that they are probably associated with the breakdown of internal atmospheric gravity waves. This is noteworthy because (as discussed in chapter 1) the phase fronts of gravity waves are rarely aligned horizontally. Thus it is probable that the specular component of the scatter rarely comes from overhead, but instead comes from an angle away from the vertical.

For these characteristics to show up under the analysis of the previous section, they must prevail for most of the data period, here 12 weeks. If this is not the case, the random scatter in the data will reduce the correlation coefficient, possibly to below the significant level ρ_{95}, and the results will be rejected.

These ideas can now be used to suggest possible mechanisms for the results presented in Figs 2-6. The SS results of Fig 2-6a) show values consistent with the lie of the land (as indicated by the arrow). This could be explained by the presence of two layers of isotropic

scatterers throughout the SS season. The shift of the value away from the predicted 0.1° may be due to the specular component of the isotropic scatter. It is not suggested that a preferred θ value exists, just that the average non-horizontal nature of the isotropic scatterers' specular component causes a bias away from the horizontal and the nearby $\theta = 0.1°$ value. The variation of the θ value with height is consistent with this idea. The regions of rejected data between 76 and 80km and above 90km could have been due to varying specularity over the 12 weeks of the data. Inspection of Fig 2-4a) shows that the ϕ value is more variable in this region than in the accepted data regions which agrees with this postulate.

The WS results of 2-6b) are considerably more difficult to justify. As stated previously, the beam angle ϕ has two different values for different heights, neither of which agree with the expected pointing angle. No physical characteristic of the Buckland Park site can be reasonably proposed that would change the beam angle by such an amount. Even if this were possible it could only explain one section of the graph as the beam cannot point both north and east simultaneously. Thus, the scattering properties of the irregularities must be used to explain these phenomena.

The high correlation observed suggests that the mechanism responsible is not highly variable. This property is also exhibited by the smooth variation of both θ and ϕ with height.

Arguments outlined earlier suggest that some form of specular reflection is required to change the beam pointing direction. However, an experiment conducted by Hocking (1979) on day 151 of 1977 (within the season of the WS data) showed that these levels returned significant power from a beam pointed 11.6° off zenith toward the east. This suggests that the scatter is isotropic. If Hocking's short-term study is applicable, then we must assume that the scatter is showing both specular and isotropic characteristics, and the specular properties are affecting the beam direction on a long-term basis.

Analysis of real-time data during the WS season has recently shown (Vincent, private communication) that the polarisation of gravity waves during this season is consistent with waves propagating generally toward the south-west. The phase front alignment for this polarisation would tilt the beam to somewhere in the north-east quadrant, which is consistent with the findings presented here. The summer polarisation is found to be less constant and thus the pointing angle would not be affected.

The possibility of a physical correlation, to explain the WS observations, has also been considered. The beam seems to move to its north and east position after the autumnal equinox, around the time of the onset of planetary wave activity. Could the relationship between horizontal and vertical velocity in these waves be causing this correlation? This possibility was dismissed, however, as the required activity would need to have a period of 7

days (or a multiple thereof) and must stay phase locked from just after the AE to the end of the WS data set to produce these results.

Because the effective pointing angle of the array varies in the way shown here, no particular beam pointing angle can be quoted and used to correct vertical velocities for the effect of horizontal winds, while the current method of real-time analysis is being used. Unfortunately, this method is susceptible to the effects of the specular returns which have the effect of changing the beam pointing direction to one normal to the scatterers' orientation. A method of vertical analysis which attempts to eliminate this effect is discussed in chapter 3 of this thesis.

It is possible, however, to calculate long-term averages (here 12 weeks) of vertical velocity, and these results are presented in Fig 2-7.

Theory predicts small magnitude rising motions in summer and downward motions in winter. However, these characteristics are not exhibited in Fig 2-7 where a downward motion in the summer is inferred at both (accepted) height ranges. The winter velocities are strongly downward at one level and less strongly upward at another level.

The incomplete understanding of the effects responsible for the winter beam characteristics lead to a cautious approach to the winter data but the summer case seems more clear and the summer data cannot be discounted.

It is interesting to note that the SS results are of similar magnitude and have the same seemingly incorrect direction as results presented by Balsley and Riddle (1984) for Poker Flat. Fritts (private communication) has indicated that the latter results may be explained by the presence of a Stokes drift (as in chapter 1). Thus, Fig 2-7 may be taken as further evidence of the existence of this phenomenon.

2.2 Other Effects Causing Apparent Vertical Velocities

In a recent paper by Balsley and Riddle (1984), possible experimental causes of error were considered in relation to VHF measurements made at Poker Flat (Alaska). Those not treated in section 2.1 are now discussed in the context of HF radars.

The effect of mesospheric electric fields was considered and reference was made to a study by Reid (1983) for Poker Flat. The angle between the horizontal, and the magnetic field lines at Adelaide is 60°compared with 77°at Poker Flat. Thus assuming similar electric field characteristics, the magnitude (only) of the effects suggested by Reid can be taken as a fair indication of the situation at Adelaide. The result is that some effect is noticeable in vertical velocities above approximately 75km. To treat the situation at Adelaide fully from this viewpoint, information on the electric field overhead is required. Unfortunately, this information is not available so that this thesis is confined to noting the possibility of this effect. As this mechanism would not be expected to change seasonally, it could not be used to explain the observations presented in section 2.1.

The presence of a horizontal electron density gradient, which would refract the radio wave path, is also considered. This would mean that a beam that pointed vertically at ground level could be bent in such a way that it was not vertical in the mesosphere. Once again,

not enough information is available to treat the problem quantitatively; however, it could only be considered a short-term effect as no mechanism can be proposed to sustain such a gradient on a long-term basis. Thus, although it may be important, it cannot be proposed as a mechanism for the findings given previously.

The apparent ray bending, due to magneto-ionic effects, is not thought to be of consequence because, although the ray path is diverted, the radio "wavefronts" remain horizontal and are just shifted sideways. Thus, the scattered power would not be Doppler shifted by the horizontal wind.

The partial reflections used to obtain Doppler velocities at BP are believed to result from changes in the electron density due to turbulence etc. From this viewpoint, it does not seem likely that a change in total electron density would change anything other than the echo reflection coefficient. Thus, it is not felt that the diurnal change in electron density would cause apparent vertical velocities.

It can be seen that some of the mechanisms mentioned in Balsley and Riddle (1984) may be important at HF. Unfortunately, information on ionospheric characteristics not immediately available is required to treat these problems fully, so they are not taken any further in this thesis.

Summary

Attempts were made to find the beam pointing angle of the Buckland Park HF array by comparing the horizontal and vertical velocities on a long-term basis and searching for a correlation between them.

Correlations were found during the summer and winter solstice seasons but in differing directions. This suggests that it was not the beam alone that determined the effective pointing direction, but the beam and the scatterers combined.

The method for obtaining the vertical velocities used in this analysis is susceptible to bias due to high power specular returns. It is concluded that a characteristic beam pointing angle of the array cannot be used to correct vertical velocities while the current method of analysis is being used.

It should be noted that From and Whitehead (1984, below) employed a technique to find the pointing angle of a HF array using E-region reflections. This method, however, is not suitable for pointing angles close to the zenith.

From, W.R. and Whitehead, J.D.
"The Calibration of an HF Radar used for Ionospheric Research".
RAD. SCI., 19, 423-428. 1984.

CHAPTER 3 : BEAM COMPARISON EXPERIMENT

3. BEAM COMPARISON EXPERIMENT

During June, 1984, the Buckland Park array was diverted from it's real-time winds program to conduct a more specialised task. Part of the analysis of the data collected in this period is presented in this chapter and has been termed the "Beam Comparison Experiment".

It was originally intended that the experiment be used to compare vertical velocities obtained from both wide and narrow beams (hence the name). Operational radars which use the spaced antenna method (Briggs, 1977) to obtain horizontal wind measurements are generally made up of three broad beam receiving arrays. The possibility of using broad beams for vertical velocity measurement instead of large arrays with narrow beams was of key interest because of the size (and cost) advantages involved. Comparisons between oblique and vertical narrow beam measurements of radial velocities were also intended.

As a results of this study, and the work presented in the previous chapter, fundamental questions were raised about the suitability of the analysis method being used. This method is outlined in the first part of this chapter. This is followed by a possible alternative in the light of the earlier results.

3.1 Experimental Configuration and Preparation

The layout of the BP HF receiving array is shown in Fig A1-2 (Appendix 1). Each of the 89 crosses shown represents a pair of half wave dipole antennas, one aligned north-south and one east-west. Each of these dipoles is connected to one of two patch boards situated in the main receiving hut. This means that two superimposed arrays are available for the reception of circularly polarised signals, as the alignment of the dipoles is unimportant for this type of radio wave.

The way in which the patch boards were configured is shown in Fig 3-1. The left-hand board (consisting of dipoles aligned north-south) provided three groups of four dipoles arranged in such a way as to be suitable for spaced antenna drift analysis. The right-hand board (of dipoles aligned east-west) was connected firstly into parallel rows and then split with power splitters. One set of power splitters was then connected together to give a nominally vertical beam. The second set of power splitters was arranged to produce an 11.6° off vertical eastward pointing beam by the inclusion of suitable lengths of cable between successive antenna rows. The value of angle, 11.6° was that determined by Hocking (1981) to be optimal as the first zero of the whole array polar diagram points upward.

During the second half of the experiment, the vertical beam of the right-hand board was phased to point at 11.6° off vertical towards the west whilst maintaining

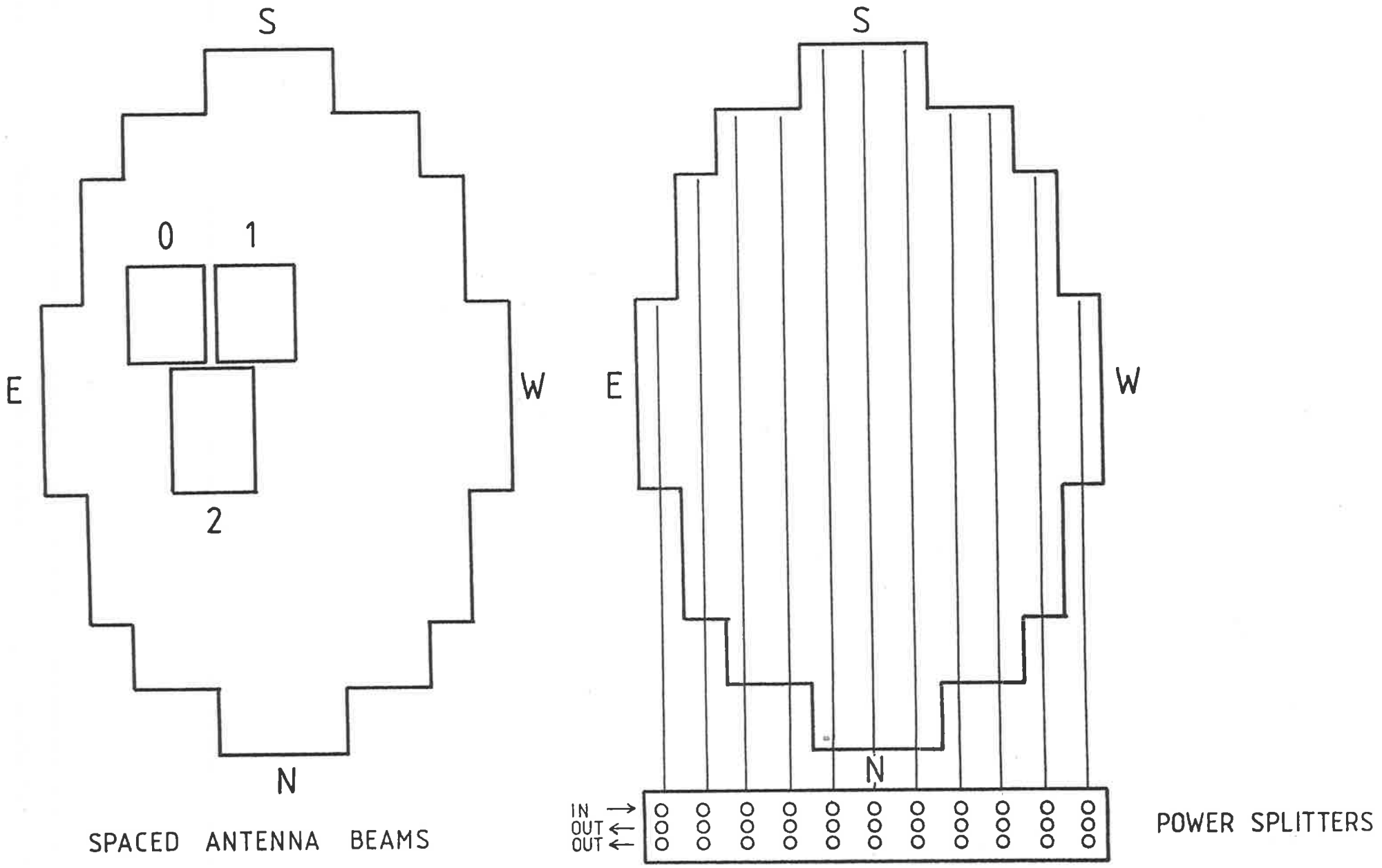

Figure 3-1. Patchboard configurations for the Beam Comparison Experiment.

the eastward beam. This was done to enable momentum flux measurements of the kind made by Vincent and Reid (1983).

The experiment lasted in total 17 days with the first part of the experiment running from 13:44 31/5/84 to 12:48 9/6/84 followed by the dual beam part from 14:50 9/6/84 to 11:06 17/6/84. These configurations and times are summarised in Fig 3-2.

Preparation for the experiment began with a check of the impedance of the array elements via the patch board sockets. In this way, faulty antennas could be identified and repaired. While the array was being configured as described, care was taken to ensure that

- good contact was made between patch board sockets and the connecting bars, and on subsequent connections to the receivers.

- connecting bars were correctly tuned to match their input lines.

- phasing cables used to tilt the narrow beam were included in the correct order.

The five receivers to be used were checked for excessive noise and the gains set to be approximately equal.

The real-time wind analysis program was used to ensure that the off vertical beam was actually pointing in the direction supposed in both parts of the experiment. This was done by comparing in sign and approximate magnit-

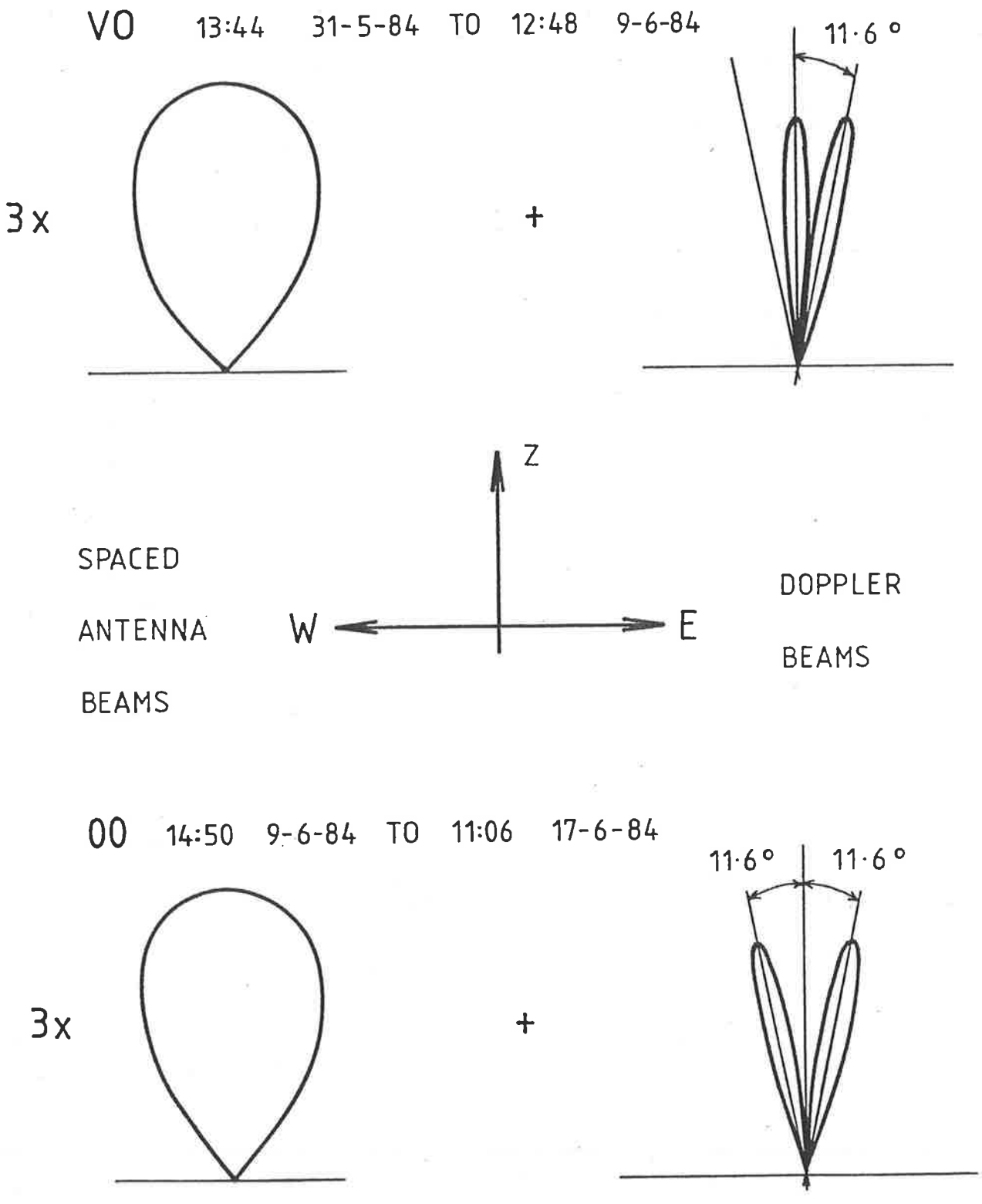

Figure 3-2. Configurations and times for the Beam Comparison Experiment.

ude Doppler inferred radial velocities from the tilted beam(s) with the horizontal velocities from the real-time spaced antenna winds analysis.

For the duration of the experiment, data were recorded every two minutes for ten heights each 2km apart within one of the sets of height ranges listed below. The mode or polarisation of transmission is also given.

0700-1700 LT : 60-78 then 80-98km using 0-mode transmission (i.e., all consecutive points at one height are 4 min apart).

1700-0700 LT : 70-88 then 80-98km using X-mode transmission (i.e., consecutive points 4 min apart 70-78 and 90-98km, 2 min apart 80-88km).

3.2. Analysis of Data Using the Phase of the Autocorrelation Function to Find Radial Velocities

Data collected during the experiment were stored on magnetic tape and later analysed to ascertain the horizontal and radial wind velocities. Analysis was carried out on the University of Adelaide's Cyber 173 mainframe computer. The horizontal wind velocities were found using the standard method of spaced antenna drift analysis (Briggs, 1977; Ball, 1981). These are sometimes used for comparison, but it is the radial velocities that are the subject of this thesis. A description of the method of analysis now follows. The computer programs used for the early analysis were developed by Reid (1984). The principles involved are best presented by assuming continuous functions and this is done here. The details of the equivalent discrete methods used in the computation by Reid are presented in the aforementioned work.

As outlined in appendix 1, Gaussian shaped pulses are transmitted at a central frequency $\omega_t = 2\pi \times 1.98$ MHz. This pulse may be expressed as

$$E(t) = E_t(t)\, e^{i\omega_t t}$$

where E_t is the amplitude of the transmitted signal and $i = \sqrt{-1}$. Refractive index fluctuations cause scattering of the wave and the backscattered component returns to the ground. Scattering theory predicts that in order for appreciable backscatter to occur, disturbances must have a scale, along the line of sight, of half the radar wave-

length (Bragg scatter). Therefore, the radar is most sensitive to disturbances of scale 75m.

The signal measured at the ground can be expressed as

$$E(t) = E_o(t)\, e^{i\omega t}$$

representing the received signal a fixed time after the transmitter pulse. This corresponds to returns from a volume of the atmosphere whose vertical scale is determined by the transmitted pulse length and horizontal scale by the receiving array polar diagram. If a scatterer within this volume is in motion, with a component of velocity V along the line of sight, the frequency ω will be Doppler shifted from ω_t thus

$$\omega = \omega_t + \omega_d = \omega_t + \frac{2V\omega_t}{c}$$

where c is the speed of light. In practice, the complex sampling of the signal has the effect of shifting the ω_t frequency component of the returned signal to zero so that any Doppler shift is away from zero frequency.

Random motions and the bulk motion of the atmosphere result in a spectrum of ω made up of contributions from the many scatterers within the sampling volume. If we compute the power spectrum $S(\omega)$ of the returned complex signal, we may use it to find the Doppler shift and thus the average velocity of the atmosphere passing through the sampling volume.

Rastogi and Woodman (1974) note that if the atmosphere is stationary, the power spectrum $S_s(\omega)$ is

positive and symmetric around zero. If the Fourier transform of this is computed to give the autocorrelation function $\rho_s(\tau)$ (by the Weiner Kintchine or autocorrelation theorem, see e.g., Bracewell, 1978) it will be real and even. A mean motion through the radar beam acts to shift this spectrum away from zero frequency, introducing a phase term thus

$$\rho(\tau) = \rho_s(\tau) \; e^{i\phi(\tau)}$$

Given that the first moment (or mean) of the power spectrum is ω_d viz.,

$$\omega_d = \int \omega \, S(\omega) \, d\omega$$

(Rastogi and Woodman, 1974) a well known Fourier theorem relating the jth order moment to the jth order derivative may be used to show

$$\omega_d = \frac{1}{i} \frac{\rho'(0)}{\rho(0)}$$

where the prime denotes differentiation with respect to τ. In combination with our expression for $\rho(\tau)$ this gives

$$\omega_d = \phi'(0)$$

that is the Doppler shift is equal to the slope of the phase of the autocorrelation function at zero lag. This can be calculated in a computationally efficient way by noting $\phi(0) = 0$ by definition and

$$\phi'(0) = \frac{\phi(\tau) - \phi(0)}{\tau} = \frac{\phi(\tau)}{\tau}$$

for a small value of τ.

This theoretical development embodies two related but separate assumptions. They are ...

1/ The unshifted (stationary atmosphere) power spectrum is symmetric around zero or equivalently the shifted power spectrum is symmetric about ω_d .

2/ The mean of the power spectrum (or 1st moment) is a measure of the average motion through the sampling volume.

If the assumption 1/ is satisfied then 2/ is acceptable, but in the real atmosphere the power spectrum is not always symmetric. Woodman and Guillen (1974) state that failure of assumption 1/ introduces an error of the order of τ^3 in the estimate of $\phi'(0)$, and by their more general formulation, show that the above theoretical arguments are still valid.

The validity of the second, almost fundamental assumption seems intuitively obvious but is questioned in the light of the results of this experiment. This should be kept in mind but further discussion of this point is deferred to section 3.3.

A typical power spectrum is shown in Fig 3-3. Its main features are the Gaussian shaped background and the presence of spectral spikes with amplitudes much greater than the Gaussian profile. Some characteristics of these power spectra make then unsuitable for the above analysis method. Thus it is necessary to introduce some rejection criteria into the operational procedure.

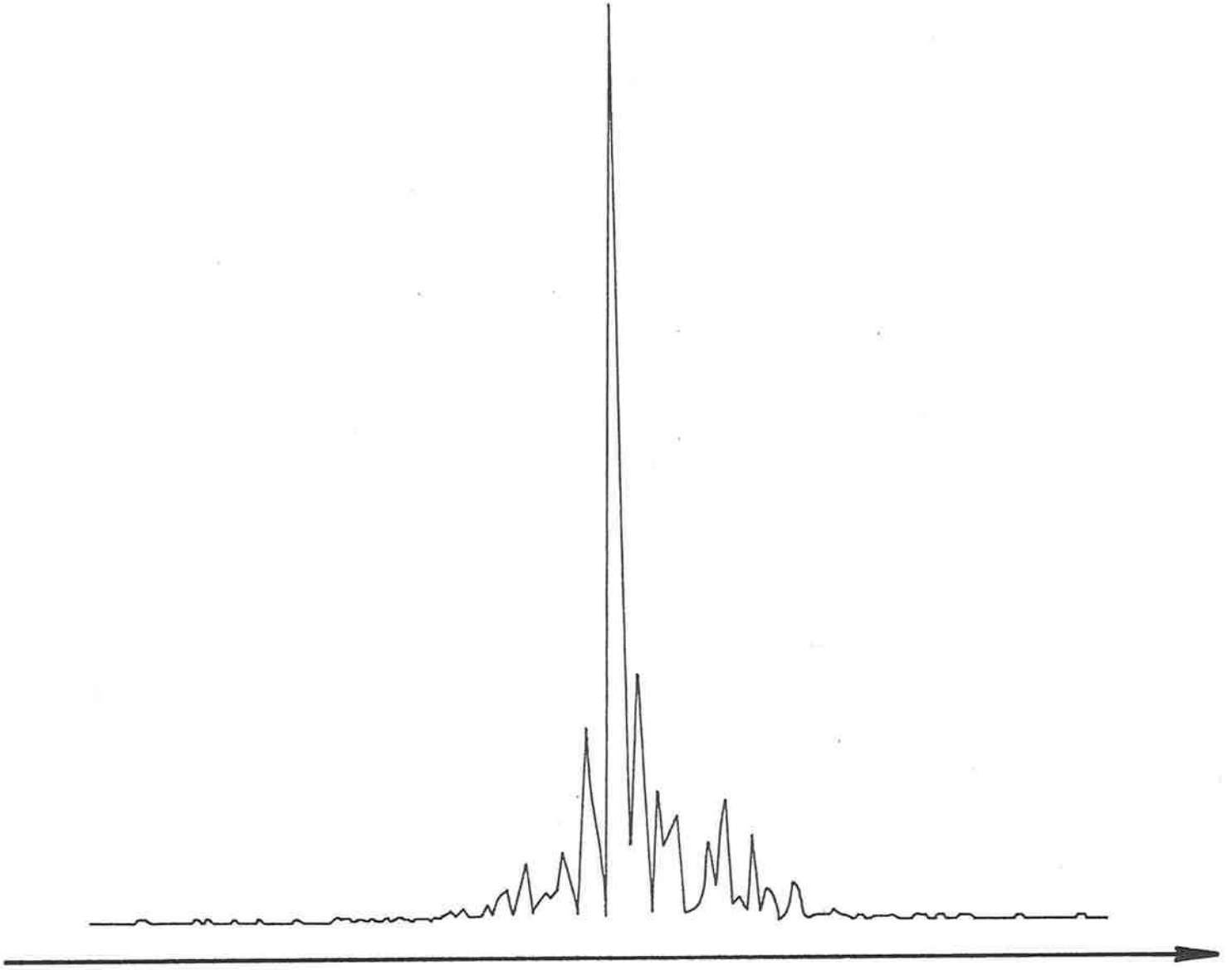

Figure 3-3. A typical power spectrum.

As it was the analysis programs of Reid (1984) that were used for this part of the experiment, it is his rejection criteria that are now described. Firstly, the data were checked to ensure that the signal levels did not correspond to saturation or noise for a significant part of the data collection period. The signal to noise ratio was calculated (see Rastogi and Woodman, 1974) and tested but, most importantly, the autocorrelation function was inspected for irregular behaviour. It was found that, on occasions, the phase of the autocorrelation function was oscillatory and thus gave spurious results. The slope at zero lag was no longer an indication of the actual slope and the results were rejected. The cause of this has been shown (Rastogi and Bowhill, 1976; Hocking, 1981) to be the beating of two or more specular components of the power spectrum. The extent of the beating depends on the number, relative powers and separation of the spikes. For example, two well separated spikes of similar amplitudes cause the ACF to oscillate considerably and result in rejection. In contrast, four or five similar spikes do not produce much oscillation of phase and will be accepted. The presence of one specular "spike" however, does not generally result in a rejection.

Using these principles, the beam comparison experiment data was analysed to find ω_d and thus V using

$$\omega_d = \frac{2V}{c} \omega_t$$

as mentioned before. The results of this analysis are now presented.

3.2.1 Results

The beam comparison experiment consisted of two configurations as stated in section 3.1 and summarised in Fig 3-2. The vertical velocities of the vertical, off-vertical (VO) part of the experiment are presented in Fig 3-4. The phase of the ACF analysis was used on two of the three wide beams as well as the narrow beams. Only the wide beam and vertical narrow beam results are presented in this figure.

It should be noted that, although data is presented over the height range 60-98km, only above approximately 80km is there data for 24 hours a day. Below this height, night-time ionospheric conditions are not suitable for consistent echo returns. This is illustrated by the computer output of Fig 3-5. Therefore, care must be taken in interpreting the absolute values below this height as only half the semi-diurnal tide is being sampled.

It is possible to obtain a vertical velocity from the dual beam (00) configuration of the second part of the experiment. The radial velocities in each beam contain information on the horizontal and vertical velocities given the off-vertical angle. For radial velocities V_E and V_W from the eastward and westward pointing beams, respectively, and assuming that a radial velocity toward the array is negative it can be shown that the vertical velocity w and the horizontal velocity u are

$$w = \frac{V_E + V_W}{2 \cos \theta}$$

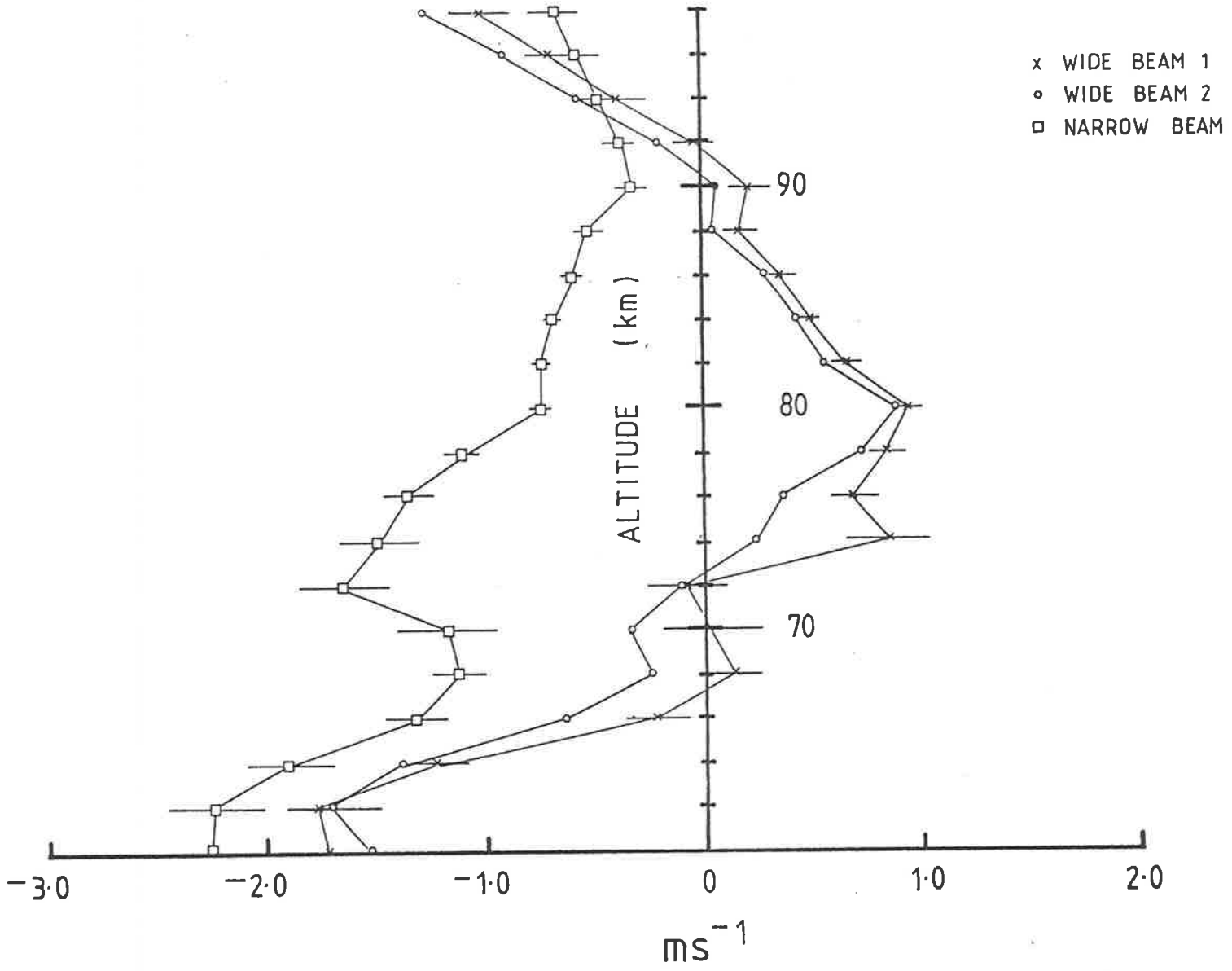

Figure 3-4. Wide and narrow beam vertical velocities.

DAY	TIME HOUR	ALTITUDE (KM) 60	62	64	66	68	70	72	74	76	78	80	82	84	86	88	90	92	94	96	98
160	1130																				
160	1200																				
160	1230	-39	-30	-16	-9	-9	-12	-16	-19	-23	-22	-9	-3	-4	-5	-6	-17	-30	-21	-22	-27
160	1300	-16	-16	-16	-19	-18	-14	-10	-11	-21	-26	1	-5	-6	-7	-7	-8	-6	-9	-18	-15
160	1330	-16	-19	-17	-10	-11	-13	-16	-20	-10	-7	-3	-2	-3	-4	-6	-10	-18	-11	-3	-3
160	1400	-13	-21	-11	-8	-5	-3	0	0	-15	-16	-6	-1	0	0	-3	-8	-29	-48	-19	-9
160	1430	-21	-21	-12	-8	-9	-9	-8	-10	-18	-16	-11	-7	-5	-6	-7	-5	3	2	-6	-4
160	1500	-8	-12	-11	-14	-14	-14	-11	-9	-12	-12	-3	-2	-8	-12	-9	-10	0	2	2	3
160	1530	-33	-29	-12	-6	-3	-7	-11	-10	-9	-6	-3	-7	-9	-9	-6	-11	3	3	3	5
160	1600	-11	-12	-11			-6	-7	-22	-34	-37	-19	-7	5	7	7	5	4	-2	-4	-4
160	1630	-23	-30	-18	-16		-9			-20	-31			6	5	3	6	32	38	17	14
160	1700	-2	-3	-15	-17	-14	-11	-16	-7	-11	-21	-18	-13	-12	-11	-10	-7	-2	58	28	-20
160	1730								0	0	-19	-6	-1	-2	-1	-2	-4	-1	-6	-8	-17
160	1800									-36	-29	-15	-1	0	0	0	-7	-9	-11	-11	-10
160	1830									-56	-25	-9	1	7	-3	-9	-3	-13	-23	-32	-42
160	1900									-49	-33	-11	-3	-2	0	-7	-10	-6	-5	-9	-17
160	1930										-19	-15	-13	2	-7	-14		-11	12	-2	8
160	2000									13	3	-6	-19	-13	1	25				13	6
160	2030									10	-2	-13	-16	-15	-5	-3	3	4	2	2	2
160	2100										-37	-2	-5	-3	-1	6	11	-11	8	6	8
160	2130											-33	-22	-18	0	5	10	8	10	8	-11
160	2200											-26	-9	-9	-10	-4	0	0	-2	-2	-11
160	2230											-11	-10	-9	-8	2	15	6	0	-14	-24
160	2300											-24	-9	-18	-16	-4	8	8	7	10	10
160	2330											11	11	-11	-14	-17	-24	-22	-8	-3	17
161	0000											-20	-15	-17	-24	5	9	22	40	58	58
161	0030											-10	-4	-8	-9	-4	-6	-8	-5	10	44
161	0100											2	-6	-2	-1	-6	-8	-9	-7	3	22
161	0130											3	-3	-2	-3	-3	0	-1	-5	-8	-8
161	0200											-16	-3	-2	-3	-2	0	2	2	6	13
161	0230											2	-13	-2	-4	-1	3	2	2	5	0
161	0300											8	6	-7	-1	3	10	13	8	4	8
161	0330										-1	-15	-13	-11	-4	1	1	1	-4	-15	-27
161	0400											-16	-7	-2	1	3	-1	-12	-19	-15	-7
161	0430										-26	-18	-17	-7	-3	-1	-2	2	20	35	21
161	0500										-22	-30	-27	-17	-2	3	0	-2	5	4	-1
161	0530										-32	-6	-6	-4	-2	1	11	18	29	8	-1
161	0600										-14	-16	-24	-22	-17	-13	-16	-11	-2	6	
161	0630									-32	-14	-12	-8	-2	0	2	5	17	11	-11	-2
161	0700			-27							1	13	-16	-17	-17	-16	-12	0	14	21	18
161	0730	-16	-13	-13	-18	-18	-1	-5			-31	-15	-7	-5	-13	-14	-4	0	-1	0	3
161	0800	-25	-28	-28	-22	-15	-14	9	1	-37	-41	-44	-34	-20	-13	-13	-20	-38	-18	-6	-5
161	0830	-21	-25	-14	-7	-3	-2	0	-11	-28	-28		-30	-8	-6	1	-3	-7	-13	-13	-10
161	0900	-25	-26	-18	-6	8	-2	3	0	-12	-17		-24	-18	-5	-6	-2	0	5	2	-1
161	0930	-21	-23	-12		-14	-10	-8	-11	-20	-34		-15	-5	-4	-8	-7	-5	0	5	12
161	1000	-4	-7	-7	-5	-5	-7	-17	-27	-30	-33		-7	-4	-8	-9	4	6	7	12	18
161	1030	-22	-27	-15	-6	-9	-4	-10	-21	-28	-22	46	0	0	8	12				0	0
161	1100	-18	-15	-13	-12	-9	-5	-8	-5	-5	-8			-4	-5	-13	-18	-17	-14	-13	-17
161	1130	-21	-17	-15	-10	-2	2	4	0	-4	-4		1	4	12	7	5	4	7	14	12
161	1200	-5	-9	-13	-3	6	11	10	6	0	1	2	1	-12	-22	-23	-22	-16	0	8	10
161	1230	1	-9	-9	-6	-3	-2	-3	-7	-14	-22		-14	-18	-14	-9	-5	-4	0	0	
161	1300																				
161	1330																				
161	1400																				

Figure 3-5. Computer output showing data acceptance.

$$u = \frac{V_E - V_W}{2 \sin \theta}$$

where θ is the angle from the vertical toward both the east and west at which the beam is pointing. The array is configured such that θ is 11.6°. However, the effective value is found to differ from 11.6° and this point will be discussed shortly. For now it is sufficient to assume $\cos \theta \simeq 1$ (as $\cos(11.6^\circ) = 0.983$). The vertical velocity values obtained in this way are presented in Fig 3-6 as well as vertical velocities from the two available wide beams.

Average horizontal velocities for the duration of the 00 part of the experiment are presented in Fig 3-7. These spaced antenna drift results can be used to find the effective value of θ, θ_{eff} for which the oblique beams give results consistent with the spaced antenna velocities. Already included in the figure is the velocity u (from the above relation) assuming that the beam is pointing at 11.6°. It is obvious that this value is not correct and the values required to match up the velocities are presented in table 3-1.

Table 3-1

Height (km)	for an 11.6° tilted beam
60	6.0°
70	6.4°
80	5.4°
90	5.3°

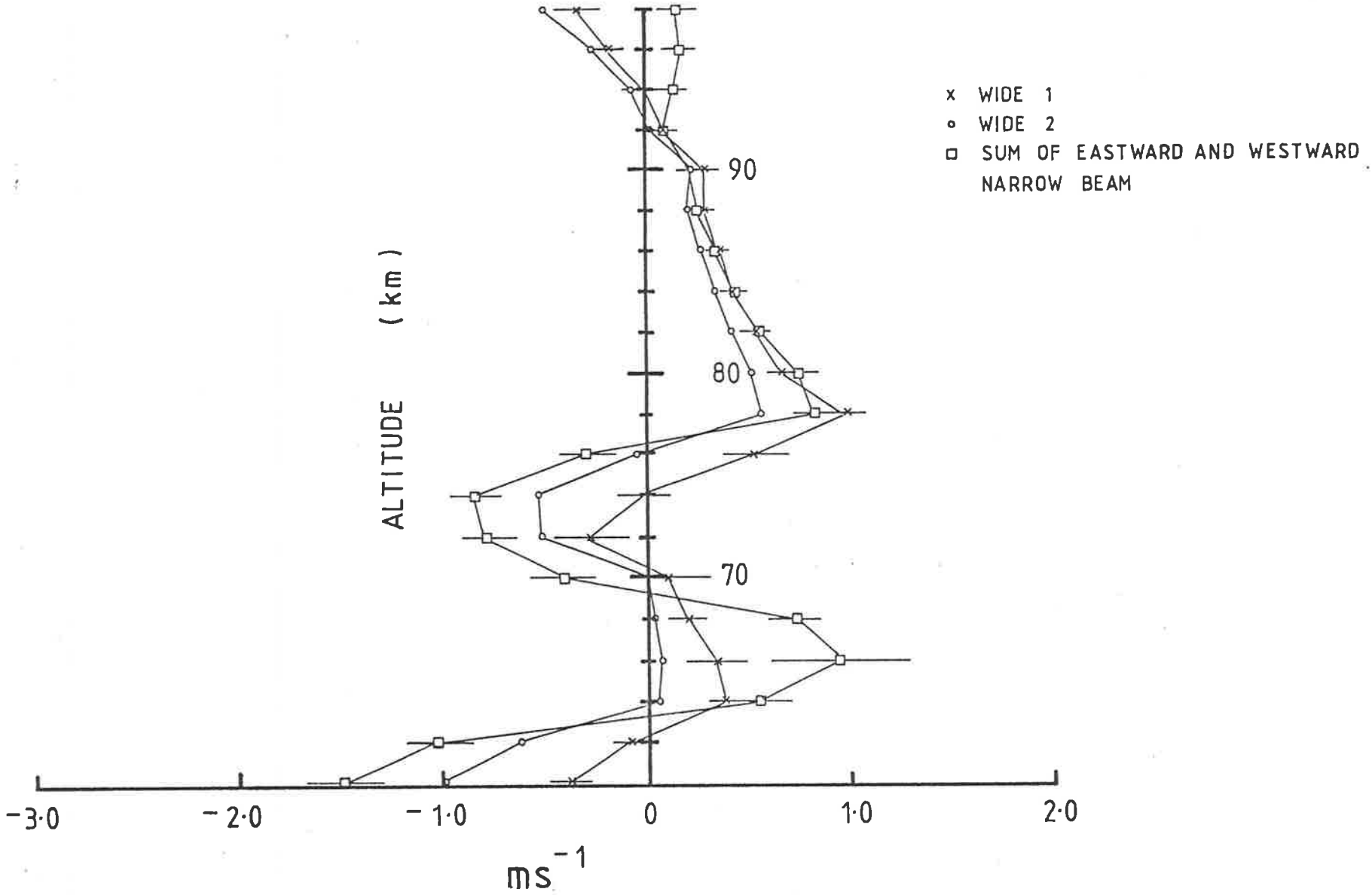

Figure 3-6. Wide beam and oblique beam vertical velocities.

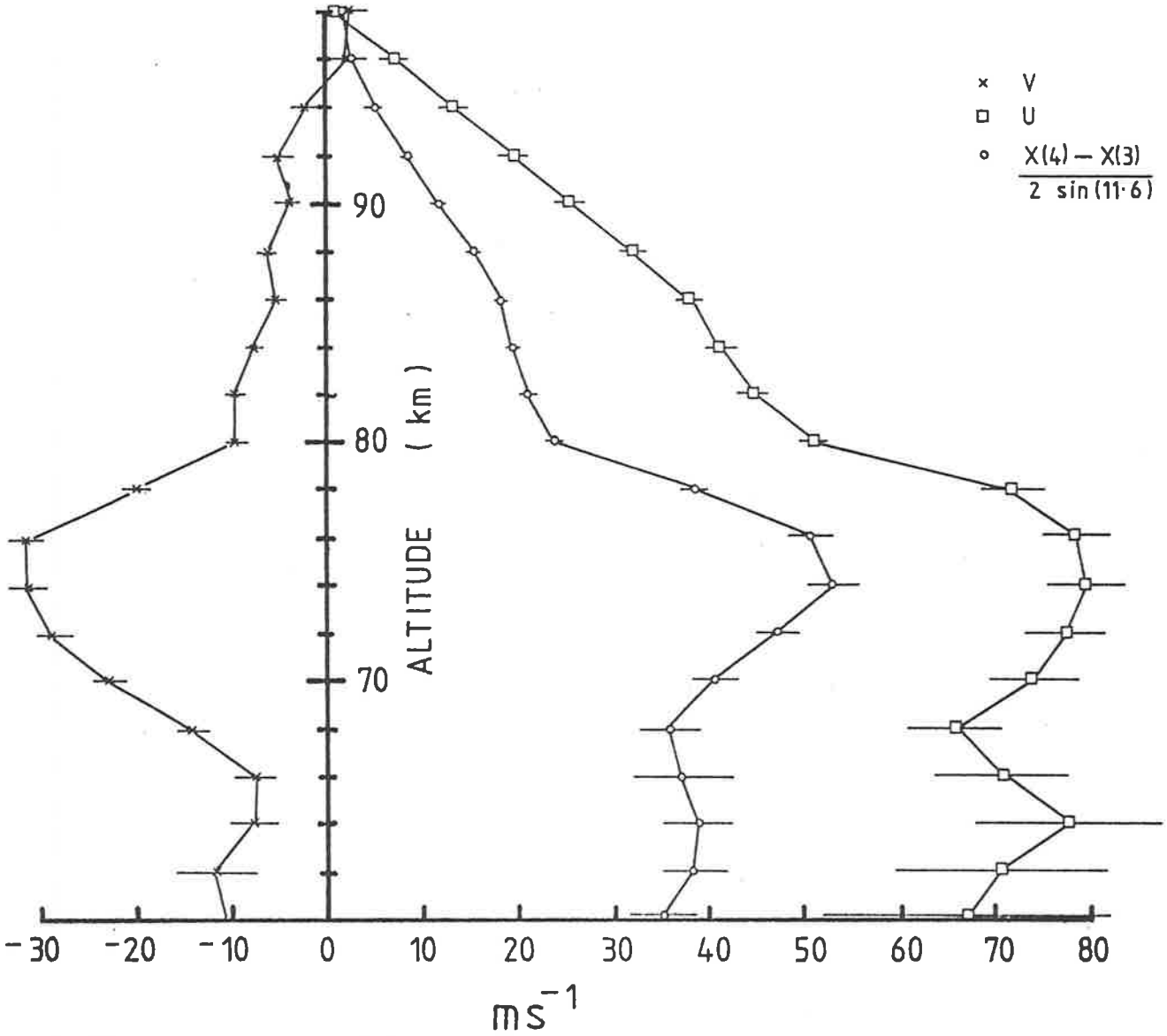

Figure 3-7. Horizontal velocities using the spaced antenna method and the oblique beams.

Because the value of θ is uncertain, all the off vertical beam results are plotted next to their range value, as compared to height from the ground. This is not considered to be a problem because, by inspection of Figs 3-5, 3-6 the features of the vertical beams do not lag the features of the oblique beams in height.

The error bars shown in Figs 3-4, 3-6 and 3-7 correspond to the error in the mean for each value. Where two wide beams are plotted, only one carries error bars as the magnitudes of the errors were similar for both. Thus, in the interest of picture clarity, one set of error bars has been omitted.

3.2.2 Discussion

Vertical velocities obtained using the method of section 3.2 and a narrow receiving beam are presented, along with equivalent wide beam results, in Fig 3-4. A wide beam can be considered to have the sampling volume of a narrow beam with extensions in a spherical shell outwards from the zenith. If we consider the atmosphere in motion through the wide beam sampling volume, then it would be expected that the power spectrum for the wide beam would be broader than that for the narrow beam, due to the returns from larger angles which have greater line of sight velocities. This broadening, however, should not affect the mean Doppler shift and thus the inferred vertical velocity. Therefore, the results of Fig 3-4, which show significant differences between the wide and narrow beams are difficult to reconcile.

With two possible velocities, it must now be considered which, if any, is correct. As an aid to answering this question it is of interest to know if any particular section of the sampling volume is contributing more to the velocity determination. This can be done by considering the sum of the velocities obtained from two oppositely pointing beams as described in the previous section. It can be seen from Fig 3-6 that there is a very good agreement between velocities found in this manner and those from the true wide beam. This suggests that most of the information contributing to the wide beam velocities is coming from angles away from the vertical. (It seems to be of no consequence that only an eastward and a westward sector of the wide beam sampling volume is used in this comparison.)

It is possible to find the effective pointing angle for a beam that is pointing nominally at 11.6° off-vertical, as stated previously, and the results were presented in table 3-1. These showed an effective pointing angle of 5 or 6 degrees for the height range of the data. Therefore, there must exist a mechanism which gives increased weight to the signals arriving from closer to overhead, thus forcing the effective pointing angle toward the vertical.

To gain an understanding of why the wide and narrow beam velocities differ, we must consider the parameters that vary in the two analyses. All the data were obtained simultaneously using reflections from the same transmitter

pulse. The electronics and data processing may vary slightly but as the two wide beams give similar answers, this is not considered important. In fact, the only difference between the two systems is the polar diagram of the receiving array being used. Thus, the differences must be due to different weightings given to signals coming in from different angles.

At this stage, nothing can be said about the scatterers other than they have characteristics that fall into two main categories (see chapter 2). The first, isotropic, refers to scatter than extends over a broad range of angles. The second category, known as specular reflection, returns signals only over a narrow range of angles.

If the receiving polar diagram is symmetric about the beam pointing angle, a steady flow of isotropic scatterers through the beam will produce the same value for the vertical velocity, irrespective of the beam width. This is because extra power spectrum contributions on the approaching side due to a broader beam will be compensated for by an equal and opposite contribution on the exit side of the beam. Thus, if the scatter is purely isotropic, there will be no difference in velocities inferred from a wide and a narrow beam, even if the ground plane is slightly tilted. (Although if the ground plane is tilted, the velocity will be incorrect.) This leaves only specular reflectors to blame, and these must now be investigated.

These thin specular reflecting layers produce high power spikes in the power spectrum of the returned signal

(Rottger, 1981; Hocking, 1983). One example of this is the power spectrum of fig 3-3 obtained during this experiment. How, then, do these "specular spikes" influence the velocity measurements?

The bulk properties of power spectra obtained from wide and narrow beams are reproduced in fig 3-8. The position of the spike in reality depends on atmospheric conditions and is positioned such as to illustrate the issues here. It is also important to note that this spike is not affected by the array polar diagram. Note also that we assume that there is only one spectral spike. It is accepted that some spike distributions will cause rejection of the data in accordance with the rejection criteria of section 3.2.

It can be seen that the Gaussian background profile of the wide beam contains more power than that of the narrow beam. We assume the spectral spikes contain the same power. How, then, will this affect the Doppler shift ...

$$\omega_d = \int \omega \; S(\omega) \; d\omega \qquad ?$$

In the narrow beam case, the spectral spike contains a large percentage of the total spectral power. Therefore, ω_d will be biased toward the spectral spike value ω_s. The wide beam, however, has more power in its Gaussian background profile and will be less affected by the presence of the spike. Thus ω_d will be closer to ω_o (see fig 3-8).

Similar arguments can be used to investigate the possible case where the specular layers are tilted and the

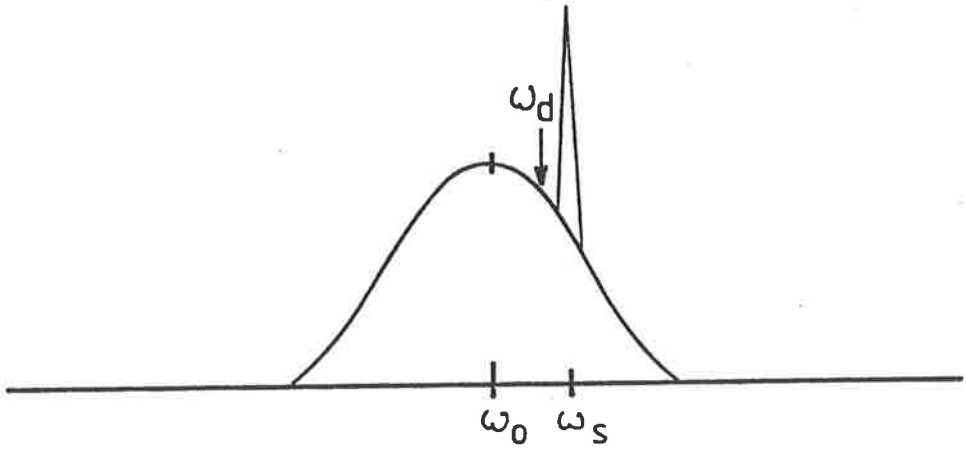

NARROW

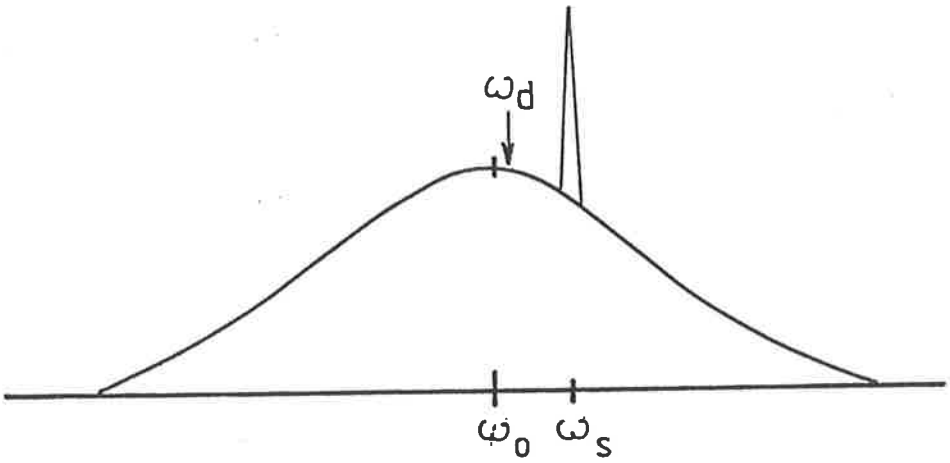

WIDE

Figure 3-8. The effect of spike rejection on ω_d

spike power is affected by the polar diagram. This case is represented by fig 3-9 where ω_o, ω_d and ω_s are as defined previously. The narrow beam, by virtue of its polar diagram, reduces the power contained within the spike at ω_s .This is not so for the wide beam, and the result is a different ω_d value (and hence velocity) for the wide beam.

One important difference between these two examples is that in the fig 3-8 case, the spike has little effect on the wide beam velocity whereas, in the fig 3-9 case, it is the narow beam that is not greatly affected.

Given this interpretation of what is occurring, which velocity do we take as a measure of the true vertical velocity? To answer this it is necessary to know whether it is the spectral spike velocity (from ω_s) or the velocity from ω_o that is of importance. The mechanisms responsible for the Gaussian background are reasonably simple (e.g., Briggs and Vincent, 1973) but this is not so for specular layers. These are now considered.

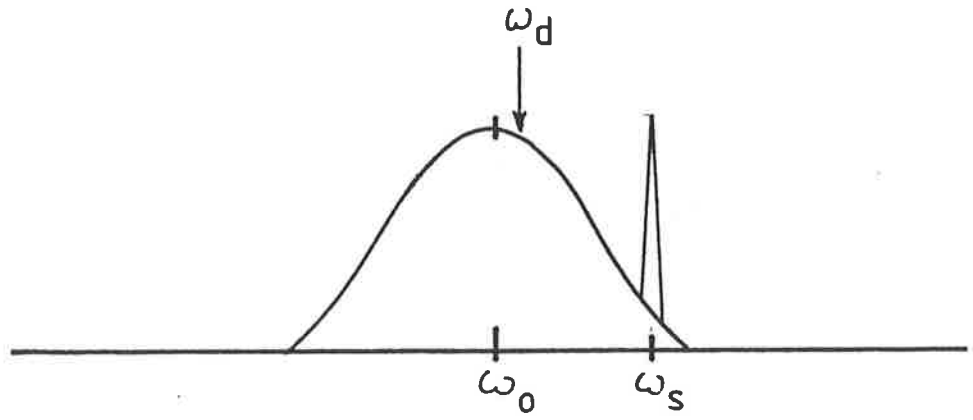

NARROW

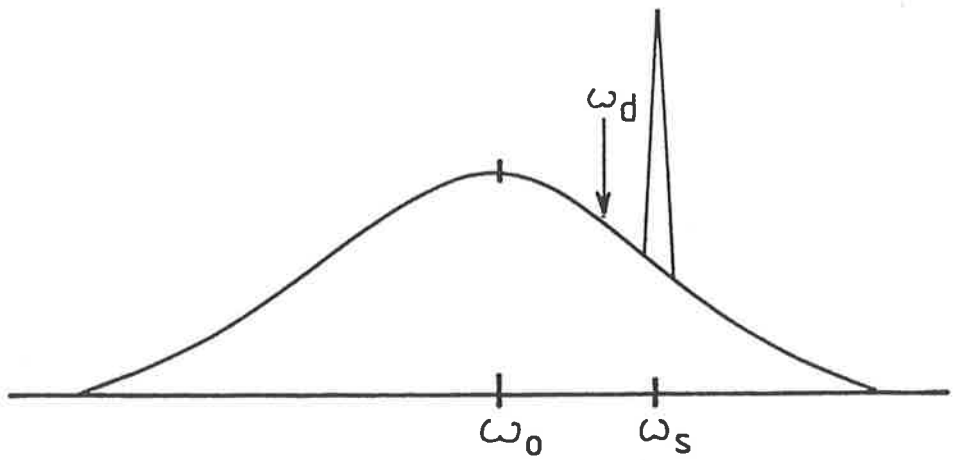

WIDE

Figure 3-9. The effect of spike rejection on ω_d .
(Spike power affected by polar diagram)

3.3. The Effect of Specular Layers on Velocity Measurement

Although specular layers may have an effect on the results obtained from an oblique beam, the following discussion will be restricted to the effects seen by a nominally vertical beam.

Of prime importance to this discussion is the orientation of the scattering layer. If the layers were aligned horizontally, the analysis of chapter 2 would have yielded pointing angles either vertical or consistent with the lie of the land. The spectral spikes described earlier would be representative of the bulk motion of the atmosphere and no difference would be observed between the wide and narrow beam results as seen in fig 3-4. (This will become more obvious through the ensuing discussion.) Thus, it would be of interest to consider specular layers that are tilted. As noted in chapter 2, the probable association with gravity wave activity would suggest that they be generally anything but horizontal. In a stratified atmosphere, however, it is unlikely that this tilt be too great but data from chapter 2 suggest tilts of around 0.5° and only a small angle is required to produce a large effect as shall now be demonstrated.

Consider a tilted specular layer moving with a general velocity $\underline{v}$. Without loss of generality, it can be assumed that motion occurs in the x-z plane, i.e., the y component of velocity is zero. The following vectors and co-ordinates are of importance.

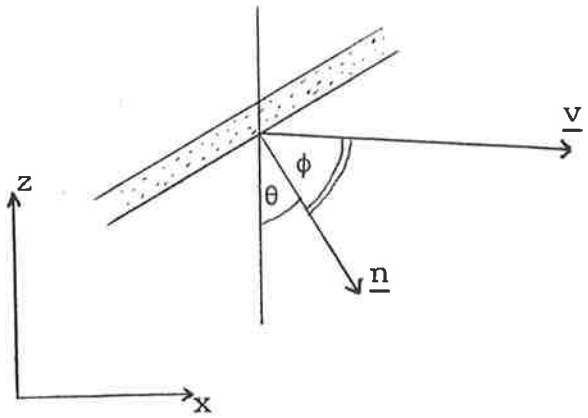

where $\underline{n}$ is the unit normal vector. The vectors $\underline{v}$ and $\underline{n}$ can then be expressed in terms of the following components:

$$\underline{v} = (v \sin(\theta+\phi),\ 0,\ -v\cos(\theta+\phi))$$

$$\underline{n} = (\sin\theta,\ 0,\ -\cos\theta)$$

Due to the specularity, radar returns will only be seen along the normal $\underline{n}$ (assuming that the transmitter and receiver are close together). Therefore, only the line of sight velocity along the normal need be considered. This velocity, v_{LOS} is

$$v_{LOS} = \underline{v}.\underline{n}$$

$$= v\sin(\theta+\phi)\ \sin\theta + v\cos(\theta+\phi)\ \cos\theta$$

where v is the modulus of $\underline{v}$. If the layer is in motion perpendicular to its orientation, $\phi=0$ and $v_{LOS} = v$ as expected. Similarly, if the layer is horizontal, $v_{LOS} = v\cos\phi$ and the true vertical component of motion results.

Of importance, however, is the case of a tilted layer moving horizontally. In this situation, $\theta+\phi = 90°$ and the expression for v_{LOS} reduces to

$$v_{LOS} = v\sin\theta \quad .$$

That is, a layer with no vertical velocity component, by virtue of the fact that it is tilted produces what could easily be interpreted as a vertical motion.

The above formulation only considers one arbitrary "point" on the specular layer. As the layer moves through the sampling volume, the reflection "point" moves along the scatterer. Thus the layer returns a signal for a finite period of time, a signal that will be Doppler shifted due to the horizontal motion, and of greater power than the isotropic returns. This will appear in the returned signal power spectrum as a spike, as seen in Fig 3-3.

It is interesting to note that the expression

$$v_{LOS} = v \sin \theta$$

is the same as that used in chapter 2 to treat the case of isotropic scatterers in motion through a beam tilted at an angle θ. It was stated there that a value of θ as small as 0.1° could have a considerable effect on the vertical velocity determination. The same is applicable here.

The effect would not be serious if the specular layers had random orientations. These contaminations could then be averaged out. However, in the light of the results of chapter 2, and the possible assocation of these layers with gravity waves, this is not likely. The stratospheric filtering discussed in chapter 1 will leave a gravity wave field with an assymetric phase speed distribution and thus a preferred orientation within the background flow. Even

if these layers are not associated with gravity waves, no explanation other than tilted specular reflectors can be proposed to explain the differences between the wide and narrow beam velocities of section 3.2.1, and as these results represent an average, the tilting cannot be purely random.

If the arguments presented are valid, then the spectral spikes seen in the returned signal power spectra should be ignored. If this is not done assumption 1/ and, more importantly, assumption 2/ of section 3.2. is no longer satisfied. The mean of the power spectrum is no longer a measure of the average motion through the sampling volume.

From a physical point of view it seems an extremely simple solution to ignore the parts of the spectrum that can tilt the beam i.e. the specular spikes, and use only the spectral information from the isotropic scatter, which does not significantly affect the beam.

We must, therefore, consider ways of removing the specular spikes from the analysis.

3.3.1 Possible methods of specular spike rejection

The most obvious way of removing the effects of tilted specular layers from vertical velocity determination is to use narrow radar beams. The "narrow" beam of the Buckland Park array is really quite wide from this point of view (half width half maximum 4.5°). An array of half width half maximum of θ_w will be sensitive to specular

layer tilts up to approximately θ_w. Thus an array would require an extremely narrow beam to remove specular effects in this way.

The possibility of removing the specular spikes from the power spectrum during analysis has been studied by Hocking (private communication). This differs from the ACF analysis of section 3.2 in that the power spectrum is computed explicitly and inspected for specular spikes. These are then removed and a Gaussian profile is fitted to the remaining data. The peak of this profile is then taken as the Doppler shift and a velocity is inferred from this.

It would be equivalent, and possibly more computationally efficient, to remove the spikes and Fourier transform back into the ACF domain. The slope of the phase method could then be used as described in section 3.2. This, however, has not yet been attempted and can only be stated as a proposal. Similarly, the optimal criteria for spike rejection have not yet been investigated. The criteria currently in use seem acceptable by physical inspection of the spectra, but further "tuning" of this may be required.

Hocking's analysis as it stands has been applied to a short (approximately 24 hours) segment of the Beam Comparison Experiment data. These results are presented in Fig 3-10 and will be briefly discussed.

The height range over which this comparison was made was limited by the results available from the spike rejection analysis. This is simply because the method has only

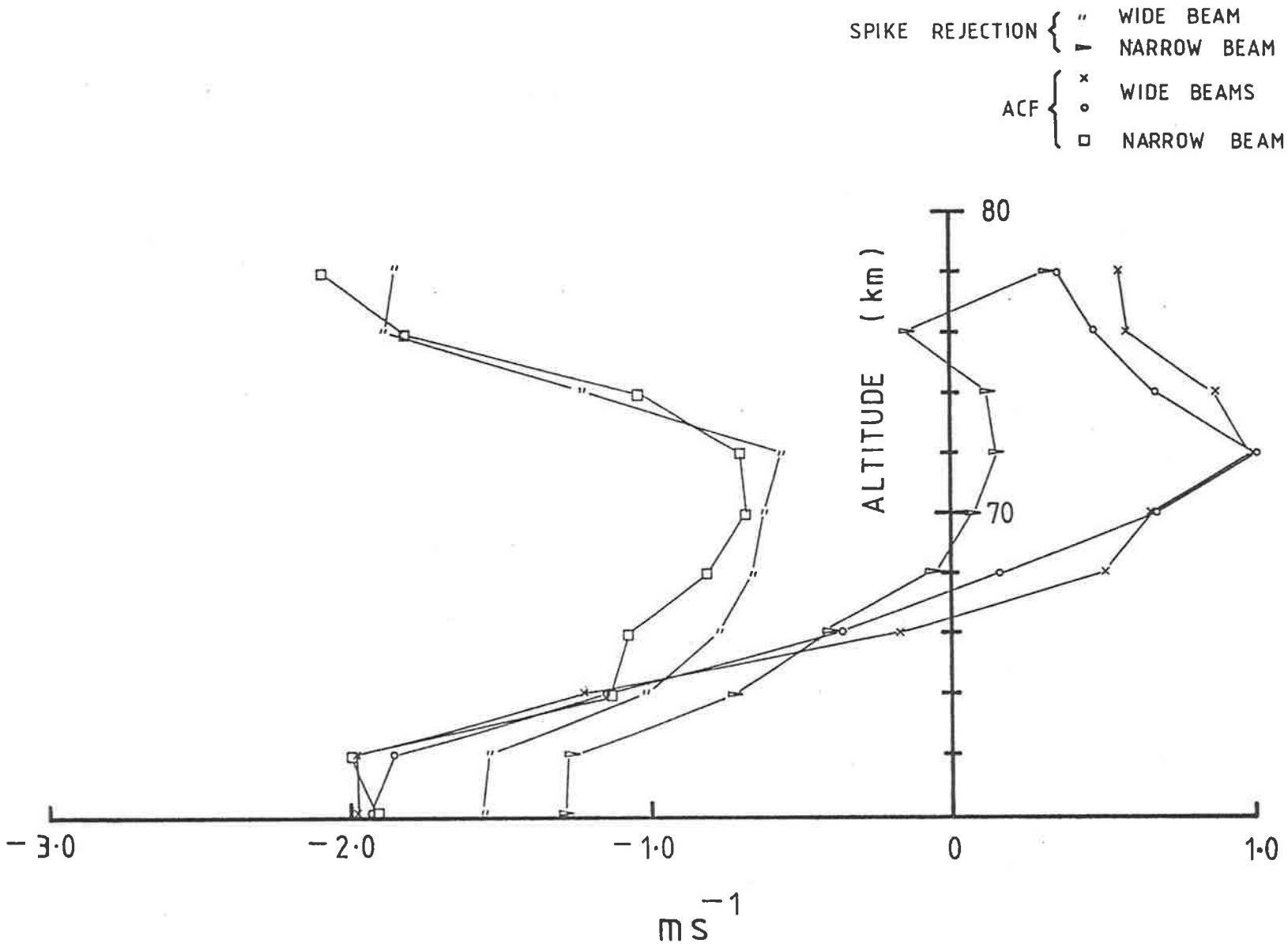

Figure 3-10. Comparison of spike rejection and ACF results.

recently been developed and has not yet been applied to other parts of the height domain. It can be seen in Fig 3-10 that the spike rejection technique has had a considerable effect on the wide beam velocity results, but has made little difference to the narrow beam results. By removing the spike, ω_d moves to ω_o, and this change is much greater for the wide beam. This suggests that something similar to that described in Fig 3-9 is occurring, even though Fig 3-9 is an ideal case. It is not suggested that the real atmosphere produces such "classic" spectra, just that a broad resemblance to Fig 3-9 is prevalent.

This result, and the mere fact that spike rejection changes the inferred velocity, leads to the following suggestions about specular reflectors, between approximately 60 and 78km ...

1/ They are generally tilted.

2/ Their tilts are, on average, of the order of the beam width of 4.5°.

Although some of these suggestions may be difficult to accept it is undeniable that spike rejection is an analysis method that warrants consideration.

Summary

In this chapter, the ACF method of inferring vertical velocities (Rastogi and Woodman, 1974) was described as part of the analysis of the Beam Comparison Experiment. The findings of this experiment could not be explained if it was assumed that specular reflectors were generally horizontal. Instead it was necessary to assume that they were tilted (probably associated with gravity waves) in a preferred direction, and were thus biasing the ACF analysis results.

The possibility of removing these contaminating effects was discussed and a method to do this, developed by Hocking (private communication), was used to obtain some preliminary results. These did in fact differ from the previous results in a manner suggestive of specular layers tilted to appreciable angles.

CHAPTER 4 : SUMMARY AND RECOMMENDATIONS FOR FUTURE WORK

4. SUMMARY AND RECOMMENDATIONS FOR FUTURE WORK

The work presented in this thesis pertains to the measurement of vertical velocities in the height range 60-100km, which encompasses the mesosphere and lower thermosphere. However, the emphasis was on ascertaining the validity of current methods of vertical velocity measurement in the light of contradictions between expected theoretical and experimentally determined values.

The first chapter set a theoretical background for the kinematics and energetics of the mesosphere region. It was found that momentum transport by internal gravity waves (Hines, 1960; Lindzen, 1981) was of great importance in this region. The possibility that the interpretation of vertical velocities may be erroneous was also discussed.

Chapter 2 decribed a method used in an attempt to find the pointing direction of the Buckland Park HF receiving array. This used statistical methods to search for a correlation between horizontal and vertical velocities. This correlation could then be used to find the parameters of what was considered to be the most likely cause of error, a beam that is tilted off vertical.

It was found, however, that for much of the year, either no significant correlation occurred or the correlation suggested a pointing direction that could not be explained by possible ground plane and, hence, beam tilts.

It was thus assumed that it was the ionospheric scatterers that were determining the pointing angle. This was further supported by the results of a study of ACF analysis carried out in chapter 3.

An experiment to investigate possible receiver beam configurations for vertical velocity measurement was carried out and was presented in chapter 3. Here it was found that the "slope of the phase of the autocorrelation function" method of Rastogi and Woodman (1974) was susceptible to contamination by tilted specular layers and the presence of these tilted layers must be accepted to explain the results of the experiment. A possible method of overcoming this problem has also been proposed by Hocking (private communication) and was outlined. Some preliminary results were also presented.

As is obvious from this summary, the nature of, and mechanisms responsible for, the radar backscatter were of considerable importance to the vertical velocities that were measured. Discussions of their effect on the vertical velocities were limited to speculation because of a lack of direct observations. If more work is to be carried out in vertical velocity determination, then a study of the scatterers, and such parameters as the angle of arrival and the relative strengths of isotropic and specular scatter, is recommended as a high priority.

The angle of arrival be studied using the BP HF array. By sampling the returned signal at various groups of antennas, beam swinging can be simulated and angular

spectra of the returned power can be computed. The same signals could also be summed to allow vertical velocity measurement, and a comparison could be made with the known angles of arrival.

BIBLIOGRAPHICAL ABBREVIATIONS

Q.J. Roy. Met. Soc.	–	Quarterly Journal of the Royal Meteorological Society
J.A.S.	–	Journal of the Atmospheric Sciences
J.A.T.P.	–	Journal of Atmospheric and Terrestrial Physics
J.G.R.	–	Journal of Geophysical Research
J. Fluid. Mech.	–	Journal of Fluid Mechanics
Can. J. Phys.	–	Canadian Journal of Physics
J. Meteor. Soc. Japan	–	Journal of the Meteorological Society of Japan
Rad. Sci.	–	Radio Science
Rev. Geophys., Space Phys.	–	Review of Geophysics and Space Physics

BIBLIOGRAPHY

Apruzese, J., Schoeberl, M. and Strobel, D. (1982) Parameterisation of I.R. Cooling in a Middle Atmosphere Dynamics Model. 1. Effects on the Zonally Averaged Circulation. J.G.R. 87, 11 pp.8951-8966.

Ball, S.M. (1981) Upper Atmosphere Tides and Gravity Waves at Mid- and Low-Latitudes. PhD Thesis, University of Adelaide, Adelaide, Australia.

Balsley, B.B., Ecklund, W.L. and Fritts, D.C. (1983) V.H.F. Echoes from the High Latitude Mesosphere and Lower Thermosphere: Observations and Interpretations. J.A.S. 40, pp.2451-2466.

Balsey, B.B. and Riddle, A.C. (1984) Monthly Mean Values of the Mesospheric Wind Field Over Poker Flat, Alaska, and a Proposed Polar Circulation Cell. Submitted to J.A.S.

Bender, C.M. and Orszag, S.A. (1978) Advanced Mathematical Methods for Scientists and Engineers. McGraw-Hill, N.Y., p.593.

Booker, J.R. and Bretherton, F.P. (1967) The Critical Layer for Internal Gravity Waves in a Shear Flow. J. Fluid. Mech. 27, pp.513-539.

Bracewell, R.N. (1978) The Fourier Transform and its Applications. 2nd Ed. McGraw-Hill, Kogakusha.

Bretherton, F.P. (1966) The Propagation of Internal Gravity Waves in a Shear Flow. Q.J. Roy. Met. Soc. 92, pp.466-480.

Briggs, B.H. (1977) The Analysis of Moving Patterns by Correlation Methods. Departmental Report ADP148, Department of Physics, University of Adelaide, Adelaide.

Briggs, B.H., Elford, W.G., Felgate, D.G., Golley, M.G., Rossiter, D.E. and Smith, J.W. (1969) Buckland Park Aerial Array. Nature 223, Sept. 27, pp.1321-1325.

Briggs, B.H. and Vincent, R.A. (1973) Some Theoretical Considerations on Remote Probing of Weakly Scattering Irregularities. Aust. J. Phys. 26, pp.805-814.

Cunnold, D., Alyea, F., Phillips, N. and Prinn, R. (1975) A Three Dimensional Dynamical-Chemical Model of Atmospheric Ozone. J.A.S. 32, 170-194.

Dickinson, R. (1973) A Method of Parameterisation for Infrared Cooling Between Altitudes of 30 and 70km. J.G.R. 78, pp.4451-4457.

Dunkerton, T.J. (1981) Wave Transience in a Compressible Atmosphere, Part I: Transient Internal Wave, Mean-Flow Interaction. J.A.S. 38, pp.281-297.

Dunkerton, T.J. (1982) Wave Transience in a Compressible Atmosphere, Part III: The Saturation of Internal Waves in the Mesosphere. J.A.S. 39, pp.1042-1051.

Eliassen, A. and Palm, E. (1960) On the Transfer of Energy in Stationary Mountain Waves. Geofysike Publikasjoner Geophysica Norvegica 22, pp.1-23.

Ference, M., Stroud, W.G., Walsh, J.R. and Weisner, A.G. (1956) Measurement of Temperatures at Elevations of 30 to 80 Kilometers by the Rocket-Grenade Experiment. J.A.S. (formerly J. Met.) 13, p.5.

Forbes, J.M. (1982) Atmospheric Tides 1. Model Description and Results for the Solar Diurnal Component. J.G.R. 87, pp.5222-5240.

Fritts, D.C. (1984) Gravity Wave Saturation in the Middle Atmosphere: A Review of Theory and Observations. Rev. Geophys., Space Phys. 22, pp.275-308.

Geller, M.A. (1983) Dynamics of the Middle Atmosphere. Space Science Reviews 34, pp.359-375.

Gossard, E.E. and Hooke, W.H. (1975) Waves in the Atmosphere: Atmospheric Infrasound and Gravity Waves - Their Generation and Propagation, Elsevier Scientific Pub. Co., N.Y., 456pp.

Groves, J. (1983) (not published) Radio Meteor Studies. Honours Report, University of Adelaide, Physics Department, Adelaide, Australia.

Haurwitz, B. (1961) Frictional Effects and the Meridional Circulation in the Mesosphere. J.G.R. 66, pp.2381-2391.

Hines, C.O. (1960) Internal Atmospheric Gravity Waves at Ionospheric Heights. Can. J. Phys. 38, pp.1441-1481.

Hines, C.O. (1974) The Upper Atmosphere in Motion (Geophysical Monograph :18). Heffernan Press, Massachusetts, 1027pp.

Hocking, W.K. (1979) Angular and Temporal Characteristics of Partial Reflections from the D-Region of the Ionosphere. J.G.R. 84, pp.845-851.

Hocking, W.K. (1981) Investigation of the Movement and Structure of D-Region Ionospheric Irregularities. 2 Vols. PhD Thesis, University of Adelaide, Adelaide, Australia.

Hocking, W.K. (1983) Mesospheric Turbulence Intensities Measured with a HF Radar at 35° S - II. J.A.T.P. 45, pp.103-114.

Hocking, W.K. and Vincent, R.A. (1982) Comparative Observations of D-Region HF Partial Reflections at 2 and 6MHz. J.G.R. 87, pp.7615-7624.

Hodges, R.R. Jr. (1967) Generation of Turbulence in the Upper Atmosphere by Internal Gravity Waves. J.G.R. 72, pp.3455-3458.

Hodges, R.R. Jr. (1969) Eddy Diffusion Coefficients Due to Instabilities in Internal Gravity Waves. J.G.R. 74, pp.4087-4090.

Holton, J.R. (1983) The Influence of Gravity Wave Breaking on the General Circulation of the Middle Atmosphere. J.A.S. 40, pp.2497-2507.

Holton, J. and Wehrbein, W. (1980) A Numerical Model of the Zonal Mean Circulation of the Middle Atmosphere. Pure and Applied Geophysics 118, pp.284-306.

Houghton, J.T. (1978) The Stratosphere and Mesosphere. Q.J. Roy. Met. Soc. 104, pp.1-29.

Kellogg, W.M. and Schilling, G.F. (1951) A Proposed Model of the Circulation in the Upper Stratosphere. J.A.S. (formerly J. Met.) 8, pp.222-230.

Leaman, K.D. and Sanford, T.B. (1975) Vertical Energy Propagation of Inertial Waves: A Vector Spectral Analysis of Velocity Profiles. J.G.R. 80, pp.1975-1978.

Leovy, C. (1964) Simple Models of Thermally Driven Mesospheric Circulation. J.A.S. 21, pp.327-341.

Lindzen, R.S. (1967) Thermally Driven Diurnal Tide in the Atmosphere. Q.J. Roy. Met. Soc. 93, pp.18-42.

Lindzen, R.S. (1981) Turbulence and Stress Owing to Gravity Wave and Tidal Breakdown. J.G.R. 86, pp.9707-9714.

Lindzen, R.S. and Forbes, J. (1983) Turbulence Originating from Convectively Stable Internal Waves. J.G.R. 88, pp.6549-6553.

Matsuno, T. (1982) A Quasi-One-Dimensional Model of the Middle Atmospheric Circulation Interacting with Internal Gravity Waves. J. Meteor. Soc. Japan 60, pp.215-226.

McComas, C.H. and Bretherton, F.P. (1977) Resonant Interaction of Oceanic Internal Waves. J.G.R. 82, pp.1397-1412.

Murgatroyd, R.J. (1969) The Structure and Dynamics of the Stratosphere. In "The Global Circulation of the Atmosphere", G.A. Corby (ed.). Roy. Met. Soc., London, pp.159-195.

Murgatroyd, R.J. and Goody, R.M. (1958) Sources and Sinks of Radiative Energy from 30 to 90km. Q.J. Roy. Met. Soc. 84, pp.225-234.

Murgatroyd, R.J. and Singleton, F. (1961) Possible Meridional Circulations in the Stratosphere and Mesosphere. Q.J. Roy. Met. Soc. 87, pp.125-135.

Ohring, G. (1958) The Radiation Budget of the Stratosphere. J.A.S. (formerly J. Met.) 15, pp.440-451.

Rastogi, P.K. and Woodman, R.F. (1974) Mesospheric Studies Using the Jicamarca Incoherent-Scatter Radar. J.A.T.P. 36, pp.1217-1231.

Rastogi, P.K. and Bowhill, S.A. (1976) Scattering of Radio Waves from the Mesosphere - 2. Evidence for Intermittent Mesospheric Turbulence. J.A.T.P. 38, 449-462.

Reid, G.C. (1975) Ice Clouds at the Summer Polar Mesopause. J.A.S. 32, pp.523-535.

Reid, G.C. (1983) The Influence of Electric Fields on Radar Measurements of Winds in the Upper Mesosphere. Rad. Sci. 18, pp.1028-1034.

Reid, I.M. (1984) Radar Studies of Atmospheric Gravity Waves. PhD Thesis, University of Adelaide, Adelaide, Australia.

Rottger, J. (1980) Reflection and Scattering of VHF Radar Signals from Atmospheric Refractivity Structures. Rad. Sci. 15, pp.259-276.

Schoeberl, M. and Strobel, D. (1978) The Zonally Averaged Circulation of the Middle Atmosphere. J.A.S. 35, pp. 577-591.

Schoeberl, M.R., Strobel, D.F. and Appruzese, J.P. (1983) A Numerical Model of Gravity Wave Breaking and Stress in the Mesosphere. J.G.R. 88, pp.5249-5259.

Spiegel, M.R. (1972) Theory and Problems of Statistics (Schaums Outline Series) McGraw-Hill, N.Y., p.359.

Strobel, D.F. (1978) Parameterization of the Atmospheric Heating Rate from 15 to 120km Due to O and O Absorption of Solar Radiation. J.G.R. 83, pp.6225-6230.

Stroud, W.G., Nordberg, W., Bandeen, W.R., Bartman, F.L. and Titus, P. (1960) Rocket-Grenade Measurements of Temperatures and Winds in the Mesosphere Over Churchill, Canada. J.G.R. 65, pp.2307-2323.

Vincent, R.A. (1984) Gravity-Wave Motions in the Mesosphere. J.A.T.P. 46, pp.119-128.

Vincent, R.A. and Reid, I.M. (1983) H.F. Doppler Measurements of Mesospheric Gravity Wave Momentum Fluxes. J.A.S. 40, pp.1321-1333.

Wehrbein, W. and Leovy, C. (1982) An Accurate Radiative Heating and Cooling Algorithm for Use in a Dynamical Model of the Middle Atmosphere. J.A.S. 39, pp.1532-1544.

Weinstock, J. (1982) Nonlinear Theory of Gravity Waves: Momentum Deposition, Generalized Rayleigh Friction, and Diffusion. J.A.S. 39, pp.1698-1710.

Weisner, A.G. (1956) Measurement of Winds at Elevations of 30 to 80 Kilometers by the Rocket-Grenade Experiment. J.A.S. (formerly J. Met.) 13, p.30.

Woodman, R.F. and Guillen, A. (1974) Radar Observations of Winds and Turbulence in the Stratosphere and Mesosphere. J.A.S. 31, pp.493-505.

APPENDICES

Appendix 1 : Description of the Buckland Park H.F. Array

Appendix 2 : Supplementary Gravity Wave Theory

Appendix 3 : Linear Regression Calculation

APPENDIX 1

DESCRIPTION OF THE BUCKLAND PARK H.F. ARRAY

Experiments described in this thesis were undertaken at the University of Adelaide's, Buckland Park Field Station. A description of the equipment used follows. A more detailed description is available in Briggs et al. (1969) and Ball (1981).

The H.F. array is situated near Adelaide at 35° 38'S, 138° 29'E and operates at a frequency of 1.98MHz. Separate aerials are used for transmission and reception. Both are now described.

Transmission

Gaussian envelope pulses of width around 25 micro-seconds are transmitted at a repetition frequency of 10Hz (variable). The transmitter peak power is about 10kW. Centre fed folded dipole aerials arranged in a square (as shown in fig A1-1) allow both O and E mode transmission by the use of a phase shifter. Circularly polarised radio waves can be synthesised by summing two mutually perpendic-ular, linearly polarised rays, that are shifted in phase (see fig A1-1). This phase shift of ±90° is inserted via the phase shifter, the sign of the shift determining the mode. The required linearly polarised beams are obtained by driving the opposite pairs of parallel dipoles together.

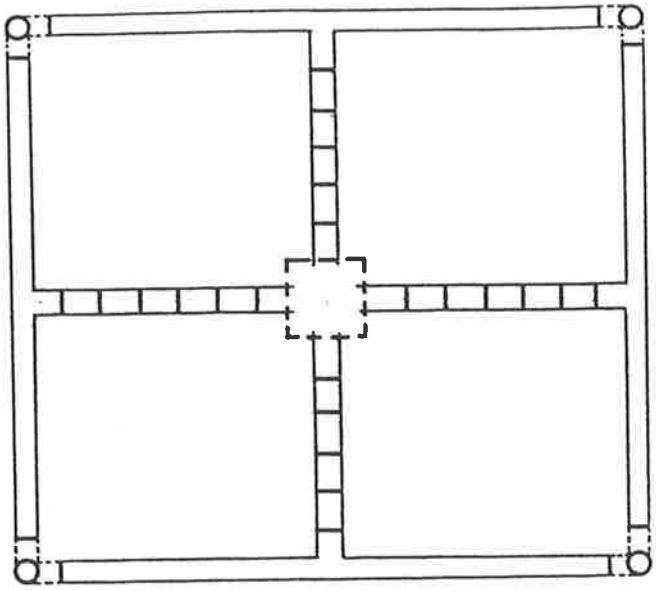

OVERHEAD VIEW

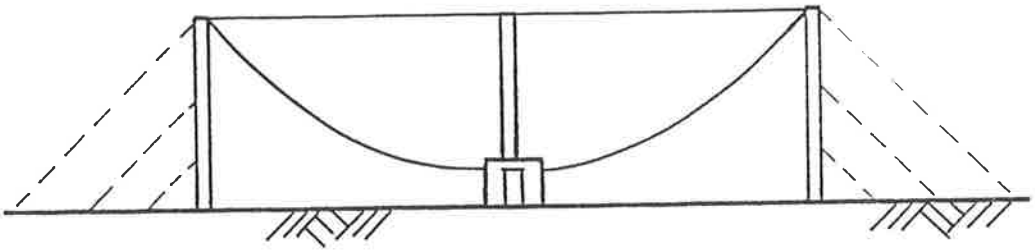

SIDE VIEW

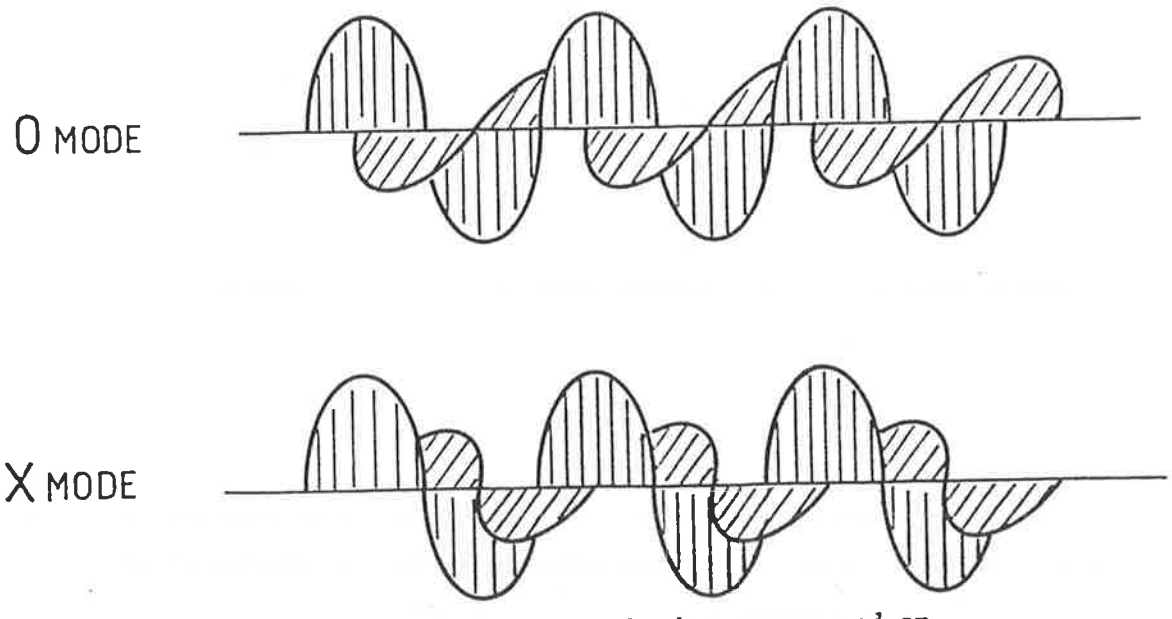

Figure A1-1. Plan of the transmitting array and an illustration of polarisation synthesis.

During the day, O-mode transmission is used because the E-mode polarisation is strongly absorbed at heights above 80km. At night, however, received powers are enhanced by using E-mode transmission.

The transmitting array (Fig A1-1) has a beamwidth (half width half maximum) of approximately 40° at 2MHz.

Reception

The receiving array consists of 2 independent sets of 89 half wave dipoles, one set aligned approximately north-south and one approximately east-west. The dipoles, made from copper wire, are 72m long and are hung from wooden poles 11m in length. These dipoles cover a circular area approximately 1km in diameter (see fig A1-2). Signals from each dipole are conveyed to the central hut via coaxial cables whose length has been cut to an integer number of wavelengths to maintain coherence. Impedance matched connecting boxes and bars are used to configure the sets of dipoles as desired, with the resulting signal going to the receivers.

When the whole array is connected as a broadside array, it has a beamwidth (half width half maximum) of around 5° with the first zero around 11.6°. The array polar diagram is as shown in fig (A1-3).

Up to 8 receivers may then be used to amplify the signals and sample as shown schematically (for 4 receivers) in fig (A1-4). The signal processors demodulate the receiver output into "in Phase" (IP) and "in Quadrature"

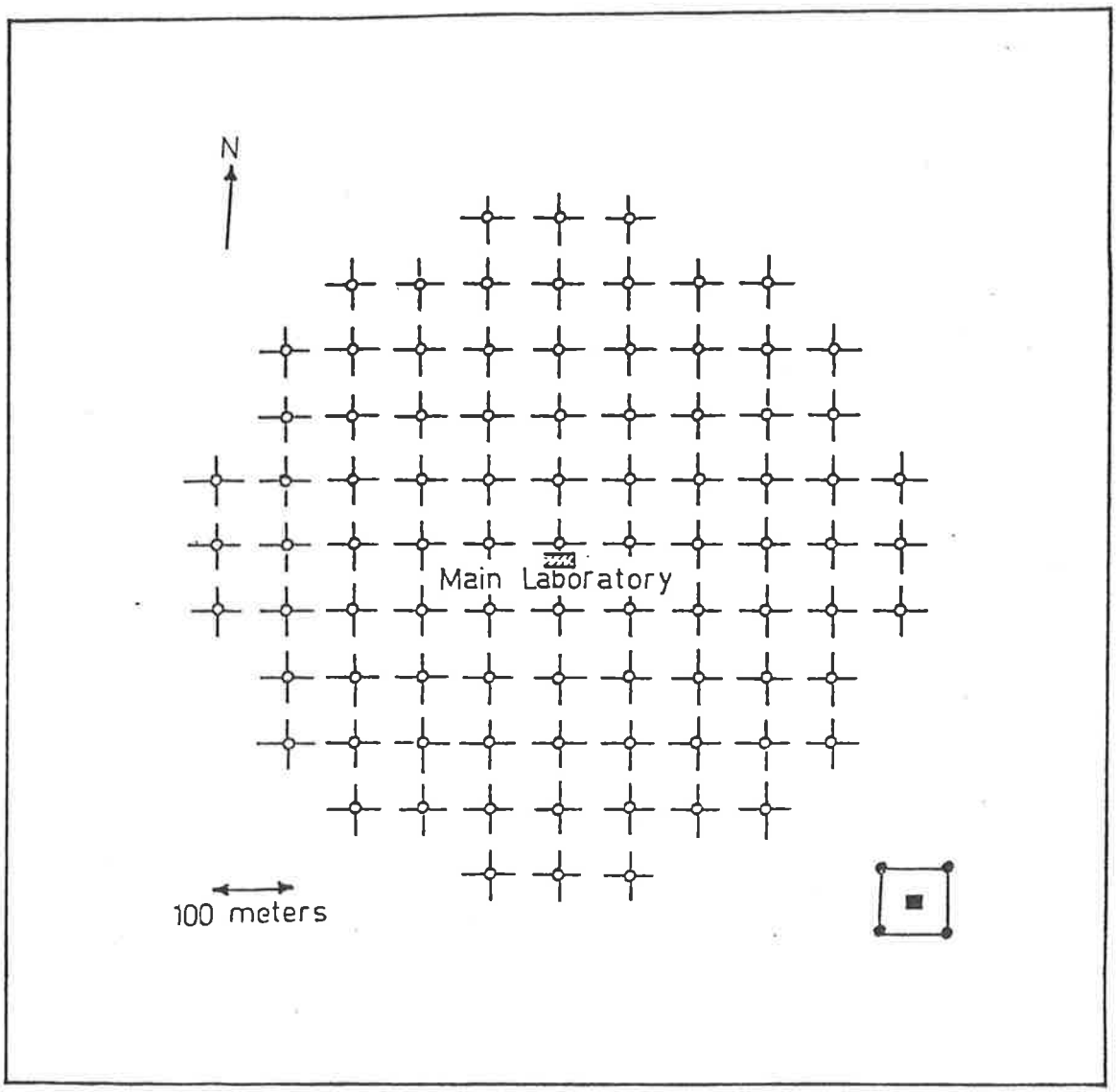

Figure A1-2. Plan of the receiving array. Each cross represents two individual dipoles.

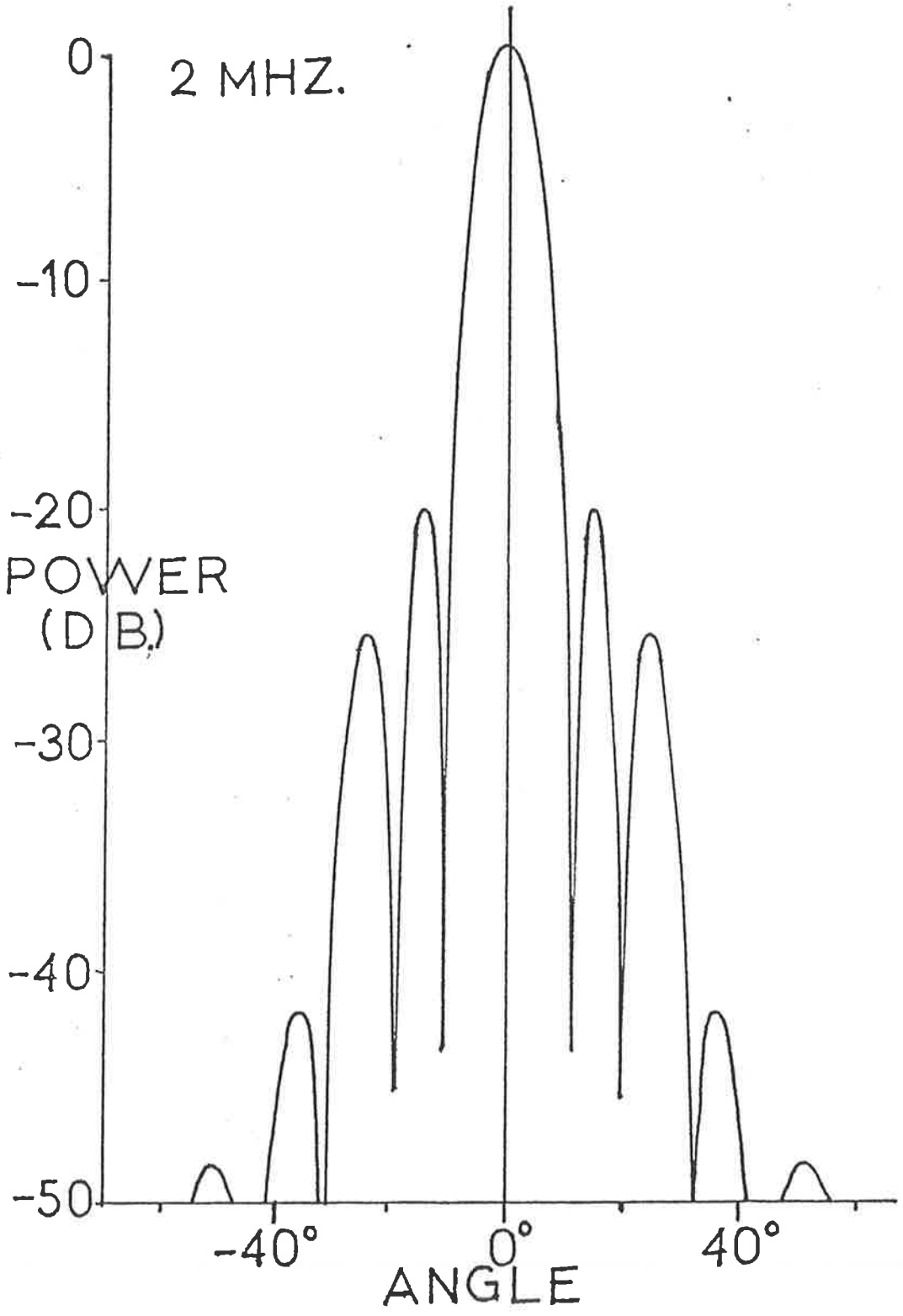

Figure A1-3. Receiving array polar diagram (after Hocking 1981).

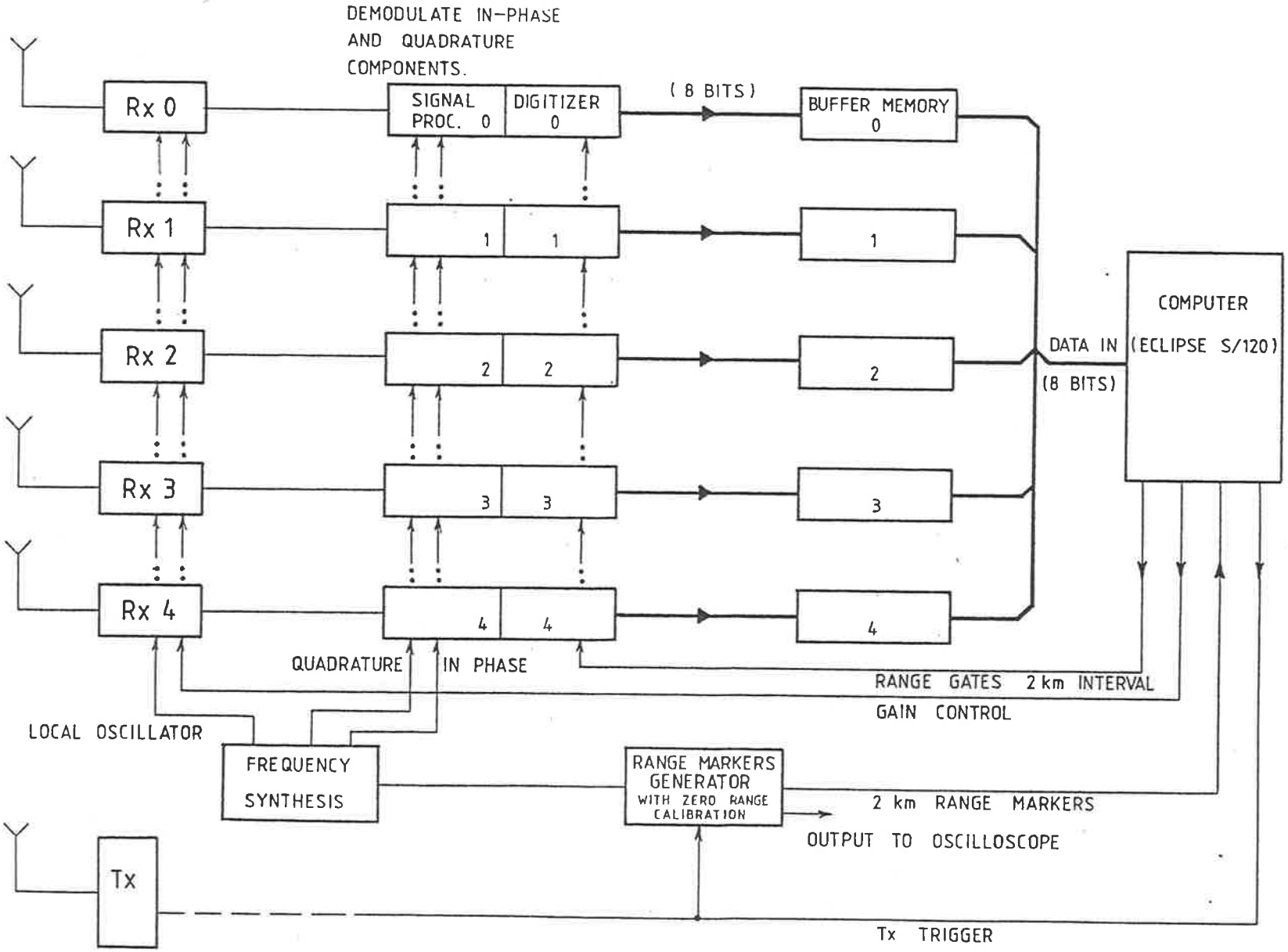

Figure A1-4. Schematic diagram of receiver and control electronics.

(IQ) components. After each transmitted pulse, the digitisers sample the IP and IQ signals at delays given by

$$\text{time delay} = \frac{2 \times \text{height}}{\text{speed of light}}$$

The hardware currently allows samples at 2km intervals between 50 and 100km. The 8-bit ($0\text{-}255_{10}$) binary signal levels are then transferred to the Eclipse S/120 minicomputer. The computer can then do primary or real-time analysis on the signals and store the results on magnetic tape. The resolution resulting from the digitisers used here is 1/256, i.e., 0.4%.

Although "range gates" at 2km intervals are indicated in fig (A1-4), range gating is not used directly. However, the finite width of the transmitter pulse produces an effect equivalent to the use of a range gate. The typical 25 microsecond pulses used here give a height resolution of 4km so that successive 2km samples are not independent.

APPENDIX 2

SUPPLEMENTARY GRAVITY WAVE THEORY

When the continuity, momentum and energy conservation equations are combined in internal atmospheric gravity wave theory, a situation results where it is convenient to work with the ratios of the perturbation quantities to their mean values (Hines, 1960). The resulting expressions, known as the "polarisation relations" are now presented. The approach used here, from Hines (1960), differs slightly from that used in chapter 1 in that the Coriolis term (and thus f) is omitted from the force equation.

The basic premise is that solutions of the basic equations will have the form

$$\frac{p'}{\bar{p}P} = \frac{\rho'}{\bar{\rho}R} = \frac{u'}{X} = \frac{w'}{Z} = Ae^{i\phi}$$

where $\phi = (\omega t - kx - mz)$

and where P, R, X, Z and A are constant and ω is real. This assumption leads to the dispersion relation (as in chapter 1) which may then be used to evaluate the constants viz.:

$$P = \gamma\omega^2 m - i\gamma g\omega^2 / C_s^2$$

$$R = \omega^2 m + i(\gamma-1)gk^2 - i\gamma g\omega^2 / C_s^2$$

$$X = \omega k m C_s^2 - ig\omega k$$

$$Z = \omega^3 - \omega k C_s^2$$

where C_s is the speed of sound, γ the ratio of specific heats, i the square root of -1 and the other quantities as previously defined.

It is then possible to assume a perturbation in one quantity (e.g., horizontal wind) and calculate the amplitude and relative phase of the other quantities. Refinements and assumptions can be made to simplify these relations even further but these are not presented in this thesis. They are, however, available in Hines (1960).

APPENDIX #3

LINEAR REGRESSION CALCULATIONS

The method used to fit straight lines to the data was the "method of least squares". This process acts to minimise the square of the vertical distance (here parallel to the $\bar{}$ axis) between the n individual data points and the fitted line. Calculus is used to obtain expressions for the line parameters and these are given here in the context of their use in this thesis. (Details are available in most statistics texts, e.g., Spiegel, 1972.)

The fitted line has the form

$$\bar{w}_m = a+cX$$

thus c is the slope and a the $\bar{w}_m$ axis intercept. To obtain this line the following sums are formed:

$$X. = \sum_{j=1}^{n} X_j \qquad \bar{w}_{m}. = \sum_{j=1}^{n} \bar{w}_{mj}$$

(where the dot denotes sum over j) and the product sums

$$\sum_{j=1}^{n} X_j^2 \qquad \sum_{j=1}^{n} X_j \bar{w}_{mj} \qquad \sum_{j=1}^{n} \bar{w}_{mj}^2$$

These are then combined into

$$P = \sum_{j=1}^{n} X_j \bar{w}_{mj} - \frac{X. \bar{w}_{m}.}{n}$$

$$Q = \sum_{j=1}^{n} \bar{w}_{mj}^2 - \frac{\bar{w}_{m}.^2}{n}$$

$$R = \sum_{j=1}^{n} X_j^2 - \frac{X.^2}{n}$$

to give the following:

$$c = \frac{P}{R} \qquad \text{the slope,}$$

$$a = \frac{(\bar{w}_{m.} - cX.)}{n}$$

$$d^2 = Q - \frac{P^2}{R}$$

with standard deviations,

$$\sigma_c = \frac{d^2}{(n-2)R}$$

$$\sigma_c = \frac{d^2 \sum_{j=1}^{n} X_j^2}{(n-2)n\ R}$$

The correlation coefficient ρ is obtained from d^2 using

$$\rho = \frac{P}{(QR)^{\frac{1}{2}}} = \left[1 - \frac{d^2}{Q^2}\right]^{\frac{1}{2}}$$